

# **Advances in Computing Science**

---

---

# Research in Computing Science

---

## Series Editorial Board

### Editors-in-Chief:

*Grigori Sidorov (Mexico)*  
*Gerhard Ritter (USA)*  
*Jean Serra (France)*  
*Ulises Cortés (Spain)*

### Associate Editors:

*Jesús Angulo (France)*  
*Jihad El-Sana (Israel)*  
*Alexander Gelbukh (Mexico)*  
*Ioannis Kakadiaris (USA)*  
*Petros Maragos (Greece)*  
*Julian Padget (UK)*  
*Mateo Valero (Spain)*

### Editorial Coordination:

*Alejandra Ramos Porras*

*Research in Computing Science* es una publicación trimestral, de circulación internacional, editada por el Centro de Investigación en Computación del IPN, para dar a conocer los avances de investigación científica y desarrollo tecnológico de la comunidad científica internacional. **Volumen 138**, noviembre 2017. Tiraje: 500 ejemplares. *Certificado de Reserva de Derechos al Uso Exclusivo del Título* No. : 04-2005-121611550100-102, expedido por el Instituto Nacional de Derecho de Autor. *Certificado de Licitud de Título* No. 12897, *Certificado de licitud de Contenido* No. 10470, expedidos por la Comisión Calificadora de Publicaciones y Revistas Ilustradas. El contenido de los artículos es responsabilidad exclusiva de sus respectivos autores. Queda prohibida la reproducción total o parcial, por cualquier medio, sin el permiso expreso del editor, excepto para uso personal o de estudio haciendo cita explícita en la primera página de cada documento. Impreso en la Ciudad de México, en los Talleres Gráficos del IPN – Dirección de Publicaciones, Tres Guerras 27, Centro Histórico, México, D.F. Distribuida por el Centro de Investigación en Computación, Av. Juan de Dios Bátiz S/N, Esq. Av. Miguel Othón de Mendizábal, Col. Nueva Industrial Vallejo, C.P. 07738, México, D.F. Tel. 57 29 60 00, ext. 56571.

**Editor responsable:** *Grigori Sidorov, RFC SIGR651028L69*

**Research in Computing Science** is published by the Center for Computing Research of IPN. **Volume 138**, November 2017. Printing 500. The authors are responsible for the contents of their articles. All rights reserved. No part of this publication may be reproduced, stored in a retrieval system, or transmitted, in any form or by any means, electronic, mechanical, photocopying, recording or otherwise, without prior permission of Centre for Computing Research. Printed in Mexico City, in the IPN Graphic Workshop – Publication Office.

# Advances in Computing Science

**Juan Carlos Chimal Eguía**  
**Horacio Rodríguez Bazán**  
**Christian E. Maldonado (eds.)**



Instituto Politécnico Nacional  
"La Técnica al Servicio de la Patria"



Instituto Politécnico Nacional, Centro de Investigación en Computación  
México 2017

**ISSN: 1870-4069**

---

Copyright © Instituto Politécnico Nacional 2017

Instituto Politécnico Nacional (IPN)  
Centro de Investigación en Computación (CIC)  
Av. Juan de Dios Bátiz s/n esq. M. Othón de Mendizábal  
Unidad Profesional “Adolfo López Mateos”, Zacatenco  
07738, México D.F., México

<http://www.rcs.cic.ipn.mx>

<http://www.ipn.mx>

<http://www.cic.ipn.mx>

The editors and the publisher of this journal have made their best effort in preparing this special issue, but make no warranty of any kind, expressed or implied, with regard to the information contained in this volume.

All rights reserved. No part of this publication may be reproduced, stored on a retrieval system or transmitted, in any form or by any means, including electronic, mechanical, photocopying, recording, or otherwise, without prior permission of the Instituto Politécnico Nacional, except for personal or classroom use provided that copies bear the full citation notice provided on the first page of each paper.

Indexed in LATINDEX, DBLP and Periodica

Printing: 500

Printed in Mexico

## Editorial

Computer Science is pervasive to the scientific endeavor. There is no area or field of study which, nowadays, can thrive without the use of computational resources, models and algorithms to analyze ever growing amounts of data in increasingly complex ways. This trend is clearly reflected in the selection of papers included in this volume of *Research in Computing Science*.

This issue presents both new and improved algorithms and methods as well as applications to other fields of study. Accepted works range from improved algorithms for solving classical computational problems, to the application of known models and techniques on biomedical challenges.

All submitted papers were reviewed by two or more independent members of the editorial committee. This volume contains revised and corrected versions of the 16 accepted papers.

Our deepest gratitude goes to all the parties involved in the creation of this volume: Foremost to the authors of the articles for their dedication to the excellence of the works presented. We are also grateful for the hard labor the members of the editorial board invested in the evaluation and selection of the highest quality papers amongst many others of high value. We are also indebted to the *Sociedad Mexicana de Inteligencia Artificial* (SMIA) for their collaboration towards the completion of this journal. Our special and profound gratefulness to the *Centro de Investigación en Computación* of the *Instituto Politécnico Nacional* (CIC-IPN) for their invaluable collaboration in the publishing of this issue. The submission, review, and selection processes were enabled by the widely adopted tool *EasyChair*, ([www.easychair.org](http://www.easychair.org)) free of charge.

*Juan Carlos Chimal Eguía*  
*Horacio Rodríguez Bazán*  
*Christian E. Maldonado*  
CIC-IPN, Mexico  
Guest Editors

November 2017



## Table of Contents

|   | Page |
|---|------|
| <b>Numerical Analysis of a Diffusion Flame Under Water Mist Jet Influence</b> .....   | 9    |
| <i>M. De la Cruz-Ávila, E. Martínez-Espinosa, G. Polupan</i>  |      |
| <b>Priority Data Transmission Schemes for a Wireless Sensor Network on BAN</b> .....  | 19   |
| <i>Sergio Martínez, Mario Rivero, Laura Garay, Issis Romero</i>   |      |
| <b>Modelo foveal rectangular a partir de un sensor de imagen comercial</b> .....  | 29   |
| <i>José Antonio Loaiza Brito, Luis Niño de Rivera y Oyarzábal</i>   |      |
| <b>Computational Intelligence Algorithms Applied to the Pre-diagnosis of Chronic Diseases</b> .....   | 41   |
| <i>Mariana Dayanara Alanis-Tamez, Yenny Villuendas-Rey, Cornelio Yáñez-Márquez</i>  |      |
| <b>Hybrid CW-GA Metaheuristic for the Traveling Salesman Problem</b> .....  | 51   |
| <i>Irma Delia Rojas Cuevas, Santiago Omar Caballero Morales</i>   |      |
| <b>Transmission of Digital Audio with Visible Light</b> .....   | 61   |
| <i>Sergio Sandoval-Reyes, Arturo Hernandez-Balderas</i>   |      |
| <b>Implicaciones computacionales de los aeromanipuladores</b> .....   | 69   |
| <i>Julio Mendoza-Mendoza, Baltazar Jiménez-Ruiz, Víctor Javier González-Villela, Mauricio Méndez-Martínez, Leonardo Fonseca-Ruiz, Erick López Alarcón</i> |      |
| <b>Lumped Parameter Estimation of a Stochastic Process of Second Order Using the Second Moment and Recursiveness</b> .....                                | 79   |
| <i>Romeo Urbietta Parrazales, José de Jesús Medel Juárez, Karen Alicia Aguilar Cruz, Rosaura Palma Orozco</i>   |      |
| <b>A Survey on Computer Science Techniques in the FOREX Market: Models and Applications</b> .....   | 89   |
| <i>Diego Aguilar, Ildar Batyrshin, Oleksiy Pogrebnyak</i>   |      |
| <b>Armagedroid, APKs Static Analyzer Software</b> .....   | 99   |
| <i>Luis Enrique Héctor Almaraz García, Eleazar Aguirre Anaya, Ponciano Jorge Escamilla Ambrosio, Raúl Acosta Bermejo</i>                                  |      |

|  |            |
|--|------------|
| <b>Experimental Comparison of Bioinspired Segmentation Algorithms Applied to Segmentation of Digital Mammographies .....</b> | <b>109</b> |
| <i>David González-Patiño, Yenny Villuendas-Rey, Amadeo J. Argüelles-Cruz</i>   |            |
| <b>Sequence Prediction with Hyperdimensional Computing.....</b>  | <b>117</b> |
| <i>Job Isaias Quiroz Mercado, Ricardo Barrón Fernández, Marco Antonio Ramírez Salinas</i>                                    |            |
| <b>Designing New CAPTCHA Models Based on the Cognitive Abilities of Artificial Agents.....</b>                               | <b>127</b> |
| <i>Edgar D. García-Serrano, Salvador Godoy-Calderón, Edgardo M. Felipe-Riverón</i>   |            |
| <b>Estimation and Identification Process Using an Exponential Forgetting Factor.....</b>                                     | <b>137</b> |
| <i>Karen Alicia Aguilar Cruz, José de Jesús Medel Juárez, Romeo Urbietta Parrazales, María Teresa Zagaceta Álvarez</i>       |            |
| <b>Análisis de readmisión hospitalaria de pacientes diabéticos mediante aprendizaje computacional .....</b>                  | <b>147</b> |
| <i>Germán Cuaya-Simbro, Elias Ruiz, Angélica Muñoz-Meléndez, Eduardo F. Morales</i>  |            |
| <b>The Mexican Magical Towns Traveling Salesman Problem: Preliminary Results .....</b>                                       | <b>159</b> |
| <i>Sandra J. Gutiérrez, Nareli Cruz, Hiram Calvo, Marco A. Moreno-Armendáriz</i>   |            |

# Numerical Analysis of a Diffusion Flame Under Water Mist Jet Influence

M. De la Cruz-Ávila<sup>1</sup>, E. Martínez-Espinosa<sup>2</sup>, G. Polupan<sup>1</sup>

<sup>1</sup> Instituto Politécnico Nacional, LABINTHAP, ESIME, CDMX, Mexico

<sup>2</sup> UNAM Ciudad Universitaria, Instituto de Ingeniería, CDMX, Mexico

mauriciodlca1@gmail.com

**Abstract.** A water mist jet for a steam generator of direct contact with a diffusion flame is numerically analyzed in this paper. Numerical simulation is conducted for an 8 Lug-Bolt array in a confined system. The diffusion flame is modelled in the Eulerian - Eulerian multiphase approach where the reaction species are oxygen which is injected by a 16.9 mm central nozzle, methane by four peripheral 5.86 mm nozzles as the water mist and with a droplet size of 10 $\mu$ m. Numerical simulations are developed with the Reynolds Averaged Navier-Stokes and the Realizable  $k$ - $\epsilon$  turbulence model is considered. The Eddy Dissipation Model is implemented in order to calculate the effect of turbulent chemical reaction rate. Predictions show some instabilities that are located within the flame structure as long as the fuel moisture percentage is less than 1%. If the mist fraction for vaporization increases, the instabilities do not affect the internal flame structure but instabilities becomes relevant to the end of the calculus domain. The decrement about 60% of the water mist velocity due to a vapor gap around the micro droplets is the mean cause of the instabilities. Therefore, a very precise control of the numerical parameters is so important for multiphase approximations.

**Keywords:** Eulerian - Eulerian multiphase approach, multiphase combustion, water mist injection, direct vaporization.

## 1 Introduction

In the open literature there are many studies focused on two gas streams, which consider an annular fuel and oxidizer injection shape. For example, the study carried out by Fossa [1], and Cioncollini [2] analyze two-phase mixture flows. Grech [3], Cutrone [4], and Smith [5] conducted numerical simulations with Reynolds-Averaged Navier-Stokes (RANS) method for diffusion combustion process in jet propulsion rockets and gas turbines. Lopez-Parra and Turan [6] have simulated a methane turbulent jet diffusion flame with the Eddy Dissipation Model (EDM) [7] and the standard

$k-\varepsilon$  turbulence model with satisfactory results. Finally, the mixing fluids process in diffusion flame systems is extremely important because the fuel and oxidizer are injected independently and combustion starts when the mixture reaches flammability limits (upper or lower) [8].

However, all this studies are focused on the flame development but not on the numerical control for a multiphase combustion-vaporization scheme. Therefore, this paper is focused on the numerical control settings for the numerical diffusion flame-water mist in a multiphase scheme approximation. The water mist injection flow for three cases are analyzed in order to compare its influence over development during the steam generation. This work allows to be applied to further numerical studies in turbulent combustion, water drops vaporization and quenching flames.

## 2 Numerical Details

Numerical simulations are conducted for 8 Lug-Bolt system where oxygen is injected in a 16.9 mm central nozzle, methane and water mist by four peripheral 5.86 mm nozzles respectively. The simulations used the standard methane, water and oxygen properties for mixture species. Jets are under atmospheric conditions of 1atm and 298K in a confined system as shown in Fig. 1.

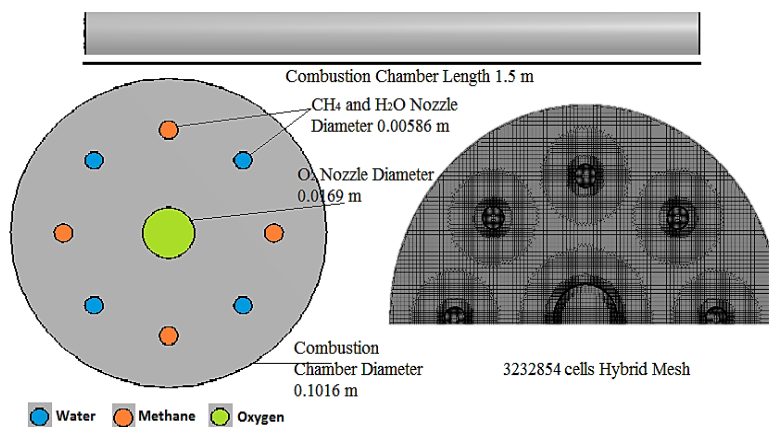


Fig. 1. Computational domain, settings and mesh.

The combustion chamber has 101.6mm diameter ( $D_c$ ) and 1500mm of total length ( $L$ ). The aim of the numerical approximations is to analyse the influence of the water mist affecting the mixture process for three flow Cases. An Eulerian-Eulerian approach was implemented for representing multiphase phenomenon and combustion species were modelled as the continuous phase ( $p$  phase 1) and the water mist as the dispersed phase ( $q$  phase 2). Simulations consider mean velocity profile of 10m/s for every stream. The water mist droplets are analysed for three different cases. The micro-droplet diameter remains constant with 10  $\mu\text{m}$  while the injection mist flow is

0.005, 0.010 and 0.015 kg/s. Pressure outlet to air was use for boundary outlet a non-slip and adiabatic treatment for the calculus domain wall was use. A mesh with 3232854 cells (Fig.1.), which is based on the proper resolution of the micro-droplets dynamics with a size of 10 microns and the gas phase flow coupling was used as described by Yuval Dagan et al [9]. Both phases are proposed as unreactive fluids to ensure a good tracking of properties at the interphase.

## 2.1 Constitutive Equations

In first instance, the numerical analysis of the oxygen-methane mixture process is of the physical nature. This implies that the equations to be solved are mass conservation, the momentum quantity, energy and chemical. These equations in multiphase Eulerian-Eulerian approach model solution are defined by the following expressions.

### Mass conservation.

$$\frac{\partial}{\partial t}(\alpha_q \bar{\rho}_q) + \nabla \cdot (\alpha_q \bar{\rho}_q \tilde{\mathbf{v}}_q) = \sum_{p=1}^n (\bar{\dot{m}}_{pq} - \bar{\dot{m}}_{qp}) + \bar{S}_q, \quad (1)$$

where  $\alpha_q$  is the volume fraction,  $\tilde{\mathbf{v}}_q$  is the velocity of phase  $q$  and  $\dot{m}_{pq}$  characterizes the mass transfer from the  $p$ th to  $q$ th phase, and  $\dot{m}_{qp}$  characterizes the mass transfer from the phase  $q$  to phase  $p$ ,  $\rho$  is the phase density and  $S_q$  is the source term.

### Momentum.

$$\begin{aligned} \frac{\partial}{\partial t}(\alpha_q \bar{\rho}_q \tilde{\mathbf{v}}_q) + \nabla \cdot (\alpha_q \bar{\rho}_q \tilde{\mathbf{v}}_q \tilde{\mathbf{v}}_q) = & -\alpha_q \nabla \bar{p} + \nabla \cdot \bar{\boldsymbol{\tau}}_q \bar{\rho}_q \bar{\mathbf{g}} + \\ \sum_{p=1}^n (K_{pq} (\tilde{\mathbf{v}}_p - \tilde{\mathbf{v}}_q) + \bar{\dot{m}}_{pq} \tilde{\mathbf{v}}_{pq} - \bar{\dot{m}}_{qp} \tilde{\mathbf{v}}_{qp}) + & (\bar{\mathbf{F}}_q + \bar{\mathbf{F}}_{\text{lift},q} + \bar{\mathbf{F}}_{\text{td},q}), \end{aligned} \quad (2)$$

where  $(K_{pq} (=K_{qp}))$  is the interphase momentum exchange coefficient and  $\tilde{\mathbf{v}}_{q,p}$  are the phase velocities. Note that represents the mean interphase momentum exchange and does not include any contribution due to turbulence. The turbulent interphase momentum exchange is modelled with the turbulent dispersion force term  $\bar{\mathbf{F}}_{\text{td},q}$  and  $\bar{\mathbf{F}}_q$  the external body forces which is equal to 0.  $\bar{\boldsymbol{\tau}}_q$  is the  $q^{\text{th}}$  phase stress tensor  $p$  and  $g$  are the pressure ante gravity respectively.

**Conservation of Energy.** To describe the conservation of energy in Eulerian multiphase applications, the equation can be written in terms of each phase:

$$\begin{aligned} \frac{\partial}{\partial t}(\alpha_q \bar{\rho}_q \bar{h}_q) + \nabla \cdot (\alpha_q \bar{\rho}_q \tilde{\mathbf{v}}_q \bar{h}_q) = \\ \alpha_q \frac{\partial \bar{p}_q}{\partial t} + \bar{\boldsymbol{\tau}}_q : \nabla \tilde{\mathbf{v}}_q - \nabla \cdot \tilde{\mathbf{q}}_q + S_q + \sum_{p=1}^n (Q_{pq} + \bar{\dot{m}}_{pq} \bar{h}_{pq} - \bar{\dot{m}}_{qp} \bar{h}_{qp}). \end{aligned} \quad (3)$$

**Conservation of Species.** The chemical species conservation equation for a multiphase mixture can be represented in the following form:

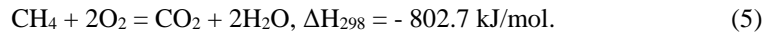
$$\frac{\partial}{\partial t} (\bar{\rho}^q \alpha^q \widetilde{Y}_i^q) + \square \cdot (\bar{\rho}^q \alpha^q \widetilde{\vec{v}}^q \widetilde{Y}_i^q) = -\square \cdot \alpha^q \widetilde{\vec{J}}_i^q + \alpha^q \mathcal{R}_i^q + \alpha^q \mathcal{S}_i^q + \sum_{p=1}^n (\bar{m}_{p^i q^i} - \widetilde{m}_{q^i p^i}) + \mathcal{R}, \quad (4)$$

where  $\mathcal{R}$  is the reaction rate and  $\bar{\tau}_q = \overline{\bar{\rho}_q \vec{v}_q \vec{v}_q} - \bar{\rho}_q \overline{\vec{v}_q \vec{v}_q}$ ,  $\bar{q}_q = \overline{\bar{\rho}_q \vec{v}_q h_q} - \bar{\rho}_q \overline{\vec{v}_q h_q}$ ,  $\bar{j}_i^q = \overline{\bar{\rho}^q \vec{v}^q Y_i^q} - \bar{\rho}^q \overline{\vec{v}^q Y_i^q}$ , are the average fluctuations of Reynolds stresses, heat fluxes and mass fluxes respectively, with the sign “ $\bar{\quad}$ ” denoting time average and “ $\widetilde{\quad}$ ” denoting Favre average.

The transport momentum equation averaging result into the appearance of terms containing the average fluctuations. Turbulence model involved in this paper (the Realizable  $k-\varepsilon$  model) is based on the Boussinesq hypothesis, which means, the Reynolds stress tensor must be modelled in order to close the RANS equations and be proportional to the mean deformation rate tensor. The Realizable  $k-\varepsilon$  turbulence model describes a two scalar transport, the turbulent kinetic energy ( $k$ ) and its dissipation rate ( $\varepsilon$ ). The model has been validated experimentally for many reactive flows simulations with satisfactory results [10-12]. Numerical simulations are developed with the alternative RANS technique and considers the Realizable  $k-\varepsilon$  [13] turbulence model for the equations system closure.

## 2.2 Constitutive Combustion Kinetics and Combustion Modelling

The energy production by the methane combustion has been well established by the next overall reaction:



This overall equation is a gross simplification by the actual reaction mechanism, which involves free radical chain reactions. The numerical simulation considers a stoichiometric reaction neglecting all other subsequent reaction in the chain reaction mechanism. Nevertheless, this work main purpose is not to analyze the secondary chemical reactions. For this reason, a single-step irreversible chemical reaction was used in order to redirect computational resources to the flow development.

The species are characterized through the involved mass fractions  $Y_i$  for  $i=1$  to  $N$ , where  $N$  is the number of species in the reacting mixture. The mass fractions  $Y_i$  are defined by:

$$Y_i = \frac{m_i}{m}, \quad (6)$$

where  $m_i$  is the mass of species  $i$  present in a given volume  $V$  and  $m$  is the total mass of gas in the volume. The numerical study of turbulent-reactive flows depends upon the combustion model adequate selection. The high non-linear production term for the species' conservation equation closure is one of the most challenging aspects when modeling turbulent combustion. The Eddy Dissipation Model (EDM) is used to calculate the turbulent chemical reaction rate effect. The EDM is based on the infinitely

fast chemistry hypothesis and assumes that the reaction rate is controlled by the turbulent mixing [14]. A generalized formulation of the EDM has been proposed in order to take into account finite-rate chemistry effects. A stoichiometric relation describing chemical reactions of arbitrary complexity can be represented by the  $r^{th}$  reaction equation [15]. The turbulent mixing rate is related to the turbulent eddies timescale present in the flow. The timescale used for this purpose is the so-called eddy lifetime,  $\tau=k/\varepsilon$ , with  $k$  being the turbulent kinetic energy,  $\varepsilon$  the turbulent dissipation rate and the chemistry typically described by relatively simple single or two-step mechanism. The species  $i$  production net-rate due to reaction  $r$ ,  $R_{i,r}$  is given by the smaller (*limiting-value*) of the two expression below.

**Base on reactants mass fraction:**

$$R_{i,r} = v'_{i,r} M_{w,i} A \rho \frac{\varepsilon}{k} \min_R \left( \frac{Y_R}{v'_{R,r} M_{w,R}} \right). \quad (7)$$

**Base on products mass fraction:**

$$R_{i,r} = v'_{i,r} M_{w,i} A B \rho \frac{\varepsilon}{k} \frac{\sum_P Y_P}{\sum_j v'_{j,r} M_{w,j}}, \quad (8)$$

where  $Y_p$  and  $Y_R$  the species mass fraction,  $A$  and  $B$  are Magnussen [14] constant for reactants (4.0) and products (0.5) respectively.  $M_{w,i}$  molecular weight  $R$  and  $P$  reactants and products respectively.

### 2.3 Numerical Fluid Reconstruction

A 3rd order *Quadratic Upstream Interpolation for Convective Kinematics* (QUICK) scheme for the convective and viscous terms was considered. However, this high-order scheme is not easy to apply to unstructured grid directly. The Leonard's QUICK scheme [16] uses a quadratic fit through two upwind nodes and one downwind cell center. To find the exact location of the next upwind cell nodes would increase the geometrical complexity and consume relatively more memory and CPU time.

In a uniform grid (Fig. 2. for definitions of points WW, W, P, E, EE), the Quick scheme at the east cell-face can be written as:

$$\begin{aligned} \phi_e &= \frac{1}{2}(\phi_P + \phi_E) - \frac{1}{8}(\phi_W - 2\phi_P + \phi_E) \quad (u \geq 0), \\ \phi_e &= \frac{1}{2}(\phi_P + \phi_E) - \frac{1}{8}(\phi_{EE} - 2\phi_E + \phi_P) \quad (u < 0). \end{aligned} \quad (9)$$

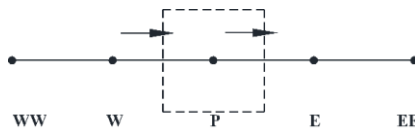


Fig. 2. QUICK scheme for a uniform grid.

This scheme is 2<sup>nd</sup>-order accurate if the definition of the truncation error is based on approximating the spatial derivative at cell centers in the linear convection equation. Other authors [14, 15] have chosen alternative definitions of the truncation error, according to which QUICK becomes 3rd-order accurate. Consequently, the implementation of both specifications (mesh/scheme) provides better approximation results in comparison to those in which use is posed separately.

The 3<sup>rd</sup>-order *Modified High Resolution Interface Capturing Scheme* (M-HRIC) for the viscous terms. For simulations using the multiphase model, upwind schemes are generally unsuitable for interface tracking because of their overly diffusive nature. Central differencing schemes, while generally able to retain the sharpness of the interface, are unbounded and often give unphysical results. In order to overcome these deficiencies, it is better to use the modified version of the High Resolution Interface Capturing (HRIC) scheme. The modified HRIC scheme is a composite normalized variable diagram (NVD) scheme that consists of a nonlinear blend of upwind and downwind differencing. First, the normalized cell value of volume fraction,  $\tilde{\phi}_c$  is computed and is used to find the normalized face value,  $\tilde{\phi}_f$  as follows:

$$\tilde{\phi}_c = \frac{\phi_D - \phi_U}{\phi_A - \phi_U}, \tag{10}$$

where A is the acceptor cell, D is de donor cell, and U is the upwind cell and

$$\tilde{\phi}_f = \begin{cases} \tilde{\phi}_c & \tilde{\phi}_c < 0 \text{ or } \tilde{\phi}_c > 1, \\ 2\tilde{\phi}_c & 0 \leq \tilde{\phi}_c \leq 0.5, \\ 1 & 0.5 \leq \tilde{\phi}_c \leq 1. \end{cases} \tag{11}$$

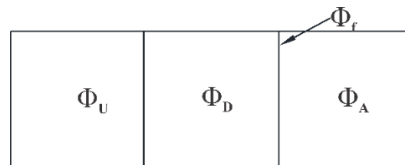


Fig. 3. Cell Representation for Modified HRIC scheme.

### 3 Results

The heat released of the combustion process directly affect the water mist flow changing its enthalpy and as a consequence the vaporization process take places. The water vapour temperature contours for the three Cases are presented in Fig.4. In Case A, the global vapour temperature ascends to 2921 K because its mass flow is 0.005 kg/s (50% less than case B and 75% less than C) and the vaporization starts in a zone near or in the flame front. Vaporization Enthalpy direct affects the micro droplet due to its proximity size (less mas flow = lager distance between droplets). The global vapour temperature for Case B is 2489 K which represents a 14.7% variation respect Case A because its droplets proximity is shorter. Then, the vaporization energy needs to be higher to reach all droplet surroundings. Thus for Case C, the global vapour temperature is 1541 K which represent a 47% respect Case A and 39% respect Case B. This

result does not mean that a proportional increase water mist mass flow must be directly proportional to a temperature decrement. All this behaviour is related to the *gap-lap* surrounding droplets and droplets proximity distance. Also, in this contours it is possible to observe vapour waves which are direct related with instabilities and associated to a density gradient at the interface when the velocity of phase  $p$  and the velocity of the phase  $q$  are the same  $v_p=v_q$ . These instabilities are exposed only at the end of the calculus domain because combustion products density are different of the water vapour and waves are present in the outer vapour structure. Results show water vapour velocity ( $v_q$ ) is equal to the combustion products velocity ( $v_p$ ) almost 60% of the injection velocity. Therefore, instabilities are more intense in case A, as shown in Fig. 4. The Fig. 5. shows droplet density contours for the maximum water mist concentration. This mist concentration is mixed with the methane stream considering it as moist fuel. When the water mist interacts with the fuel, a methane displacement occurs, thereby does not allows a correct fuel-oxygen mixture. For a water mist jet mass flow, humidity ratio and moist percent by species volume mixture is shown in Table 1. The mist concentration % represent a methane direct displacement %. This percent is lower than the Upper Flammability Limit density species mixture (UFL). The flammability limits in a combustion process moist free is considered as a reference case. The reference case and moist mixture for three cases are shown in Table 1.

**Table 1.** Moist variation for the mixture process.

| Case      | Moist Fuel Concentration (kg/m3) | Moist Mixture Concentration (kg/m3) | Variation | Variation % | CH4 mixture % | O2 mixture % |
|-----------|----------------------------------|-------------------------------------|-----------|-------------|---------------|--------------|
| Reference | 0.6558                           | 0.8100                              | 0         | 0           | 60.88         | 39.12        |
| A         | 0.6564                           | 0.8198                              | 0.00983   | 1.21        | 59.67         | 40.33        |
| B         | 0.6674                           | 0.8236                              | 0.01358   | 1.67        | 58.00         | 42.00        |
| C         | 0.6732                           | 0.8279                              | 0.01793   | 2.21        | 55.79         | 44.21        |

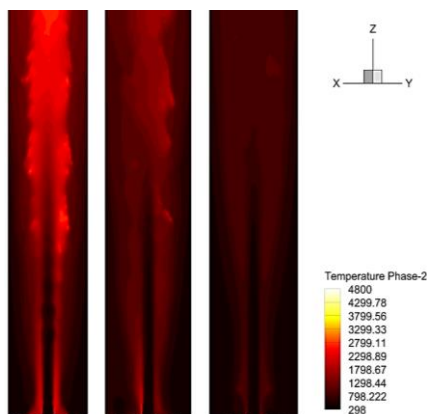


**Fig. 4.** Contours of water vapour Case A, B and C temperature K.

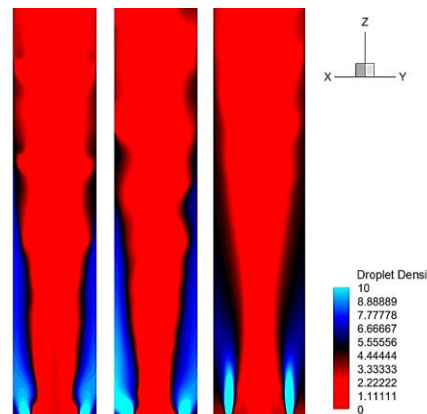


**Fig. 5.** Density contours Case A, Case B and Case C [dim less].

The fuel-oxygen mixture is produced by the turbulence induced in the methane-oxygen stream at the outlet burner and the density difference between the central jet and surroundings (mixture layer around the oxygen jet potential core). On one hand, numerical predictions show a drag effect on methane jet by the oxygen flow because the oxygen jet core has a greater amount of flow. The same behaviour is present in the three cases. Therefore, for the most relevant zone to the species mixture is located between the methane jets and oxygen stream where the flammability limits are reached. The flammability limits are represented by a methane-oxygen mixture density an optimal composition that is reached for combustion reaction. Since this global mixture have 0.8% of moist, the global density mixture increases its value in 1.21% to reach the UFL and the reaction zone is extended in the combustion chamber (represented through the iso-surfaces in Fig. 6). Whilst the reaction zone increases, the recirculation zones remain unchanged. But on the other hand, the drag effect and the recirculation also affect the water mist flow. Besides the drag effect, the velocity contraflow product of the vortex has a direct impact on the jets momentum reducing the velocity of the eight jets flow as the streamlines exhibit in Fig 7. For the three case the most affected is the case A with a water mist velocity reduction in a 60%.

Considering two fluid regions,  $v_p > v_q$ . The fluid  $p$  has uniform velocity  $v_p = 10$  m/s while  $q$   $v_q = 4$  m/s although the fluid injection  $V = 10$  m/s for both phases. The velocity difference mentioned before is a direct consequence of the water vapour gap surrounding every droplet as mentioned by Korlie [17]. This velocity gradient causes a special offset between the mixture interfaces. It is assumed that the flow is inviscid at  $T_{pq} < T_{sat}$  in this case  $T_{pq} < T_{React}$  where  $T_{pq}$  is the mean temperature between phases and  $T_{React}$  is the mean exothermic reaction temperature. Therefore it can suffer a tangential velocity discontinuity at the interfacial area concentration,  $A_{p,i}$  and  $A_{p,j}$  just before the methane and oxygen potential cores. Those discontinuities are shown in Fig 8. Since the velocity gradient is sufficient to inflict a shear at the fluid interface, is possible to define a shear velocity or friction velocity.

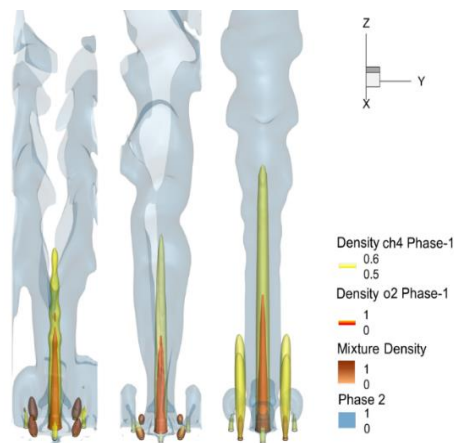


**Fig. 6.** Iso-surfaces of mixture components Case A, B and C.

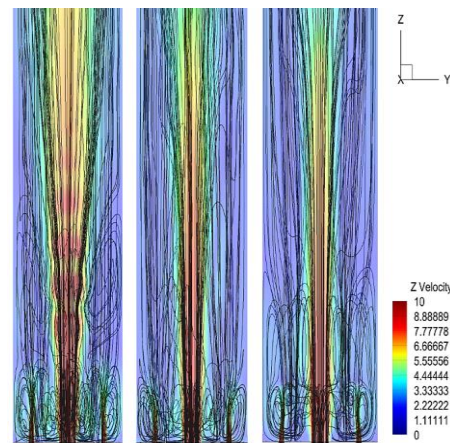


**Fig. 7.** Streamlines and recirculation zones Cases A, B and C.

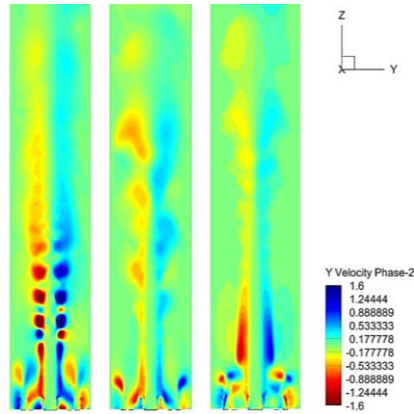


**Fig. 8.** Contours of tangential velocity of water mist phase [m/s].

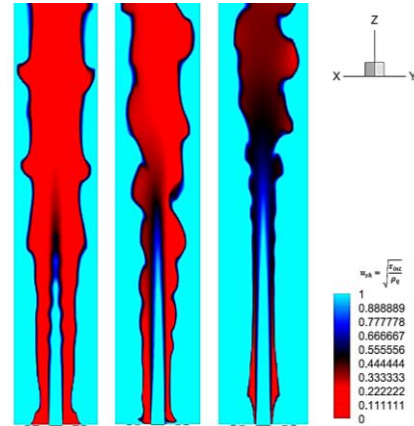


**Fig. 9:** Contours of  $u_{sh}$  [dim less].

This kind of shear stress may be re-written in units of velocity. It is useful method to compare true velocities, such as the velocity of a mist flow in a stream and the shear between layers of flow and it is shown that in many case this velocity is  $u_{sh} \approx 1/10 v_p$ . Before the flickering zone the outer instabilities at the outer flame layer are present. In most cases the inner instabilities are present within flame-mist layer.

The Fig. 9. demonstrates the instabilities by means of waves. The waves destabilize the structure of the oxygen jet. The outer waves destabilize the vapour-combustion products mixture structure. With the increment of mist flow the inner waves tend to diminish and the outer instabilities tends to increase.

## 4 Conclusions

The vaporization starts in a zone near the flame front and vaporization Enthalpy direct affects the micro droplet due to its proximity establishing the relation *less mass flow equal to lager distance between droplets*. Then, the vaporization energy needs to be higher to reach all droplet surroundings which means a flame front temperature reduction. All this behaviour is related to the “*gap-lap*” surrounding droplets and droplets proximity distance. Since the mean velocity of both phases are the same  $v_p = v_q$ , the outer instabilities are intense by water vapour and combustion products mixing process.

Furthermore, in a fuel moisture percentage less than 1%, the instabilities are conserved within the flame structure. If the vaporization mist fraction increases, the instabilities do not affect the internal structure where the methane-oxygen mixing process occurs. However, these instabilities are transferred to the outer structure of the flame by means of waves since the density variation between water vapour and combustion products is emphasized. Even the methane-oxygen reaction zone increases its value (distance) in a 68% is not a participant cause for any both kind of instabilities. The direct mechanism for these instabilities is an intensified vaporization process affecting directly the velocity of the water mist injection jets. Therefore, the vaporization effect is the leading cause of both types of instabilities.

## References

1. Fossi, M.: A Simple Model to Evaluate Direct Contact Heat Transfer and Flow Characteristics in Annular Two-Phase Flow. *International Journal of heat and mass flow* vol. 16, 272–279 (1995)
2. Cioncollini, A., Thome J., Lombardi C.: Algebraic Turbulence Modelling in Adiabatic Gas–Liquid Annular Two-Phase Flow. *International Journal of Multiphase Flow* vol. 35, pp. 580–596 (2009)
3. Grech, N., Mehdi, A., Zachos, P. K., Pachidis, V., Singh, R.: Effect of Combustor Geometry on Performance of Airblast Atomizer Under Sub-Atmospheric Conditions. *Engineering Applications of Computational Fluid Mechanics* vol. 6, pp. 203–213 (2012)
4. Cutrone, L., Ihme, M., Herrmann, M.: Modelling of High Pressure Mixing and Combustion in Liquid Rocket Injectors. *Center for Turbulence Research*, pp. 269–281 (2006)
5. Smith J. J., Schneider G., Suslov D., Oschwald M., Haidn O.: Steady-State High Pressure LO<sub>x</sub>/H<sub>2</sub> Rocket Engine Combustion. *Aerospace Science and Technology* vol. 11, pp. 39–47 (2007)
6. Lopez-Parra, F., Turan A.: Computational Study on the Effects of Non-Periodic Flow Perturbations on the Emissions of Soot and NO<sub>x</sub> in a Confined Turbulent Methane/Air Diffusion Flame. *Combustion Science and Technology* 179 (7): 1361–1384 (2007)
7. Magnussen, B. F.: On the Structure of Turbulence and a Generalized Eddy Dissipation Concept for Chemical Reaction in Turbulent Flow. *AIAA Paper* 1981-42 (1981)
8. De la Cruz, M., Polupan, G., Martínez, E., Carvajal, I.: Estudio Numérico del Efecto de la Presión en el Proceso de Mezcla Metano-Oxígeno en un Arreglo de Chorros 4-Lug Bolt. *Información Tecnológica, CIT Chile*, vol. 26, no. 2, pp. 153–162 (2015)
9. Dagan, Y., Arad, E., Tambour Y.: On the Dynamics of Spray Flames in Turbulent Flows. In: *Proceedings of the Combustion Institute* vol. 35, issue 2, pp. 1657–1665 (2015)
10. Vicente, W., Salinas-Vázquez, M., Martínez, E., Rodríguez, A.: Numerical Simulation of a Turbulent Lean, Premixed Combustion with an Explicit Algebraic Stress Model. *J. Math. and Statistics*: 1, 86–90 (2005)
11. Lin, Z. Q., Wei, F., Jin, Y.: Numerical Simulation of Pulverized Coal Combustion and No Formation. *Chemical Engineering Science*: 58, 5161–5171 (2003)
12. Herrmann, M.: Numerical Simulation of Turbulent Bunsen Flames with a Level Set Flamelet Model. *Combustion and Flame*: 145, 357–375 (2006)
13. Shih, T.-H., Liou, W. W., Shabbir, A., Yang, Z., Zhu, J.: A New k-ε Eddy-Viscosity Model for High Reynolds Number Turbulent Flows Model Development and Validation. *Computers and Fluids* 24(3): 227–238 (1995)
14. Waterson, N.P., Deconinck, H.: A Unified Approach to the Design and Application of Bounded Higher-Order Convection Schemes. In: *Proceedings of the 9th International Conference on Numerical Methods in Laminar and Turbulent Flow*, Pineridge Press, Swansea, p. 203, Atlanta (1995)
15. Gaskell, P.H., Lau, A.K.C.: Curvature-Compensated Convective Transport: Smart, a New Boundedness-Preserving Transport Algorithm. *International Journal for Numerical Methods in Fluids*, Vol. 8, p. 617 (1988)
16. Leonard, B.P., Leschziner, M.A., McGuirk, J.: The QUICK algorithm: a uniformly 3rd-order finite-difference method for highly convective flows. In: *Numerical methods in laminar and turbulent flow: proceedings of the first international conference*, p. 807, Swansea, (1978)
17. Korlie, M.S.: Three-Dimensional Computer Simulation of Liquid Drop Evaporation. *Computers and Mathematics with Applications* 39, pp. 43–52 (2000)

# Priority Data Transmission Schemes for a Wireless Sensor Network on BAN

ISSN 1870-4069

Sergio Martínez<sup>1</sup>, Mario Rivero<sup>2</sup>, Laura Garay<sup>1</sup>, Issis Romero<sup>1</sup>

<sup>1</sup> Instituto Politécnico Nacional,  
Unidad Profesional Interdisciplinaria en Ingeniería y Tecnologías Avanzadas,  
CDMX, Mexico

<sup>2</sup> Instituto Politécnico Nacional, Centro de Investigación en Computación,  
CDMX, Mexico

smartinezc1403@alumno.ipn.mx, lgaray@ipn.mx,  
iromero@ipn.mx, mriveroa@ipn.mx

**Abstract.** Among the most recurrent Wireless Sensor Network (WSN) employment is the biopotential signals monitoring (e.g. electrocardiograms, electroencephalograms, electrogastrograms) that allows transmitting the body organ response from a person. Within the WSN's focused on bioelectrical studies, the energy analysis is essential indeed, given that sensors are devices of minimal dimensions and implies batteries tend to be small and have short-lifetime. In the present research we proposed two priority schemes to enhance the network performance by giving transmission priority to certain nodes. In a first scheme, nodes have different priorities according to the data type they are reporting on. Hence, nodes that sense more relevant data have higher priority to use the channel compared to nodes reporting less important data. For the second scheme, the aim is to prolong the system lifetime by assigning higher transmission probability to nodes with higher residual energy levels while nodes with little energy left, perform fewer transmissions. We show that the performance of the system is indeed enhanced by the introduction of such schemes.

**Keywords:** Wireless Sensor Network (WSN), Body Area Network (BAN), Cognitive Ratio (CR).

## 1 Introduction

Nowadays, the implementation of wireless and ambulatory technologies in medical applications has important relevance [1]. Take into consideration, the multiple areas joint effort to work on e-health applications, which primary goal is to increase life quality of people. Within e-health, it is required the gauge of constant signals emitted by the body. That is why tools are required that are capturing the electrical measures generated by the human being. These are known as bioelectrical studies. For biopotential signals monitoring, different solutions have emerged and an alternative relies on wireless sensor networks [2].

However, based on [3] and [4] the WSN confront an inherent conflict that intrinsically depends on batteries dimensions and capacities. In this context, batteries require an important energy performance analysis given that life-battery

is shorter than current energy systems [5]. Nevertheless, studies of network energy behavior focus either on the adaptation of protocols [6], packet size optimization [7] or materials properties analysis giving greater capacity [8]. The present research proposed to design and simulate the energy performance of a WSN focused on the study of biopotential signals.

We analyze that in practical applications two common situations are presented, in one there are sensors that have priority over others because they are giving attention to a specific body area, consequently exist nodes that have more importance than others generating the priority based scheme. In other case, there are medical applications where the aim is to extend the lifetime batteries as much as possible. This second scheme requires an analysis of the remaining battery energy giving rise to the residual energy based scheme.

## 2 System Design and Parameters Description

A wireless sensor network is a set of devices placed in a certain area capable of performing basic operations, sensing and communicate with other sensors [9]. Let both describe a bioelectrical potential as the representation of the ion flow through the cell membrane and can be measured by invasive or non-invasive nodes for nerves and muscles in the human body [10].

The proposed system is composed of a set of nodes in sensors that measure bioelectrical signals assuming that all are placed in the body of a single person. The intercommunication distance responds to less than 3.28 ft, thus the sensors work on a body area network (BAN) [5] with e-health application. The system is designed considering that any biopotential study cited in the table bellow can be transmitted.

**Table 1.** Most used bioelectrical studies [11].

| Study | Description   | Voltage        | Frequency(Hz) |
|-------|---|----------------|---------------|
| ECG   | <b>Electrocardiogram.</b> Representation of heart electrical signals                                  | 0.5–4 mV       | 0.01–250 Hz   |
| EEG   | <b>Electroencephalogram.</b> Depiction of electrical signals produced by the brain.                   | 5–300 $\mu$ V  | 150 Hz DC     |
| EGG   | <b>Electrogastrogram.</b> It is the representation of the electrical signals produced by the stomach. | 10 $\mu$ V–1mV | 1 Hz DC       |
| EMG   | <b>Electromyogram.</b> Measures the electrical activity of muscles.                                   | 0.1–5 mV       | 10 KHz        |

### 2.1 Communication Parameters

The following describes the general properties of the communication scheme used in the network:

- The communication scheme or protocol is TDMA since it requires a minimum hardware-software processing for its implementation and considers a deterministic system assuring the information transmission of each node in its respective slot.
- A hybrid network is understood in this project when it is used two different kinds of networks. The primary network consists of sensors that transmit continuously. On the other hand, the secondary network will transmit sporadically (i.e. event monitoring) [12].

- The cognitive radio in the communication system network design is presented in the inclusion of on/off processes that represent a method of modeling traffic in stationary communications networks. To consider on/off processes, the following premises must be considered:
  - The nodes of the continuous monitoring network (primary network) will be on for a specific period called time on.
  - There will also be time periods for primary network nodes where they will be 'turned off'. In this sense, these periods are known as time off. When primary network has some turned off node, the respective slot will be free to transmit information that is generated from secondary network nodes. It is very important to indicate that the sensors work all the time and implies energy consumption at any time.

The communication protocol has as reference the work done in [12] and [13] where both focus on epilepsy, however at the present design is open to any biopotential study cited in Table 1.

### 3 Energy Analysis

There is clearly a great compromise between the information amount tolerance that can be lost from continuous monitoring and the energy consumption reduction. We estimate results for knowing in detail the network behavior and to carefully analyze this dependence. We consider  $M$  as the number of slots for each frame.

To specify the quantitative analyzes, it is considered to evaluate the data in specific values. Let the primary network be an electroencephalogram composed of a set of 22 nodes. The secondary network will be monitoring a 4-channel electrogastrogram. Thus:  $M = 22$  nodes and  $n_e = 4$  event monitoring nodes (secondary network nodes).

#### 3.1 Energy Consumption And Packet Loss For WSN

In the primary network there are in total  $M$  nodes and the information will be transmitted continuously. In this case, it is remembered that it is a deterministic protocol so that each of the nodes of the electroencephalogram has a reserved slot to transmit. However, when the on/off processes are included, there is a change in the energy consumption derived from the on and off times. Therefore, the energy in the primary network is analyzed through two cases:

- Case 1. The node is active. The node is on (i.e. slot is related to an on time) and the usual energy transmission is taken. This energy will be evaluated by  $E_{[tx]}$  referring to the unit of energy consumption per packet transmission.
- Case 2. The node is in sleep mode. It refers to the node being switched off and therefore not transmitting EEG information. However, when the sensor is on (even if not send data), a certain amount of energy is being used which is much smaller than the active node. The energy is determined by:

$$E_s = 0.1E_{[tx]}, \quad (1)$$

where

$E_s$  = Sleep node energy consumption,  
ISSN 1870-4069

$E_{[ts]}$  = Active node energy consumption.  
*Sergio Martínez, Mario Rivero, Laura Garay, Issis Romero*

The WSN performance is evaluated by variables  $E_{[ts]}$  (for energy consumption) and Packets (for system loss). In both cases, there is a probability that the packet has been successfully transmitted. This is defined as the probability of successful packet transmission.

The secondary network is based on the  $n_e$  nodes occupied. In numerical terms, for this analysis are four. In order to be able to relate the energy used by the primary network.

However, the applications of bioelectrical studies are variable, depending on the medical requirement, the analysis must be adapted. On the one hand, we have the circumstance where the study has a set of nodes that monitor a specific area. Consequently, the priority of some sensors is greater than the rest. In this way, the communication and analysis scheme focuses on the priority that each sensor has.

In the other hand, there is a primordial interest on the network energy optimization. In that case, it is much more convenient to modify the perspective so that the analysis is applied on the lifetime of the batteries and their respective residual energy.

### 3.2 Priority Based Scheme Model

There are scenarios where one sensor has more importance than the others. For example, in an EGG, there is an area with greater gastric movement and takes precedence over the rest. For this case, the first scheme based on priorities is proposed.

This scheme considers an amount of  $M$  continuous monitoring nodes and  $n_e$  event-monitoring. In each frame, on and off time will be generated. When some node in the primary network is off, then secondary network information can be transmitted through one of the four nodes that monitor the stomach. Each of these nodes will have an assigned priority. Only two priorities are presented: high or low. To differentiate them, each of them will have an assigned transmission probability, the one of high priority will be greater than the others. Therefore, it is proposed: Transmission probability of high priority node = 0.85 and Transmission probability of low priority node = 0.25.

Each node will have its own transmission probability determined by its respective priority, so  $\rho_i$  represents the probability of transmission of an  $i$ -event monitoring node. Based on the above, there will be three possible cases:

- 1 . One high priority node and three low priority nodes ( $\rho_0 = 0.85, \rho_1 = 0.25, \rho_2 = 0.25$  and  $\rho_3 = 0.25$ )
- 2 . Two high priority nodes and two low priority nodes ( $\rho_0 = 0.85, \rho_1 = 0.85, \rho_2 = 0.25$  and  $\rho_3 = 0.25$ )
- 3 . Three high priority nodes and only one low priority node ( $\rho_0 = 0.85, \rho_1 = 0.85, \rho_2 = 0.85$  and  $\rho_3 = 0.25$ )

It is necessary to indicate that the transmission probability of high or low priority is independent of the probability of successful transmission of the packet ( $\epsilon$ ).

### 3.3 Residual Energy Based Scheme Model

*Priority Data Transmission Schemes for a Wireless Sensor Network on BAN*

When nodes that are monitoring are equally important, all nodes can transmit with the same priority. However, depending on the case, there are sensors that monitor much more than others, so the battery-lifetime of these becomes shorter. In other words, its efficiency and probability of sending the data will depend on how much energy is available from the battery. In this way the residual energy scheme is proposed. This second scheme shares the same basis as the priority scheme, it has a primary network of  $M$  nodes and a secondary network composed of  $n_e$  nodes. In this case, we will consider a transmission probability dependent of the energy still holding the battery for each sensors. This is called residual energy and is directly related to the probability of transmission of each of the event-monitoring node.

$$\rho_i = \gamma e^{-\gamma E_0/E_R} \quad (2)$$

where  $\rho_i$  = transmission probability for i-node,  $\gamma$  = Battery decay factor,  $E_0$  = Initial battery energy,  $E_R$  = Residual battery energy

It is again emphasized that the probability of transmission by residual energy is independent of the probability of successful transmission ( $\epsilon$ ).

## 4 WSN Performance Simulations And Results

The network performance was applied by discrete event simulations. The results will be display for the primary and secondary network divided into the two proposed schemes (by priority and by residual energy). The scale for energy consumption depends on lifetime battery of  $1 * 10^9 E_{[ts]}$ .

All the graphs shown below are determined by the variables:  $P_{ON}$  which represents the on time probability per frame and  $\epsilon$  which indicates the probability that an event is successfully transmitted.

### 4.1 Priority Based Scheme Model

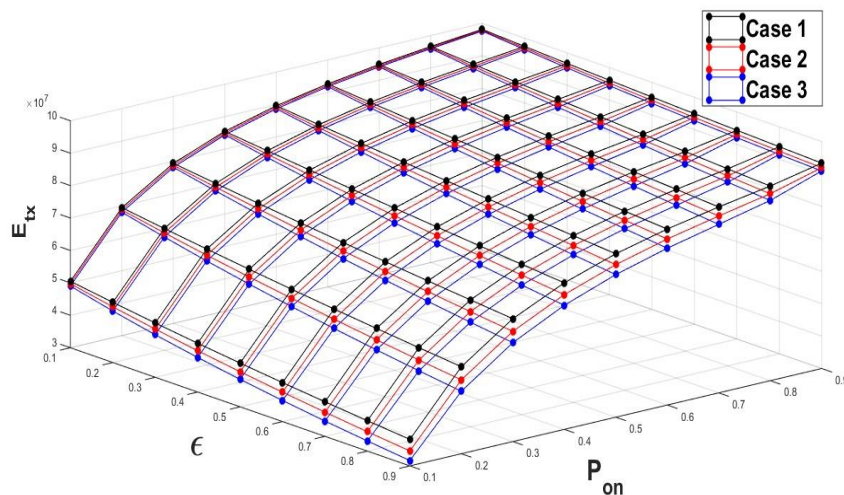


**Fig.1.** Primary Network Energy consumption (active nodes).

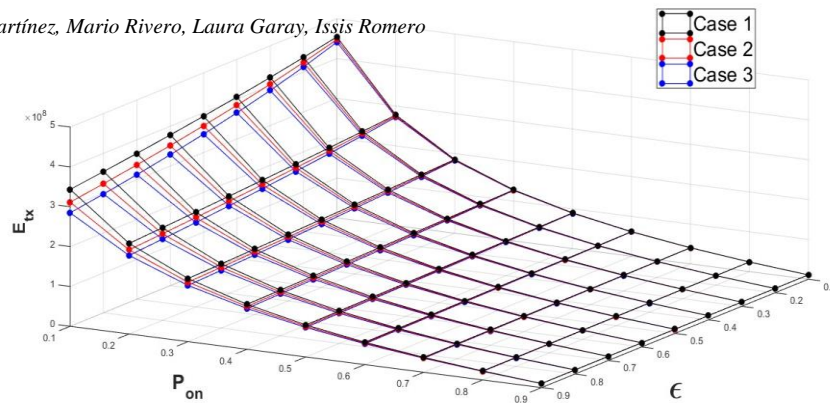


**Fig.2.** Primary Network Energy consumption (sleep mode nodes).

In these first figures it is possible to show the behavior of the primary network respect to the energy consumption for active and sleep nodes. These graphs show the three possible cases identified in section 3.2. Specifically, it can be considered that as the on time probability increases, the amount of energy consumption increases. It can also be denoted that for the minimum turned-on time and a maximum probability of successful packet transmission, the scheme that has three high priority nodes and one low one presents the least amount of energy consumed. It is important to remind that Case 1:  $\rho_0 = 0.85$ ,  $\rho_1 = 0.25$ ,  $\rho_2 = 0.25$  and  $\rho_3 = 0.25$ , Case 2:  $\rho_0 = 0.85$ ,  $\rho_1 = 0.85$ ,  $\rho_2 = 0.25$  and  $\rho_3 = 0.25$  and Case 3:  $\rho_0 = 0.85$ ,  $\rho_1 = 0.85$ ,  $\rho_2 = 0.85$  and  $\rho_3 = 0.25$

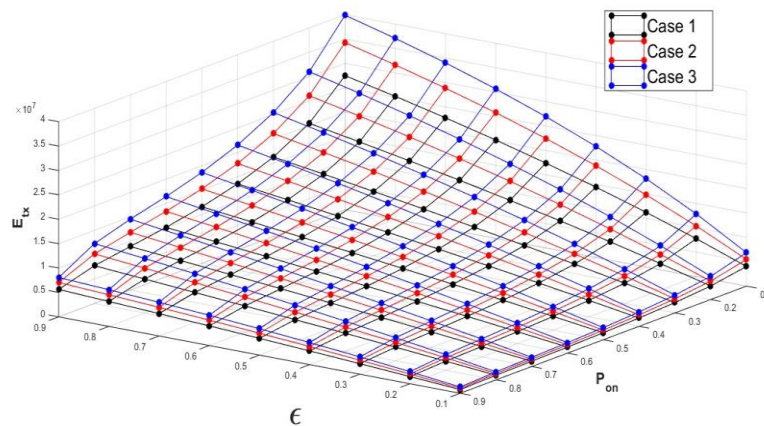


**Fig.3.** Secondary Network Total Energy Consumption.

For the secondary network it can be seen that the system has a maximum energy consumption when the on time is very low and the probability of successful transmission is high. Although within the three cases, the scheme of three high priority and one low node is the one that requires the maximum energy consumption, so this scheme is not optimum when there is a large amount of monitoring per event.

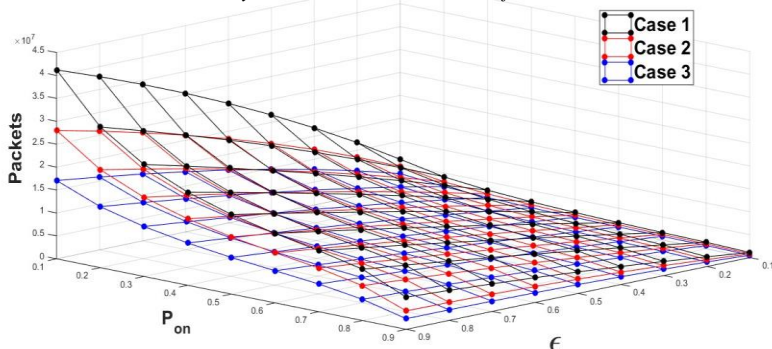


Fig.4. Network Packet Loss (non reported packets).

In the subsequent figure, it can be seen the loss of packets due to a lack of reporting (i.e., not falling into the probability of transmission by priority, they are not transmitted.) In this sense, it can be denoted that the maximum number of lost packets are when there is only one high priority sensor.

#### 4.2 Residual Energy Based Scheme

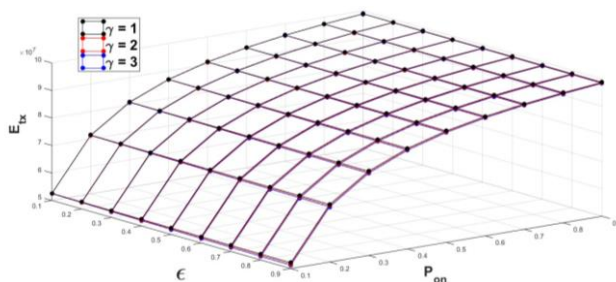


Fig.5. Primary Network Energy consumption (active nodes).

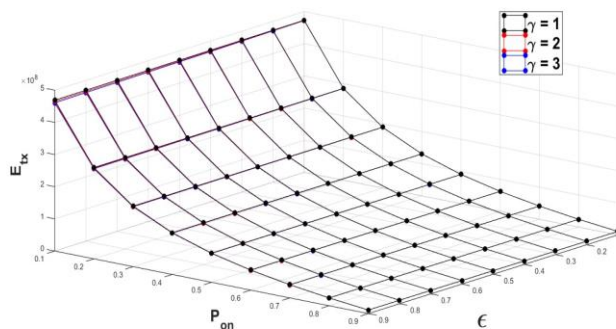
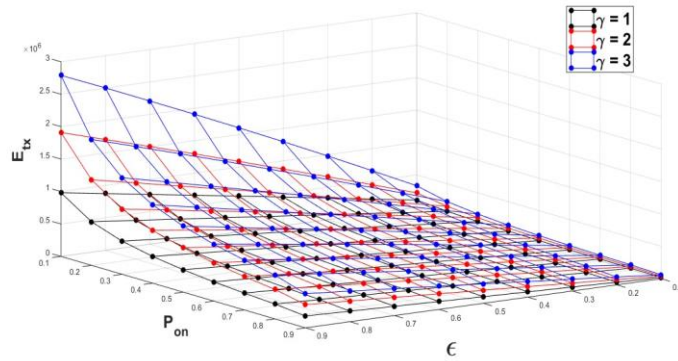


Fig.6. Primary Network Energy consumption (sleep mode nodes).

In these figures we present a behavior quite similar to the system by priorities, where at greater on time probability, successful transmission of more packets is shown and the energy used in active nodes is greater. However, unlike the priority scheme, the energy consumption for this network is lower.



**Fig.7.** Secondary Network Total Energy Consumption.

The secondary network in this case shows a considerable difference with respect to the decay factor of the battery, where the higher the factor, the higher the energy consumption obtained by the secondary network.

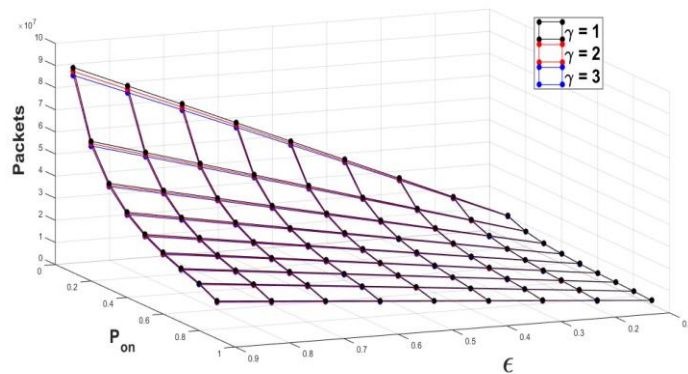


**Fig.8.** Network Packet Loss (non reported packets).

Regarding the loss of packets, it can be denoted that the behavior for the different battery decay factor is practically the same, where the greatest loss occurs when there is the maximum information transmission request and the minimum amount of on time probability. It should be considered that the packet loss here involves the packets of the primary network.

## 5 Conclusions

In the present research a WSN focused on biopotential studies was proposed that works with TDMA deterministic protocol and uses cognitive radio through on/off

processes to reduce the number of slots used on each frame. Energy performance was evaluated through two schemes: priority based scheme where sensors have different importance (some body parts are more important than the others) and residual energy scheme where the aim is to decrease the battery energy consumption. The network is represented by discrete event simulations.

Therefore, a priority scheme can be considered to generate lower energy consumption in the primary network, more variable consumption in the secondary network but more losses than the residual energy scheme. If the application requires few monitoring per event, it is advisable to use a scheme based on priorities, otherwise the residual energy scheme is recommended.

## References

1. Nakajima, T.: Aspects of Information Communications Technology for Better Medical Control, International Journal of E-Health and Medical Communications (IJEHMC), 1, 18–27, (2010)
2. Mahmoudi, R., Inieviski, K.: Low power emerging wireless technologies, 2, CRC Press, (2012)
3. Dargie, W., Poellabauer, C.: Fundamentals of Wireless Sensor Network. Chichester: John Wiley & sons Ltd, p. 34, (2010)
4. Castillejo, P., Martínez, J., Rodríguez, M.: Integration of wearable Devices in a wireless sensor network for an e-health application. Institute of Electrical and Electronics Engineers, 13, 38–49 (2013)
5. Shaikh, A., Pathan, S.: Research on Wireless Sensor Network Technology. International Journal of Information and Education Technology, 2, 476–479 (2012)
6. Chatzigiannakis, I., Kinalis, A., Nikolettseas, S.: Wireless sensor networks protocols for efficient collision avoidance in multi-path data propagation. In: Proceedings of the 1st ACM international workshop on Performance evaluation of wireless ad hoc, sensor, and ubiquitous networks (PE-WASUN '04), ACM, 8–16 (2004)
7. Sankarasubramaniam, Y., Akyildiz, I., McLaughlin, S.: Energy Efficiency Based Packet Size Optimization. In: Wireless Sensor Networks IEEE International Workshop on Sensor Network Protocols and Applications, 1–8 (2003)
8. Rodriguez, J.: Digital Advances in Medicine, E-health, and communication technologies. Digital: IGI Global, p. 12 (2013)
9. Dargie, W., Poellabauer, C.: Fundamentals of Wireless Sensor Network. John Wiley & sons Ltd: Chichester, p. 24 (2010)
10. Ganong, W.: Review of Medical Physiology. McGrawHill: New York, p. 576 (2005)
11. Enderle, J., Blanchard, S., Bronzino, J.: Introduction to biomedical engineering. Elsevier academic press: California, p. 323 (2004)
12. Martinez, S., Rivero, M., Garay, L.: Design of hybrid wireless sensor network to monitor bioelectric signals focused on the study of epilepsy. Research in Computing Science, 75, 43–49 (2014)
13. Martinez, S., Rivero, M., Garay, L.: Performance Analysis of Preemptive and Non-Preemptive Schemes in Hybrid Wireless Sensor Networks focused on the study of epilepsy. Research in Computing Science, 101, 29–42 (2015)



## Modelo foveal rectangular a partir de un sensor de imagen comercial

José Antonio Loaiza Brito, Luis Niño de Rivera y Oyarzábal

Instituto Politécnico Nacional, Sección de Estudios de Posgrado e Investigación,  
ESIME Culhuacan, México

jloaiza@ipn.mx, luisnino@rivera@gmail.com

**Resumen.** Este trabajo propone la implementación del modelo foveal tipo rectangular a la imagen generada en un sensor convencional. La principal problemática en los sensores foveales basados en el modelo log polar es que cada fotosensor está diseñado con geometrías y tamaños diferentes. Los sensores convencionales tienen una distribución de M por N píxeles en un arreglo rectangular, en tanto que en los modelos foveales, los elementos de imagen se encuentran distribuidos en círculos concéntricos. El diseño de cada sensor debe ser específico de acuerdo a la aplicación que se requiera. Esto ocasiona una limitación en el desarrollo de sistemas con distintas configuraciones de retinas, debido a que es necesario cambiar los diseños para diferentes aplicaciones con el respectivo análisis. La propuesta consiste en una nueva estrategia para generar una imagen foveal desde un sensor de imagen convencional, que utiliza un algoritmo de transformación log polar en un modelo rectangular, donde se promedian los valores de los elementos fotosensores vecinos en una regla de crecimiento geométrico. Los resultados muestran las imágenes obtenidas desde un sensor de imagen comercial, aplicando el algoritmo de transformación log polar a un esquema de rectángulos circunscritos con crecimiento geométrico.

**Palabras clave:** modelo foveal, modelo log polar, sensor de imagen, visión foveal.

### Foveal Rectangular Model from a Commercial Image Sensor

**Abstract.** This work proposes the implementation of the rectangular model foveal to the image generated in a conventional sensor. The main problem in foveal sensors based on the log polar model is that each photosensor is designed with different geometries and sizes. Conventional sensors have a distribution of M by N pixels in a rectangular array, whereas in foveal models, the elements of image are distributed in concentric circles. The design of each sensor must be specific according to the application that is required. This causes a limitation in the development of systems with different configurations of retinas, because it is necessary to change the designs for different applications with the respective

analysis. The proposal consists of a new strategy to generate a foveal image from a conventional image sensor, which uses a log polar transformation algorithm in a rectangular model, where the values of the neighboring photo-sensor elements are averaged in a geometric growth rule. The results show the images obtained from a commercial image sensor, applying the log polar transformation algorithm to a scheme of circumscribed rectangles with geometric growth.

**Keywords:** foveal model, log polar model, image sensor, foveal vision.

## 1. Introducción

El modelo foveal está inspirado en los sistemas de visión de los animales debido a que se trata de emular el comportamiento de la retina biológica, basándose en la distribución geométrica de las células fotorreceptoras en humanos o animales [1,2,3]. En la retina biológica se tiene la mayoría de los fotorreceptores concentrados en la zona foveal y disminuyen en número en dirección a la periferia [4,5,6]. Esta organización de los fotorreceptores tiene propiedades significativas debido a la variación en la resolución en el campo visual. A esto se le conoce como *visión espacio-variante* [5,7]. Existen numerosos estudios en que han desarrollado sensores con estructuras foveales, destacando la tecnología CMOS debido a sus capacidades y calidad en resolución [6,7,8]. Sin embargo, el diseño y fabricación de este tipo de sensores aún tienen problemas que deben ser resueltos.

Aunque algunos autores han sugerido una aplicación ingeniosa en VLSI, éstas aún requieren un proceso de fabricación no estándar [7,8]. Pardo et al. presentaron el diseño de un sensor foveal CMOS utilizando ajustes en la geometría de cada fotosensor de acuerdo a la ubicación desde el centro hasta la periferia, utilizando una rotación de ejes, los cuales, van creciendo en tamaño en los diferentes niveles de la fovea para producir corrientes fotogeneradas proporcionales al área de incidencia [7,8,9]. Sin embargo, ésta se debe compensar debido al crecimiento de los sensores. Nuevas soluciones se encuentran en la literatura especializada que proponen la construcción de elementos de detección de tipo logarítmico para compensar dichos problemas [4,5,7,8].

F. Pardo, B. Dierickx, D. Schaffer, F Paillet y P. Zeferino analizaron en detalle el procedimiento de diseño de una celda básica para un fotodiodo con tecnología CMOS [7,8,9,10]. El Patrón de Ruido (FPN), debido al factor de escala en la fabricación y los efectos de canal angosto, es un gran reto que todavía no está resuelto. Pardo et al. proponen reducir el FNP generado por la escala de diseño, utilizando una estructura cartesiana de píxeles para la región de mayor resolución y posteriormente una transformación log polar en la región periférica. P. Pardo muestra una transformación de ejes cartesianos para rotar los polígonos [7]; sin embargo, al momento de realizar el diseño de todo el sensor, es necesario construir un modelo de anillos concéntricos con un factor de escalamiento geométrico. Es por ello que sería necesario rotar la célula básica y escalarla, (figura 1). El modelo foveal representa la base de los sistemas de visión foveal; sin embargo, el problema principal para poder llevar diversos análisis de estructuras foveales, representa el inconveniente de su fabricación.

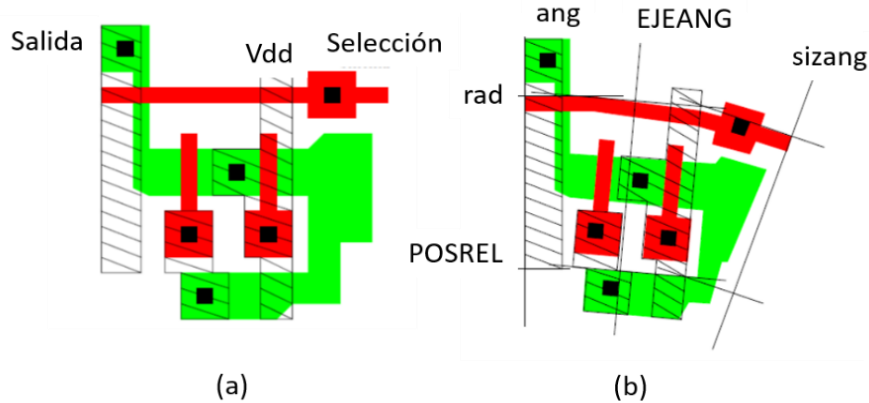


**Fig. 1.** Diseño de una celda básica de fotodetección. a) Celda original con sus líneas de acceso. b) Rotación establecida para el campo receptivo, en la que se muestran los ejes modificados [7].

## 2. El modelo foveal

El modelo foveal es una transformación matemática de una imagen desde un plano polar a un plano rectangular a través de un mapeo logarítmico y luego regresarla para su interpretación. La representación log-polar [7,8,11,12,13] es el mapeo de puntos del plano polar o también llamado plano retínico  $(\rho, \eta)$  a un plano complejo logarítmico, nombrado plano cortical  $(\xi, \gamma)$ .

De acuerdo con [11,14], la imagen foveal es, en resumen, una representación en un plano discreto de la transformación log-polar. Esto es, una imagen es representada en coordenadas rectangulares de acuerdo con:

$$z = x + jy, \quad (1)$$

$$z = \rho e^{j\eta}, \quad (2)$$

donde:

$$\rho = \sqrt{x^2 + y^2}, \quad (3)$$

$$\eta = \tan^{-1}\left(\frac{y}{x}\right). \quad (4)$$

Por lo que las coordenadas  $x$ ,  $y$  se pueden expresar como:

$$x = \rho \cos(\eta), \quad (5)$$

$$y = \rho \sin(\eta). \quad (6)$$

Lo anterior representa la ubicación de un elemento de imagen en el plano rectangular. Cualquier pixel queda perfectamente ubicado bajo estas coordenadas. De la investigación de Volker Krüger, una imagen cortical quedaría representada a través de un mapeo al plano logarítmico complejo por la siguiente regla de correspondencia:

$$w = \ln(\rho e^{j\eta}). \quad (7)$$

El origen del plano x-y no se puede mapear por la singularidad presentada en  $\rho=0$ . Por lo que es necesario definir un intervalo muy cercano al origen de la imagen. La representación de la imagen tiene un crecimiento geométrico o exponencial, por lo que se utiliza un logaritmo arbitrario de base “a” [14]. Así, para el mismo punto de imagen z:

$$z = \rho a^{j\eta}. \quad (8)$$

La base “a” es la contraparte del *factor de magnificación cortical*. Entonces:

$$w = \log_a(\rho) + j\eta. \quad (9)$$

Para realizar el proceso de visión por computadora o utilizar un procesador digital, los componentes radiales y angulares deberán ser digitalizados. Por ello se consideran las siguientes coordenadas:  $\xi$  = Componente radial,  $\gamma$  = Componente angular.

Las variables  $N_r$  y  $N_a$  definen la resolución máxima radial y angular del plano log polar, respectivamente. El mapeo de las coordenadas polares ( $\rho, \eta$ ) a las coordenadas ( $\gamma, \xi$ ) en el plano log polar, está dada por [14]:

$$\xi = \log_a\left(\frac{\rho}{\rho_0}\right), \quad (10)$$

$$\gamma = \frac{N_a}{2\pi}\left(\eta + \frac{\pi}{2}\right). \quad (11)$$

La figura 2 muestra una representación de la transformación con las coordenadas de (10) y (11). El plano cortical aún sigue siendo un plano rectangular en donde queda representada la imagen en coordenadas logarítmicas. Para obtener la representación foveal de dicha imagen, es necesario obtener la transformación inversa, que es en realidad, la transformación log polar. Las coordenadas se definen como:

$$x = \rho_0 a^{\xi} \text{Cos}(\eta), \quad (12)$$

$$y = \rho_0 a^{\xi} \text{Sen}(\eta), \quad (13)$$

donde los valores de las coordenadas quedan en un intervalo de  $0 \leq \xi \leq N_r, 0 \leq \gamma \leq N_a$ . De igual manera, en [13,14], se establece lo siguiente:

$$\rho_0 a^{N_r} = \rho_{max}, \quad (14)$$

donde es posible observar que el tamaño de la imagen transformada queda relacionado por el factor “a”. La forma de la ecuación es una función de crecimiento geométrico.

### 3. Metodología

En este trabajo se discute la manera de utilizar la transformación log polar para generar un modelo rectangular e implementarlo desde un sensor de imagen comercial.

Así, cualquier elemento de fotodetección queda especificado por un pixel, llamado *celda básica*, (figura 2). La propuesta consiste en realizar agrupaciones de celdas básicas para hacer crecer zonas de incidencia hacia la periferia. La distribución en un plano polar (figura 2a.) queda determinada por medio de campos receptivos. Así, al colocar agrupaciones de celdas básicas, éstas pueden cubrir áreas completas si se realiza una distribución rectangular o cuadros concéntricos. Los campos receptivos se presentan como rectángulos con crecimiento geométrico.

Una primera evaluación consiste en superponer el conjunto de celdas rectangulares sobre la estructura polar, generando diferentes zonas blancas sobre el plano polar. Sin embargo, las zonas blancas decrecen cuando se trata de rectángulos concéntricos. Este nuevo enfoque reduce las zonas blancas y produce una mejor distribución sobre el diseño.

Las trayectorias rectas concéntricas en la figura 2-b se mueven gradualmente hacia la periferia siguiendo el modelo log polar conocido. Lo relevante es que la ubicación de cada celda básica sigue las ecuaciones (12) y (13) haciendo posible reorganizar los pixeles de una imagen en una nueva estructura foveal, pero rectangular. Esta agrupación respeta el modelo espacio-variante del sensor foveal estudiado. El ajuste se realiza utilizando asociaciones de elementos de imagen siguiendo una función polinomial:

$$f(k) = b^k, \quad (15)$$

donde “b” es la base en la que se trabaja la serie y “k” equivale al número de capas o niveles en los que dividirá la imagen foveal.

En esta propuesta, se establece la base 2, debido a que las asociaciones serán en grupos de dos, cuatro o más celdas básicas, como se puede observar en la figura 2-b.

Este nuevo modelo es equivalente al modelo log polar convencional, ya que las trayectorias se extienden por la misma ley de crecimiento geométrico de los círculos de la estructura espacio-variante. Es importante mencionar que la ley de crecimiento de las celdas que componen cada rectángulo circunscrito en la nueva distribución foveal está controlada por el Factor de Crecimiento S.

De acuerdo con (14) y (15), se propone que, el elemento de imagen más pequeño se designa como  $W_0$ , el cual tiene un crecimiento geométrico rectangular con un factor de crecimiento S. El tamaño del i-ésimo elemento de imagen está dado por:

$$W_i = S^i W_0. \quad (16)$$

Por lo que el tamaño semi radial del sensor será:

$$rd = \sum_{i=0}^N W_i, \quad (17)$$

$$rd = W_0 \left( \frac{S^{N+1}-1}{S-1} \right), \quad (18)$$

donde N es el número de capas del modelo foveal. Sin embargo, si se toma como centro el elemento mínimo de imagen, se presentará una singularidad (cuando S=1). Es por ello, que se deberá tomar lo siguiente:

$$rd_{max} = rd_0 + W_0 \left( \frac{S^N+S-2}{S-1} \right), \quad (19)$$

$rd_{max}$  queda determinado por la suma del radio del elemento mínimo de imagen ubicado en el centro más el radio ( $rd$ ) de todo el sensor. Cada elemento rectangular de tamaño  $W_i$  queda representado en el plano rectangular, como se observa en la figura 3.

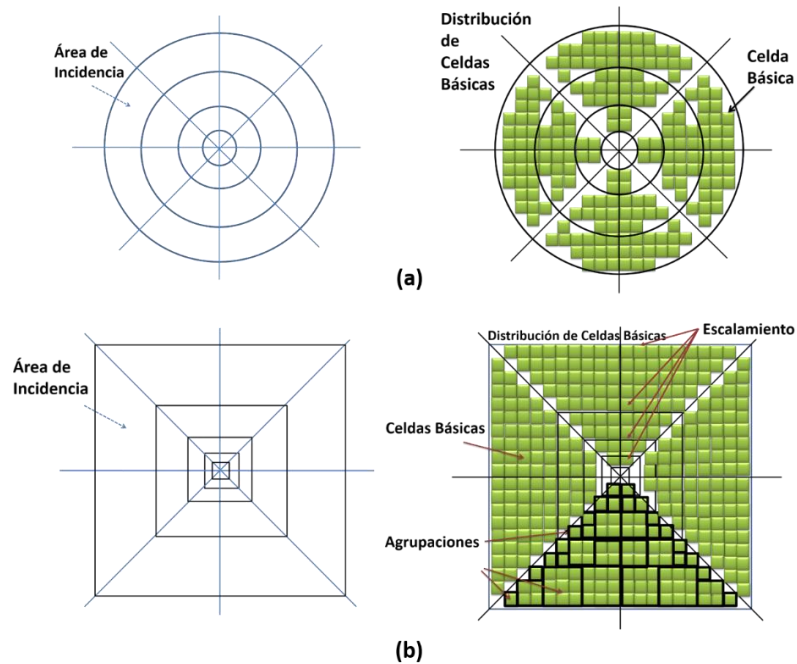


**Fig. 2.** Correspondencia entre un modelo de círculos concéntricos y uno rectangular. En (a) se muestra la distribución de celdas básicas en los diferentes anillos. En (b) se puede observar una propuesta de distribución de celdas en un formato rectangular basado en agrupaciones de acuerdo al área de incidencia.

La magnitud de  $W_0$  tiene valores reales positivos que dependen de la tecnología de fabricación para el fotodetector o simplemente adquieren valores enteros positivos cuando se trata de una imagen en píxeles. El crecimiento geométrico de los elementos de imagen, sirve de base para la transformación de la imagen original en un modelo polar, visto desde un plano rectangular.

Una vez definida la celda básica, es posible generar toda la retina y la fóvea en una matriz concéntrica rectangular distribuyendo los píxeles. Los fotorreceptores están representados con cuadros distribuidos en polígonos concéntricos alrededor del centro del sensor cuya separación aumenta de forma exponencial. Lo anterior posibilita que cualquier circuito de fotodetección sea una celda básica, evitando una rotación de ejes en el diseño de la estructura.

La figura 4 representa la forma de agrupar los elementos de imagen para llevar a cabo la distribución foveal de la imagen. La selección de filas y columnas es necesaria al tratarse de un arreglo matricial; sin embargo, la línea de selección de “anillo” es fundamental

para seleccionar un contorno cuadrado similar a los anillos o circunferencias en una representación polar.

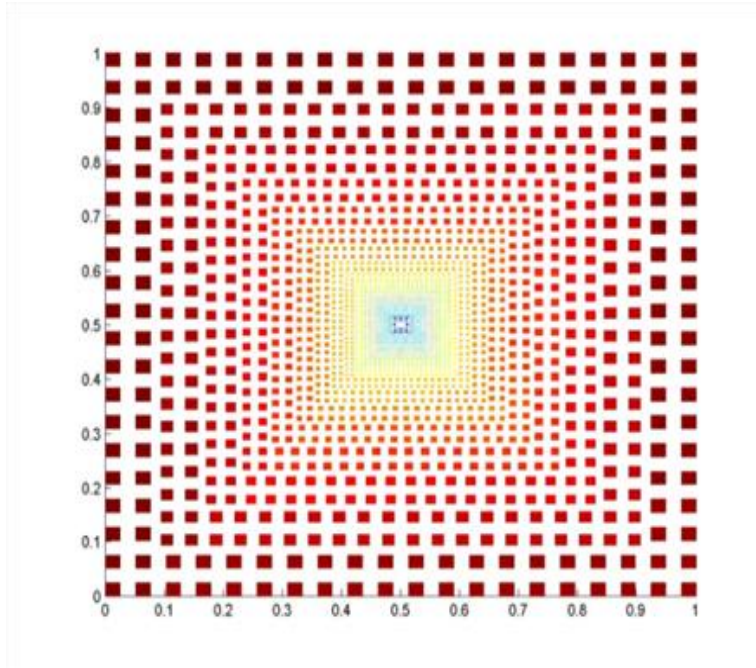


**Fig. 3.** Representación de la transformación por agrupación de celdas utilizando el modelo rectangular.

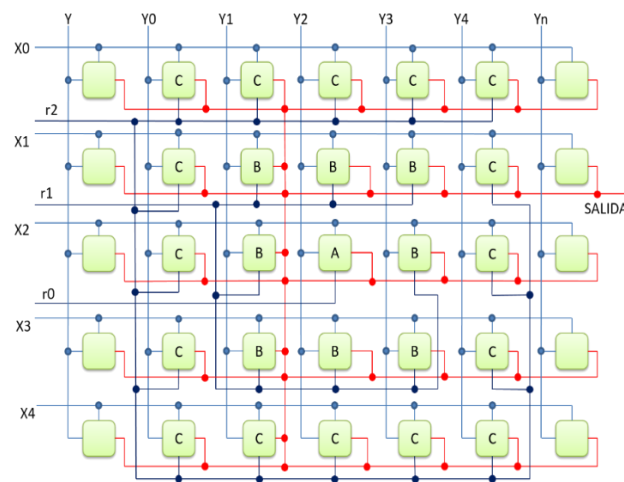


**Fig. 4.** Estructura del modelo foveal rectangular donde las coordenadas X, Y son para seleccionar cada pixel. La variable r representa la manera con la cual se agrupan los elementos de imagen.

El modelo conecta celdas básicas formando un contorno. Por ejemplo, la celda básica central es individual y se selecciona mediante las líneas  $(r_0, X_2, Y_2)$ . El contorno siguiente puede seleccionarse mediante  $(r_1, X_1-X_2-X_3, Y_1-Y_2-Y_3)$ , lo anterior significa que se pueden generar las siguientes coordenadas para seleccionar cada una de las celdas  $(r_1, X_1, Y_1)$ ,  $(r_1, X_2, Y_1)$ ,  $(r_1, X_3, Y_1)$ , etc. Para el siguiente contorno, se realiza de la misma manera  $(r_2, X_0-X_1-X_2-X_3-X_4, Y_0-Y_1-Y_2-Y_3-Y_4)$ .

#### 4. Resultados

El modelo propuesto presenta que es posible realizar agrupaciones de celdas con el objeto de tener áreas de incidencia mayores sin modificar el tamaño del pixel. La salida será la suma de las corrientes fotogeneradas o del valor promedio de los pixeles en las celdas agrupadas. De acuerdo con (18) y (19) y considerando el elemento mínimo igual 1 y 480 como el máximo, se obtienen los valores correspondientes al Factor de Crecimiento S, (figura 5).

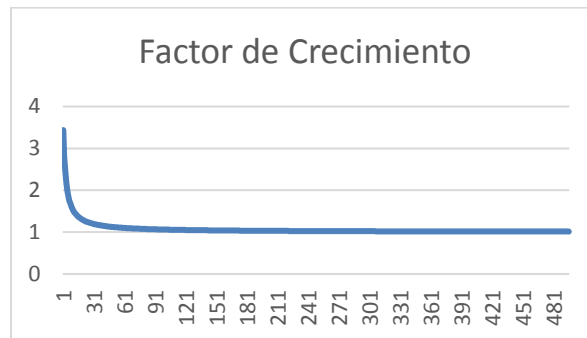


Fig. 5. Gráfica del número de capas (resolución en pixeles) contra el factor de crecimiento (escalamiento).

Al aproximarse a los 480 pixeles el factor de crecimiento varía muy poco. Aplicando el procedimiento a las imágenes de prueba es posible obtener una imagen foveal como se muestra en la figura 6.

El valor de  $N=240$  se toma como un valor máximo de acuerdo a la resolución de la imagen original que es de 480 pixeles. Las figuras en 6(a) son imágenes tomadas por un sensor de imagen comercial OV7670 con una resolución de  $640 \times 480$  pixeles. Desarrollando el procedimiento de transformación foveal rectangular (figura 3 y 4), es posible observar que se mantiene una alta resolución en el centro de la imagen y que decrece hacia la periferia.

El cuadro blanco en el centro de la imagen se debe a que se consideró como el elemento más pequeño a un grupo de pixeles para conformar la fovea; sin embargo, eso no es necesario ya que es completamente viable considerar a un pixel como el elemento

básico de imagen. Lo anterior se puede observar en la primera figura foveal, en la que el cubo tiene un intervalo de área central de píxeles.

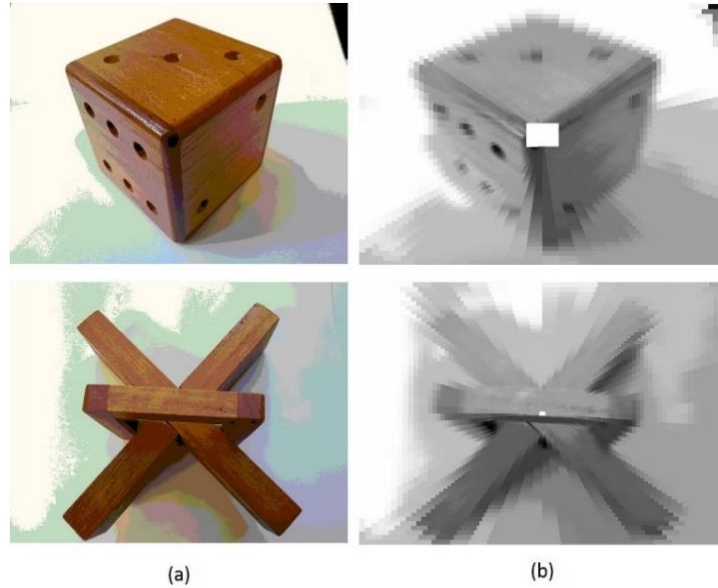


**Fig. 6.** Transformación Foveal Rectangular. a) Imágenes originales tomadas del sensor comercial. b) Imágenes que han sido transformadas siguiendo la estructura de la figura 4.

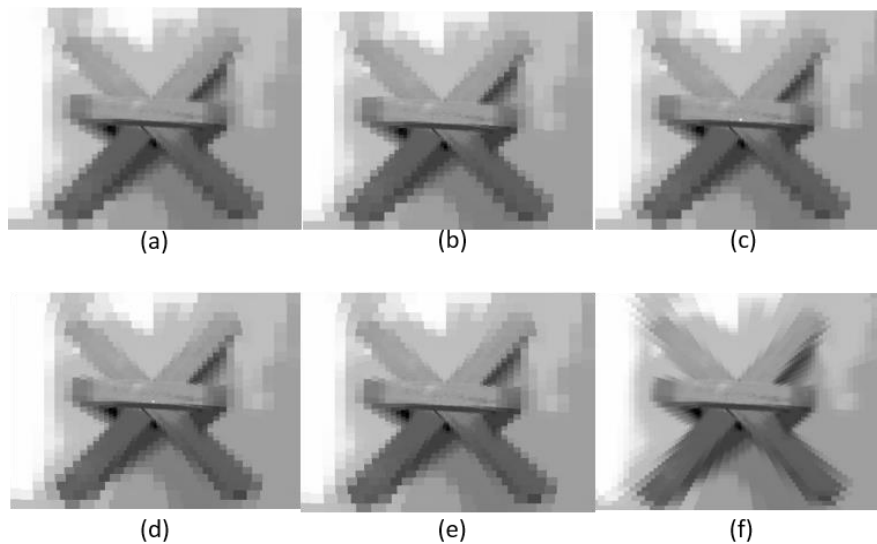


**Fig. 7.** Conversión foveal rectangular con una imagen tomada desde el sensor OV7670 con una resolución de 640x480 píxeles. (a)  $S=10$ ,  $N=120$ . (b)  $S=10$ ,  $N=240$ . (c)  $S=50$ ,  $N=120$ . (d)  $S=50$ ,  $N=240$ . (e)  $S=100$ ,  $N=120$ . (f)  $S=100$ ,  $N=240$ .

El valor se toma considerando un píxel a la derecha e izquierda de un punto central. De igual manera, un píxel superior e inferior. Debido al escalamiento, esto se ve reflejado en un cuadro blando notorio en el centro de la imagen. Para la imagen inferior, solo se tomó un píxel como intervalo central. Nótese que el área blanca se encuentra reducida.

Las imágenes de la figura 7, muestran el efecto con diferentes valores de  $S$  y un valor constante del número de capas en 120 y 240.

## **5. Conclusiones**

Los resultados muestran que la estructura propuesta basada en fotosensores rectangulares funciona correctamente para implementar sensores de visión foveal a partir de estructuras de sensores convencionales. Este nuevo enfoque de los sensores foveales preserva las propiedades de la transformada log polar. Además, es posible trabajar con diseños VLSI convencionales y sin requisitos previos de fabricación de sensores estándar. Por el contrario, los chips foveales (que son de fabricación no estándar) son una de las razones que han dificultado la aplicación en la visión foveal. Este modelo puede aplicarse a nuevos chips foveales dedicados basados en fotodiodos, fototransductores CMOS convencionales o fototransistores.

La celda básica puede ser cualquiera que haya sido empleada en diferentes modelos retinales, estableciendo un modelo foveal ortogonal con cuadros concéntricos y agrupación de elementos de imagen del mismo tipo sin realizar ninguna transformación de ejes. El punto clave es asegurar que esas estructuras sean capaces de tener un acceso independiente a cada píxel a través de una lógica de control apropiada.

La transformación log polar a través de software dedicado ha visto una aplicación limitada debido a los tiempos de transformación y procesamiento impuestos por la lógica de programación. El modo de transformación propuesto en este artículo, que utiliza un espacio variable rectangular, permite realizar la transformación foveal directamente sin llevar a cabo una transformación previa cortical y así obtener de forma directa una reducción en la cantidad de información que podrá ser procesada posteriormente.

## **Referencias**

1. Palanker, D., Vankov, A., Huie, P., Baccus, S.: Design of a high resolution optoelectronic retinal prosthesis. Department of Ophthalmology and Hansen Experimental Physics Laboratory, Stanford University, Institute of Physics Publishing 2 S105–S120 (2002)
2. Weber, C., Trisch, J.: Implementations and Implications of Foveated Vision. *Recent Patents on Computer Science* 2, 75–85 (2009)
3. Bolduc, L.: A review of biologically motivated space variant data reduction models for robotic vision. *Computer Vision and Image Understanding*, vol. 69, 170–184 (February 1998)
4. Traver, V. J., Pla, F.: Designing the lattice for log-polar images. *Discrete Geometry for computer Imagery, Proceedings*, vol. 2886, 164–173 (2003)
5. Melnyk, P.: Biologically Inspired Composite Image Sensor for Deep Field Target Tracking. Thesis. University of New Hampshire.

6. Niño-de-Rivera, L., Calzada Salas, R., Duchén Sánchez, G., Loaiza Brito, J.A.: Visual Simulation of Retinal Images Through Microstructures. *Microelectronic Engineering*. Vol. 90, pp. 159–162 (2012)
7. Pardo, F., Dierickx, B., Scheffer, D.: Space-Variant Nonorthogonal Structure CMOS Image Sensor Design. *IEEE Journal of Solid-State Circuits*, Vol. 33, No. 6 (June 1998)
8. Pardo, F., Dierickx, B., Scheffer, D.: CMOS foveated image sensor: Signal scaling and small geometry effects. *IEEE Transactions on Electron Devices*, Vol. 44, No. 10 (October 1997)
9. Paillet-Damien, F., Thierry, M., Bernard, M.: Second Generation Programmable Artificial Retina. CTA/GIP ENSTA/LEI. 32. 75015 Paris, France (2000)
10. Zeferino-Tomas, P. F.: Bio-Inspired Processing Module for the development of an artificial retina. Universidade Tecnica de Lisboa. Instituto Superior Tecnico. Licenciatura em Engenharia Electrotecnica e de Computadores. Relatório de Trabalho Final de Curso 157/2002/M (Setembro de 2003)
11. Pardo-Carpio, F.: Sensor Retínico Espacio Variante basado en Tecnología CMOS. Tesis. Departamento de Informática y Electrónica Universidad de Valencia (24 de septiembre de 1997)
12. Christos-Savvas, D. B.: Reconfigurable Foveated Active Vision System. In: 3rd International Conference on Sensing Technology, Taiwan (2008)
13. Javier-Traver, V., Bernardino, A.: A review of log-polar imaging for visual perceptions in robotics. *Robotics and Autonomous Systems* 58 (2010)
14. Volker, K.: Optical Flow Estimation in the Complex Logarithmic Plane. Instituts für Informatik und Praktische Mathematik der Christian Albrechts Universität zu Kiel (1995)



# Computational Intelligence Algorithms Applied to the Pre-diagnosis of Chronic Diseases

Mariana Dayanara Alanis-Tamez<sup>1</sup>, Yenny Villuendas-Rey<sup>2</sup>,  
Cornelio Yáñez-Márquez<sup>1</sup>

<sup>1</sup> Instituto Politécnico Nacional, Centro de investigación en Computación,  
Mexico

<sup>2</sup> Instituto Politécnico Nacional, Centro de Innovación y Desarrollo Tecnológico en Cómputo,  
Mexico

**Abstract.** Classification models applied to medicine have become an increasing area of research worldwide. Such as, the application and development of known models and algorithms for disease diagnosis and prediction have been an active research topic. The present article is a study of the classification algorithms most used in the literature, and its application to the diagnosis of chronic diseases. More specifically, we tested five classification models, over medical data. The application of the supervised classification algorithms is done over the Knowledge Extraction based on Evolutionary Learning (KEEL) environment, using a Distributed optimally balanced stratified 5-fold cross validation scheme. In addition, the experimental results obtained were validated to identify significant differences in performance by mean of a non-parametric statistical test (the Friedman test). The hypothesis testing analysis of the experimental results indicates which supervised classification model outperforms others for medical diagnosis.

**Keywords:** classification models, medical informatics, disease prediction and diagnosis, computational intelligence.

## 1 Introduction

For medical diagnosis, computational applications have been developed mainly in two principal areas: algorithm development and system development for supporting diagnosis. Among others, several web-based systems, as well as tools for teleradiology and telemedical devices can be mentioned [1, 2, 3].

Chang et al. [1] developed a Web-based decision support system that considers the sensitivity analysis as well as the optimal prior and posterior decisions applied for some chronic diseases. The purpose of their work is to review several approaches and to develop a Web-based decision support system (DSS).

Sanchez-Santana et al. [2] introduced another computational approach for medical diagnosis. They propose a new teleradiology environment for the detection of cardiovascular problems and allows medical staff to semi-automatically identify and quantify a patient's potential cardiovascular complications.

In addition, Havlik et al [3] propose a solution for remote monitoring, rapidly developing devices for telemedical applications and assistive technologies. The approach used was to design and realize a modular system consisting of input modules for signal acquisition, a control unit for signal pre-processing, handshaking of data communication, controlling the system and providing the user interface and communication modules for data transmission to a superordinate system.

In this paper, for assisting medical diagnosis, several algorithmic solutions have been proposed in recent years (section 2). We study the different classification algorithms most used in the literature, and its application to the diagnosis of chronic diseases (section 3). The different datasets have: imbalanced data, mixed categorical and numerical attributes, and missing values. In addition, we used 15 medical related datasets (section 4) to test all the classification models and the numerical experiments performed in the comparison between the different classification algorithms applied to the medical diagnosis. Finally, we offer the conclusion and some lines of future work (section 5).

## 2 Background

For medical diagnosis, several algorithmic solutions have been proposed in recent years.

Aiping Lu et al. [4] used pattern classification as a guideline in disease classification in Traditional Chinese medicine (TCM) practice and has been recently incorporated with biomedical diagnosis. They describe the historical evolution on the integration of the TCM pattern classification and disease diagnosis in biomedicine, the methodology of pattern classification for diseases

Timothy J. W. Dawes et al. [5] used a machine-learning survival model that uses three-dimensional cardiac motion which predicts outcome independent of conventional risk factors in patients with newly diagnosed pulmonary hypertension. It is used to determine if patient survival and mechanisms of right ventricular failure in pulmonary hypertension could be predicted by using supervised machine learning of three-dimensional patterns of systolic cardiac motion.

Yu Sun et al. [6] used the performance of a support vector machines (SVM) algorithm to predict prostate tumor location using multi-parametric MRI (mpMRI). They used a Gaussian kernel SVM which was trained and tested on different patient data subsets. Parameters were optimized using leave-one out cross validation.

Fazekas [7] addressed the examination of the periodicity of the childhood leukemia in Hungary using seasonal decomposition time series. The dataset used was from the Hungarian Pediatric Oncology Workgroup, and contained the data of all the patients with lymphoid leukemia diagnosed between 1988 and 2000. These data highlight the role of the environmental effects, like viral infections, epidemics, among others on the onset of the disease.

To sum up, Zheng et al. proposed a data informed framework for identifying subjects with and without Type 2 Diabetes Mellitus from Electronic Health Records via feature engineering and machine learning [8]. The objective of this work is to develop

a semi-automated framework based on machine learning as a pilot study to liberalize filtering criteria to improve recall rate with a keeping of low false positive rate.

### **3 Datasets and Algorithms**

In this section, a summary of the classification algorithms applied and the datasets related to medical diseases are presented.

#### **3.1 Datasets Related to Medical Diseases**

The used datasets include information about different diseases, such as breast cancer, thyroid diseases, heart diseases, liver disorders, diabetes, and others, all related to mainly with chronic diseases. The datasets used in this paper were taken from online information provided by KEEL dataset repository [9]. We used the medical related standard classification datasets.

In the following, a description of each of the datasets used is shown.

**Breast Cancer dataset:** It is one of three domains provided by the Oncology Institute, which has repeatedly appeared in the machine learning literature. This dataset has two classes, 201 instances of one class and 85 instances of another class. The instances are described by nine attributes, some of which are linear and some are nominal.

**Liver Disorders (BUPA) dataset:** It analyzes some liver disorders that might be because of the excessive alcohol consumption. The objective is to select if a given individual suffers from alcoholism.

**Heart Disease (Cleveland) dataset:** It is a part of the Heart Disease Dataset (the part obtained from the V.A. Medical Center, Long Beach and Cleveland Clinic Foundation), using a subset of 14 attributes. The objective is to detect the presence of heart disease in the patient.

**Haberman's Survival dataset:** It contains cases from a study that was conducted between 1958 and 1970 at the University of Chicago's Billings Hospital on the survival of patients who had undergone surgery for breast cancer. The objective is to determine if the patient survived 5 years or longer (positive) or if the patient died within 5 years (negative).

**Statlog (Heart) dataset:** The objective is to detect the absence or presence of heart disease.

**Hepatitis dataset:** It contains a mixture of integer and real valued attributes, with information about patients affected by the hepatitis disease. The objective is to predict if these patients will die or survive.

**Mammographic Mass dataset:** It can be used to predict the severity (benign or malignant) of a mammographic mass lesion from BI-RADS attributes and the patient's age. The data was collected at the Institute of Radiology of the University Erlangen-Nuremberg between 2003 and 2006.

**Thyroid Disease (New Thyroid) dataset:** It is one of the several databases about Thyroid available at the UCI repository. The objective is to detect if a given patient is normal or suffers from hyperthyroidism or hypothyroidism.

Pima Indians Diabetes dataset: The diagnostic, binary-valued variable investigated is whether the patient shows signs of diabetes according to World Health Organization criteria

Post-Operative dataset: The classification objective of this database is to determine where patients in a postoperative recovery area should be sent to next. Because hypothermia is a significant concern after surgery, the attributes correspond roughly to body temperature measurements.

South African Hearth dataset: A retrospective sample of males in a heart-disease high-risk region of the Western Cape, South Africa. The class label indicates if the person has a coronary heart disease: negative or positive.

SPECTF Heart dataset: It describes diagnosing of cardiac Single Proton Emission Computed Tomography (SPECT) images. Each of the patients is classified into two categories: normal or abnormal.

Thyroid Disease (thyroid0387) dataset: The objective is to detect is a given patient is normal or suffers from hyperthyroidism or hypothyroidism. This dataset is one of the several databases about Thyroid available at the UCI repository.

Breast Cancer Wisconsin (Diagnostic) dataset: It contains 30 features computed from a digitized image of a fine needle aspirate (FNA) of a breast mass. The objective is to determine if a found tumor is benign or malignant.

Breast Cancer Wisconsin (Original) dataset: It contains cases from a study that was conducted at the University of Wisconsin Hospitals, Madison, about patients who had undergone surgery for breast cancer. The objective is to determine if the detected tumor is benign or malignant.

**Table 1.** Description of the datasets used.

|     | Datasets       | Attributes |             | Imbalance analysis |        | Missing values | Classes |
|-----|----------------|------------|-------------|--------------------|--------|----------------|---------|
|     |                | Numeric    | Categorical | Instances          | IR     |                |         |
| 1.  | breast         | 0          | 9           | 277                | 2.420  | Yes            | 2       |
| 2.  | bupa           | 7          | 0           | 345                | 1.379  | No             | 2       |
| 3.  | cleveland      | 13         | 0           | 297                | 12.308 | Yes            | 5       |
| 4.  | haberman       | 3          | 0           | 306                | 2.778  | No             | 2       |
| 5.  | heart          | 13         | 0           | 270                | 1.250  | No             | 2       |
| 6.  | hepatitis      | 19         | 0           | 80                 | 5.154  | Yes            | 2       |
| 7.  | mammographic   | 6          | 0           | 830                | 1.060  | Yes            | 2       |
| 8.  | newthyroid     | 5          | 0           | 215                | 5.000  | No             | 3       |
| 9.  | pima           | 8          | 0           | 768                | 1.866  | No             | 2       |
| 10. | post-operative | 0          | 8           | 87                 | 62.000 | Yes            | 3       |
| 11. | saheart        | 8          | 1           | 462                | 1.888  | No             | 2       |
| 12. | spectfheart    | 44         | 0           | 267                | 3.855  | No             | 2       |
| 13. | thyroid        | 21         | 0           | 7200               | 40.157 | No             | 3       |
| 14. | wdbc           | 30         | 0           | 569                | 1.684  | No             | 2       |
| 15. | wisconsin      | 9          | 0           | 683                | 1.858  | Yes            | 2       |

In table 1, a summary of the description of the datasets is given. The summary includes the amount of numerical and categorical attributes, the number of instances, the Imbalance Ratio (IR) among majority and minority classes, the presence or not of missing values, and the number of classes.

For validation purposes, we used the Distributed optimally balanced stratified cross validation procedure (dob-scv) with five folds, introduced by [10] and recommended for imbalanced scenarios.

### 3.2 Performance Measures and Statistical Tests

Firstly, when imbalanced datasets were used for classification, the usual performance measures become inadequate [11]. This is because of the bias that such measures have towards the majority class, which in turn may yield to misleading conclusions. For evaluating the performance over imbalanced datasets with multiple classes, the use of the average True Positive Rate for each class [11] have been raised.

Therefore, in a two classes problem, the true positive rate (TPR) (as well-known as recall or sensitivity) considers the total of positive instances correctly classified, relative to the total of instances of the positive class, considering True Positives (TP), True Negatives (TN), False Positives (FP), and False Negatives (FN). See equation (1).

$$\text{Classification Sensitivity} = \text{TPR} = \text{Recall} = \frac{TP}{TP + FN}. \quad (1)$$

In fact, in a problem with  $k$  classes, the classification sensitivity takes into consideration the total of correctly classified instances from class  $j$ , relative to the total of instances of the  $j$ -th class. Therefore, the classification sensitivity for class  $j$  calculate the probability of correctly classifying an instance from class  $j$ . For the computation of such classification sensitivity, let  $n_j$  be the number of correctly classified instances (in a confusion matrix of  $k$  classes), and let  $t_j$  be the total of instances belonging to class  $j$ . So, for this reason the classification sensitivity (also recall or true positive rate) of class  $j$ , denoted by  $S_j$ , is computed as follows:

$$S_j = \text{Recall}_j = \text{TPR}_j = \frac{n_j}{t_j}. \quad (2)$$

The minimum classification sensitivity is given by [7]:

$$\text{Minimum} = \min_{j=1..k} \{S_j\}. \quad (3)$$

Although minimum classification sensitivity allows handling multiple classes, it only considers the lesser of the correctly classified rates among the classes. That is why in this paper, a measurement of performance is giving the same weight to each of the classes, independently from the number of samples each has, was chosen. The performance measure used here is the average classification sensitivity per class [10] which is defined as:

$$\text{Average} = \frac{1}{k} \sum_{i=1}^k S_j. \quad (4)$$

In the previous equation  $k$  is the number of classes and  $S_j$  is the classification sensitivity for the  $j$ -th class. This performance measure allows us to evaluate the global performance of classification algorithms over all the classes in the problem, not only

over the minority class. The use of the average classification sensitivity per class allows taking into consideration all the classes, without bias towards any one. Figure 3 presents an example of how the minimum classification sensitivity and the average classification sensitivity are computed, with  $k = 3$  classes:

|                        |          | <i>Real Class</i> |          |          |
|------------------------|----------|-------------------|----------|----------|
|                        |          | <i>X</i>          | <i>Y</i> | <i>Z</i> |
| <i>Predicted class</i> | <i>X</i> | 2                 | 8        | 0        |
|                        | <i>Y</i> | 3                 | 3        | 4        |
|                        | <i>Z</i> | 6                 | 2        | 2        |

$$S_A = \frac{2}{10} = 0.2, S_B = \frac{3}{10} = 0.3, S_C = \frac{2}{10} = 0.2$$

a)  $Average = \frac{0.2+0.3+0.2}{3} = \frac{0.7}{3}$       b)  $Minimum = \min\{0.2, 0.3, 0.2\} = 0.2$

**Fig. 1.** An example of computation of performance measures given a confusion matrix for three classes taking in consideration the average classification sensitivity and the minimum classification sensitivity.

To determine which classification algorithms got the better experimental results while predicting voting intentions and hypothesis testing was used. Statistical hypothesis tests evaluate whether there is a significant difference in the performance given by different classification algorithms, talking about their prediction of the voting intentions. Regarding the works of [12,13], non-parametric tests were chosen for the current research. Particularly, the Friedman test is widely recommended for this kind of works so it was selected.

In addition, the Friedman test is a statistical non-parametric test developed by Friedman [14], which turns out to be the non-parametric equivalent to the two-way ANOVA analysis. The Friedman test consists of ordering the samples and replacing them by their respective ranks like: the best result corresponds to rank 1, the second best to rank 2, the third to rank 3 and so on. After that, the existence of identical samples is taken into consideration, in which case they are assigned an averaged rank.

### 3.3 Classification Algorithms

Firstly, a decision tree [15] is a predictor that indicates the label associated with an instance by traveling from a root node of a tree to a leaf, the leaf will be the assigned class. At each node on the root to leaf, the successor child in the tree is chosen based on a splitting of the input space. **C4.5** is a decision tree which is an extension of the ID3 algorithm, this algorithm is almost always referred to as a statistical classifier.

Another algorithm used is **kNN** [15] or  $k$  nearest neighbor algorithm, it is a supervised classification method whose training phase consists of storing the characteristic vectors and class labels of training examples. The distance between the stored vectors is calculated and the “ $k$ ” nearest instances are selected; the selected instance is sorted with the most repeating class.

**Logistic** [15] or Logistic Regression, is a type of regression analysis used to predict the outcome of a categorical variable as a function of independent or predictor variables. However, logistic regression is used for classification tasks: We can interpret  $h(x)$  as the probability that the label of  $x$  is 1.

**MLP** [15] or Multilayer Perceptron is a network of simple “neurons” or “perceptrons”. It has its neurons grouped in layers of distinct levels. Each of the layers is formed by a set of neurons and three different types of layers are distinguished: the input layer, the hidden layers and the output layer.

Finally, **SMO** [16] or Sequential minimal optimization is an algorithm for solving the quadratic programming problem that arises during the training of support vector machines, it was implemented by John Platt's for the machines learning tool called WEKA (Waikato Environment for Knowledge Analysis).

The classification algorithms described in this section were used to evaluate the datasets proposed in the next section.

## 4 Experimental Results and Discussion

This section presents the experimental results obtained for medical diagnosis, using the classification models proposed, as well as other state of art models. Figure 2 illustrates the schematics of the experiment design carried out.

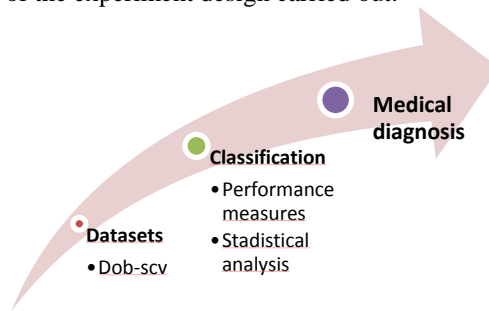


Fig. 2. Schematic of the experimental design.

Five state-of-the-art classification algorithms were selected. All of them can deal with mixed and incomplete data. This selection includes Nearest Neighbor (NN) (using  $k=3$ ), Multilayer Perceptron (MLP), C4.5, SMO and Logistic. For MLP, C4.5, Logistcs and SMO, we used the default parameter values offered in the KEEL software package.

For the Nearest Neighbor classifier, the HEOM dissimilarity was used [17] which handles mixed and incomplete data descriptions. Considering that  $max_a$  and  $min_a$  are the maximum and minimum values of the feature  $a$ , if it is a numerical attribute, the HEOM dissimilarity is computed as:

$$HEOM(x,y) = \sqrt{\sum_{a=1}^n d_a(x_a, y_a)}. \quad (5)$$

$$d_a \begin{cases} 1 \text{ if } x_a \text{ or } y_a \text{ are unknown,} \\ \text{overlap}(x_a, y_a) \text{ if } a \text{ is numerical,} \\ \text{diff}(x_a, y_a) \text{ if } a \text{ is categorical,} \end{cases}$$

$$\text{overlap}(x_a, y_a) = \begin{cases} 0 \text{ if } x_a = y_a, \\ 1 \text{ otherwise,} \end{cases}$$

$$\text{diff}(x_a, y_a) = |x_a - y_a| / \max_a - \min_a .$$

Table 2 shows the results obtained by the analyzed classification algorithms, for the medical diagnosis problems considered. Best results are highlighted in bold.

**Table 2.** Average True Positive Rate obtained by the classification algorithms.

| Datasets          | C4.5         | kNN          | Logistic     | MLP          | SMO          |
|-------------------|--------------|--------------|--------------|--------------|--------------|
| breast            | 0.591        | 0.605        | 0.595        | <b>0.659</b> | 0.632        |
| bupa              | 0.614        | 0.652        | <b>0.659</b> | 0.535        | 0.500        |
| cleveland         | 0.292        | 0.297        | <b>0.319</b> | 0.298        | 0.310        |
| haberman          | 0.578        | 0.583        | 0.564        | <b>0.649</b> | 0.500        |
| heart             | 0.775        | 0.803        | <b>0.835</b> | 0.833        | 0.833        |
| hepatitis         | 0.679        | 0.732        | 0.641        | <b>0.820</b> | 0.693        |
| mammographic      | <b>0.838</b> | 0.818        | 0.828        | 0.459        | 0.824        |
| newthyroid        | 0.894        | 0.914        | <b>0.956</b> | 0.695        | 0.767        |
| pima              | 0.687        | 0.690        | <b>0.730</b> | 0.708        | 0.714        |
| post-operative    | 0.328        | 0.343        | 0.326        | <b>0.641</b> | 0.336        |
| saheart           | 0.618        | 0.607        | 0.669        | 0.643        | <b>0.688</b> |
| spectfheart       | 0.565        | <b>0.701</b> | 0.606        | 0.579        | 0.509        |
| thyroid           | <b>0.976</b> | 0.593        | 0.724        | 0.447        | 0.518        |
| wdbc              | 0.479        | 0.475        | 0.487        | <b>0.500</b> | 0.477        |
| wisconsin         | 0.502        | 0.511        | <b>0.512</b> | 0.510        | 0.503        |
| <b>Times Best</b> | 2            | 1            | <b>6</b>     | 5            | 1            |

To find the best classification algorithm is more appropriate for the correct diagnosis of diseases, the Friedman test [13] was applied.

**Table 3.** Algorithms rankings according to the Friedman: the best performer is Logistic.

| No. | Algorithm | Ranking |
|-----|-----------|---------|
| 1   | Logistic  | 2.267   |
| 2   | MLP       | 2.767   |
| 3   | kNN       | 3.000   |
| 4   | SMO       | 3.300   |
| 5   | C4.5      | 3.667   |

The algorithms rankings according to the Friedman test are shown in table 3, where the best classifier for this task is, apparently, Logistic.

Considering the results of the Friedman Test, it rejects the hypothesis having an adjusted value lower or equal than 0.05. The test indicates that the probability of Friedman is 0.149, this value is greater than 0.05 thus the result confirms that although the Logistic model was the number one in the ranking, the Friedman test did not find significant differences in the performance of the five classifiers analyzed.

## 5 Conclusions and Future Work

In this paper, it is proposed to study and evaluate the different classification algorithms most used in the literature, in order to determine which of these is the best in terms of medical diagnosis. These classification algorithms were selected because all of them can deal with mixed and incomplete data.

The result was that among the selected algorithms, in the analysis of diagnosis of several diseases, the logistic model obtained very good results; due to it significantly outperform other classifiers in medical diagnosis. According to the Friedman test, the best classifier in the experiments carried out is Logistic; but, considering the results of the probability of Friedman that is 0.149 and this value is greater than 0.05 we conclude that although the Logistic model was the number one in the ranking, the Friedman test did not find significant differences in the performance of the five classifiers analyzed.

As a future work, we would propose a new algorithm, different from those already evaluated in the literature, that competes with the evaluated classifiers and that also has significant differences against the others. This new algorithm should be proposed taking into consideration that it is able of handling mixed, incomplete and multiclass data.

**Acknowledgements.** The authors would like to thank the Instituto Politécnico Nacional (Secretaría Académica, COFAA, SIP, CIDETEC, and CIC), the CONACyT, and SNI for their economic support to develop this work.

## References

1. Chang, C. C., Cheng, C. S., Huang, Y. S.: A Web-Based Decision Support System for Chronic Diseases. *JUCS (Journal for Universal Computer Science)*, 12(1), 115–125 (2006)
2. Sanchez-Santana, M. A., Aupet, J. B., Betbeder, M. L., Lapayre, J. C., Camarena-Ibarrola, A.: A tool for telediagnosis of cardiovascular diseases in a collaborative and adaptive approach; *JUCS (Journal for Universal Computer Science)*, 19(9), 1275–1294 (2013)
3. Havlik, J., Lhotska, L., Parak, J., Dvorak, J., Horcik, Z., Pokorny, M.: A Modular System for Rapid Development of Telemedical Devices; *JUCS (Journal for Universal Computer Science)*, 19(9), 1242–1256 (2013)
4. Lu, A., Jiang, M., Zhang, C., Chan, K.: An integrative approach of linking traditional Chinese medicine pattern classification and biomedicine diagnosis. *Journal of ethnopharmacology*, 141(2), 549–556 (2012)
5. Dawes, T. J., de Marvao, A., Shi, W., Fletcher, T., Watson, G. M., Wharton, J., Cook, S. A.: Machine learning of three-dimensional right ventricular motion enables outcome prediction in pulmonary hypertension: a cardiac MR imaging study. *Radiology*, 283(2), 381–390 (2017)
6. Sun, Y., Reynolds, H., Wraith, D., Williams, S., Finnegan, M. E., Mitchell, C., Haworth, A.: Predicting prostate tumor location from multiparametric MRI using Gaussian kernel

- support vector machines: a preliminary study. *Australasian physical & engineering sciences in medicine*, 40(1), 39–49 (2017)
7. Fazekas, M.: Analysing Data of Childhood Acute Lymphoid Leukaemia by Seasonal Time Series Methods. *JUCS (Journal for Universal Computer Science)*, 12(9), 1190–1195 (2006)
  8. Zheng, T., Xie, W., Xu, L., He, X., Zhang, Y., You, M., Chen, Y.: A machine learning-based framework to identify type 2 diabetes through electronic health records. *International Journal of Medical Informatics*, 97, 120–127 (2017)
  9. KEEL dataset repository Homepage, <https://www.keel.es>
  10. López, V., Fernández, A., García, S., Palade, V., Herrera, F.: An insight into classification with imbalanced data: Empirical results and current trends on using data intrinsic characteristics. *Information Sciences*, 250, 113–141 (2013)
  11. Fernández, A., López, V., Galar, M., Del Jesus, M. J., Herrera, F.: Analysing the classification of imbalanced data-sets with multiple classes: Binarization techniques and ad-hoc approaches. *Knowledge-based systems*, 42, 97–110 (2013)
  12. Demšar, J.: Statistical comparisons of classifiers over multiple datasets. *Journal of Machine Learning Research*, 7, 1–30 (2006)
  13. García, S., Fernández, A., Luengo, J., Herrera, F.: Advanced nonparametric tests for multiple comparisons in the design of experiments in computational intelligence and data mining: Experimental analysis of power. *Information Sciences*, 180(10), 2044–2064 (2010)
  14. Friedman, M.: A comparison of alternative tests of significance for the problem of m rankings. *Annals of Mathematical Statistics*, 11, 86–92 (1940)
  15. Duda, R. O., Hart, P. E., Stork, D. G.: *Pattern classification*. Wiley, New York (1973)
  16. SMO Homepage. <http://weka.sourceforge.net/doc.dev/weka/classifiers/functions/SMO.html>
  17. Wilson, D. R., Martinez, T. R.: Improved heterogeneous distance functions. *Journal of Artificial Intelligent Research*, 1–34 (1997)

# Hybrid CW-GA Metaheuristic for the Traveling Salesman Problem

Irma Delia Rojas Cuevas, Santiago Omar Caballero Morales

Universidad Popular Autónoma del Estado de Puebla A.C., Puebla, Puebla,  
Mexico

irmadelia.rojas@upaep.edu.mx, santiagomar.caballero@upaep.mx

**Abstract.** The Traveling Salesman Problem (TSP) is one of the most challenging problems in Logistics and Supply Chain Management. Its relevance in routing planning and distribution has significant impact on reduction of operative costs for all enterprises. However, due to its NP-hard complexity, it is difficult to obtain optimal solutions for TSP instances. This paper describes a hybrid approach based on Clarke and Wright (CW) and Genetic Algorithms (GA) to provide near optimal solutions for the TSP. Performance of this meta-heuristic was assessed by comparing it with other well-known methods such as CW, GA and Tabu-Search (TS). Results obtained from experiments with TSP instances corroborated the suitability of the hybrid approach for the TSP.

**Keywords:** traveling salesman problem, tabu search, metaheuristics, Clarke and Wright, genetic algorithms.

## 1 Introduction

The Traveling Salesman Problem (TSP) [1] is one of the most important and challenging problems in Logistics and Supply Chain Management. This is because operative costs associated to transportation and distribution are correlated to the efficiency of route planning, and TSP is focused on finding the route of minimum distance to cover a set of customer points.

However, solving the TSP is a computational task of NP-hard complexity. Thus, it is difficult to obtain exact or optimal solutions for large instances of the TSP (number of customer points higher than 100). This is the reason why the TSP is one of the combinatorial optimization problems that has attracted many researchers to propose and analyze metaheuristic algorithms to solve it in polynomial time. Among the algorithms used for this purpose, the following can be mentioned: Genetic algorithms (GA) [2], Tabu-Search (TS) [3], Clarke and Wright (CW) [4].

For GAs different strategies and implementations have been proposed. This has led to different reported performance for the TSP: average errors from best-known solutions between 1.56% and 7.64% for 14 TSP instances [5], 0.00% to 1.62% for 40 instances [6], 0.00% to 2.54% for 22 TSP instances [7], 0.00% to 2.46% for 29 instances

[8] and 0.00% to 0.61% for six TSP instances [9]. On the other hand, with TS, average errors from best known solutions of 0.00% to 6.00% have been reported [10]. However, in some cases, TS has provided better solutions than best-known solutions as reported in [11].

This work is focused on providing a hybrid metaheuristic to provide near-optimal solutions to different TSP instances. Based on work reported in the literature, the metaheuristic is aimed to provide solutions with an average error less than 7.64% [5]. The metaheuristic is integrated by the CW algorithm and a GA (CW-GA metaheuristic). This was performed in order to achieve sequential improvement on CW solutions by means of evolutionary operators. Comparison with the hybrid CW-TS approach led to confirm that GA can be a more suitable metaheuristic for hybridization with other methods for sequential improvement of TSP solutions.

The present work is structured as follows: in Section 2 the details of the CW, GA and TS algorithms are presented. Then, in Section 3 the assessments of the CW, GA, TS, CW-GA and CW-TS methods are presented and discussed. Finally, the conclusions are presented in Section 4.

## 2 Development of the Metaheuristics

In this section, the metaheuristics used for the hybrid approach are described. In Section 2.1 the CW algorithm is described while in Section 2.2 the TS algorithm is described. Then, in Section 2.3 the elements of the GA are described.

### 2.1 Clarke and Wright (CW)

Clarke and Wright is commonly used for Vehicle Routing Problems (VRP). In this case it is used for the TSP (VRP is also known as the multiple TSP or *m*TSP). The CW algorithm is described as follows:

- First the Euclidean distance between all customer points is computed:

$$c_{ij} = \sqrt{(x_i - x_j)^2 + (y_i - y_j)^2}, \quad (1)$$

where  $(x_i, y_i)$  and  $(x_j, y_j)$  are the geographical locations of customer point  $i$  and  $j$  respectively.

- Second, the saving value between customer  $i$  and  $j$  is computed as:

$$s_{ij} = c_{Di} + c_{jD} - c_{ij}, \quad (2)$$

where  $c_{Di}$  is the traveling distance between the Depot (start-end point for the TSP route of minimum distance) and customer  $i$ ,  $c_{jD}$  is the traveling distance between customer  $j$  and the Depot, and  $c_{ij}$  is the traveling distance between customer  $i$  and  $j$ . Eq. (2) is not the original proposed by Clarke and Wright, it is the modified expression proposed by Bodin [12]. After computation, all savings values are stored in a *savings list* with its corresponding customer points.

- Third, the values in the *savings list* are sorted in decreasing order. Finally, the route is constructed by continuous merging of customer points  $(i,j)$  with the highest saving value. Thus, the merging procedure starts from the top of the *savings list*. Figure 1 presents an extension of the description of the CW algorithm.

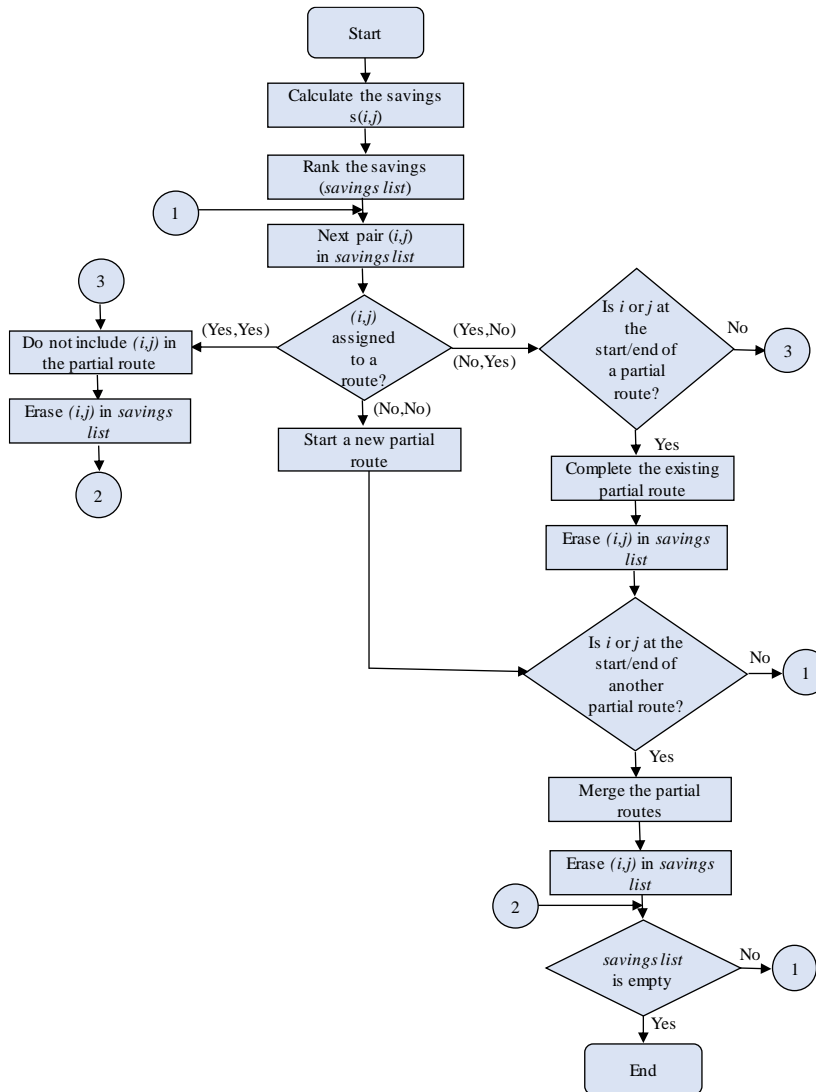


Fig. 1. Description of the Clarke and Wright (CW) algorithm.

## 2.2 Tabu Search (TS)

TS considers a neighborhood search procedure to iteratively move from one potential solution  $S_0$  to an improved solution  $sBest$  in the neighborhood of  $S_0$ . In order to avoid

revisiting previous solutions a *tabu list* is considered. This list keeps the last movements that led to a solution *hidden* from the search process during a number of iterations. The overall TS process is as follows [13]: a *tabu list* of size  $N/4$  is considered for a 2-opt movement strategy with a *Stop Condition* of 1000 iterations. A generation of feasible solutions (neighborhood) is obtained with the 2-opt strategy and assessment for the *tabu list* is based on the minimum distance criteria. If the movement that led to the solution of minimum distance is not in the *tabu list* and this solution is better than the best solution previously found then the movement is applied, the best solution is updated, and the movement is added the *tabu list*. If the movement does not improve the quality of the solution, the movement is just added to the *tabu list*. If the movement is already in the *tabu list* then no change or update is performed. Figure 2 presents an extension of the description of the TS algorithm.

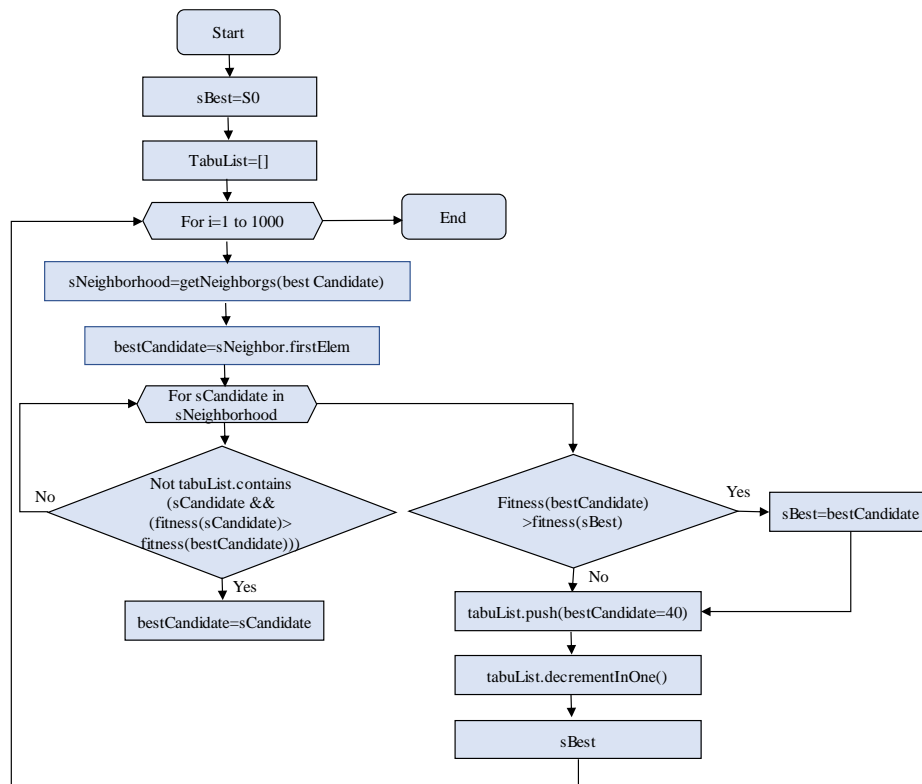


Fig. 2. Description of the Tabu-Search (TS) algorithm.

### 2.3 Genetic Algorithm (GA)

In a GA, a population of candidate solutions for an optimization problem is evolved to obtain better solutions. Each candidate solution has a set of properties which can be

mutated or be used to exchange information with other solutions. In this case, the properties are the sequences of nodes in a tour or route of minimum distance.

The GA begins with an initial population of  $A$  individuals which can be randomly generated or be obtained by another method. Then, this population is evolved by producing *offspring* from selected individuals (*parents*). Potential parents were selected based on their *fitness* to solve the combinatorial problem. On each generation, the fitness of every individual in the population is evaluated; the fitness is the value of the objective function to be solved (in this case, the total distance of the TSP route). For this case, parents were randomly selected from the best 50% of individuals.

Then, offspring were obtained by means of the *reproduction operators* known as *crossover* and *mutation*. For this case,  $0.80 \times A$  offspring were produced with OX crossover,  $0.05 \times A$  were produced with CX crossover, and  $0.15 \times A$  were produced with 2-opt, 1-opt and shift mutation. Figure 3 presents the extended description of the GA.

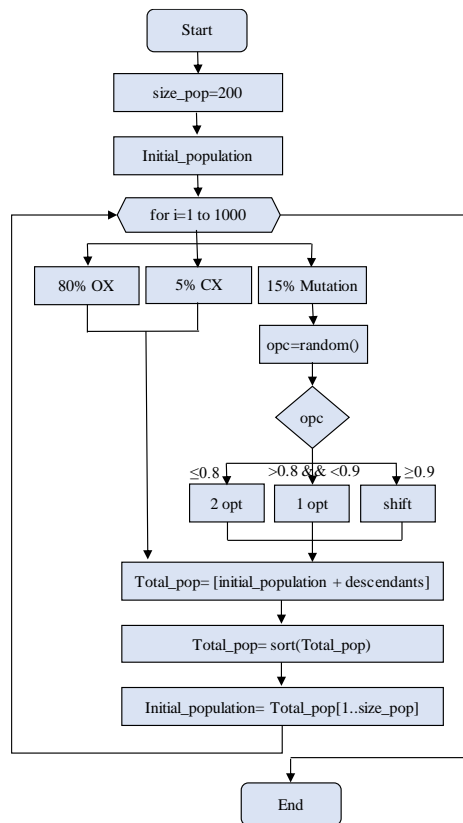


Fig. 3. Description of the Genetic Algorithm (GA).

- **2-opt:** Figure 4 presents the reproduction mechanism of this operator. In the first step (a) two points are random selected. Then, in the second step (b) the points are reconnected and the cost (total distance) of the route is computed. If the cost of this

route is better than the previous cost, the two points remain in the new position, otherwise, they return to their original position. With the **1-opt** operator, a single point is selected and it is moved to a randomly selected location.

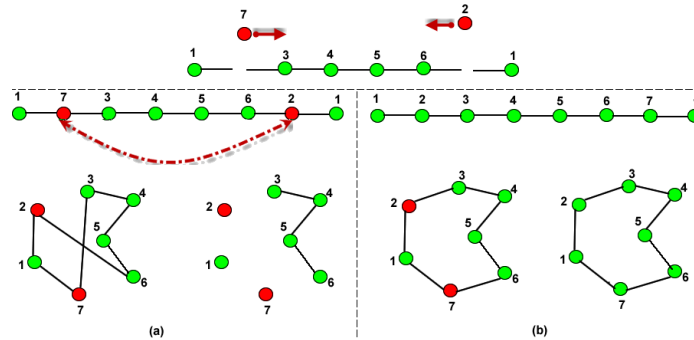


Fig. 4. Sample tour with seven locations: (2, 7) are swapped.

- **Shift:** Figure 5 presents the two steps of this process. In the first step (a) two points are randomly selected. Then, in the second step (b) the order of all points between the two selected points (including these points) is reversed. If the cost of the new route is better than the previous cost, the shifted points remain in their new positions, otherwise, they are returned to their original position.

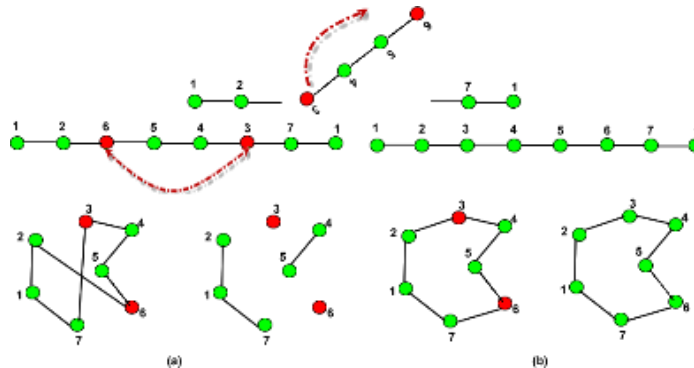


Fig. 5. Sample tour with seven locations: (2,7) are shifted.

- **Cycle Crossover (CX) and Order Crossover (OX):** With these operators, points between parent solutions can be exchanged, leading to offspring that contain route information from different solutions.

### 3 Assessment

A set of 30 symmetric TSP instances were considered to assess the approach [14]. For this case, GA and TS were initialized with randomly generated solutions. As shown in

Table 1, the constructive method CW has the lowest average error (8.39%) from well-known solutions. GA follows with 47.50% and TS has the highest average error with 106.01%. Also, as presented in Figure 6, GA has better and faster convergence than TS. However, none of them reach the optimal solution, or are close to the performance of CW.

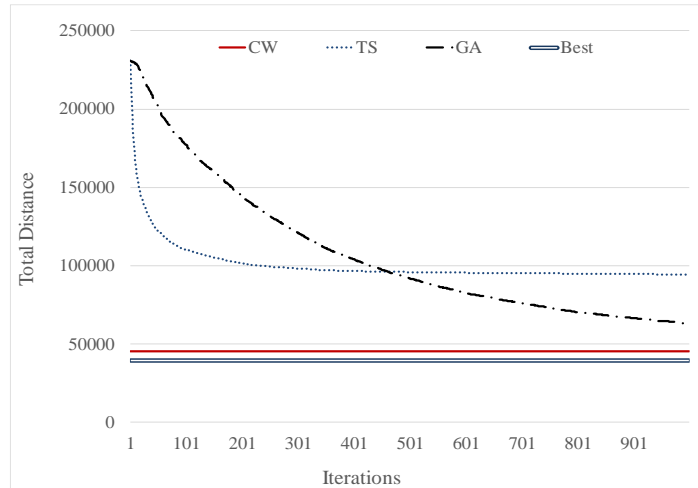


Fig. 6. Convergence of CW, TS, and GA algorithms.

In order to assess the hybrid approach, the initial solutions for TS and GA were obtained with the CW algorithm. This led to the hybrid metaheuristics CW-TS and CW-GA. As presented in Table 1, the CW-GA outperforms CW, TS, GA and the CW-TS method by obtaining an average error of 5.57%. In contrast, CW-TS achieved an average error of 6.61%. Convergence of CW-GA and CW-TS is presented in Figure 7.

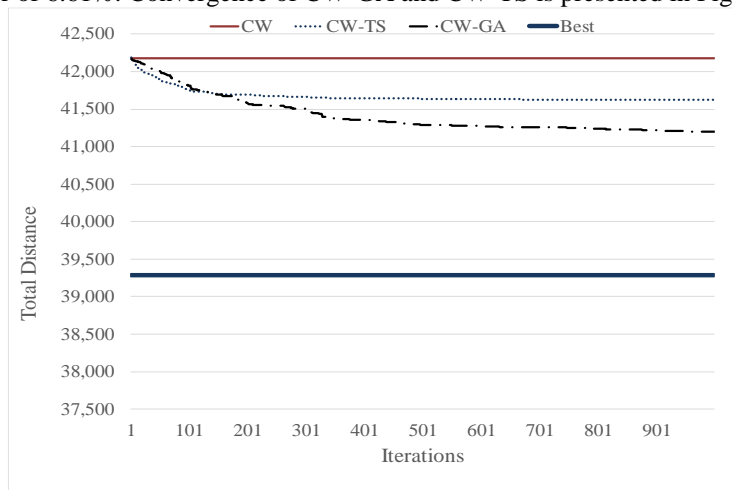


Fig. 7. Convergence of CW, CW-TS and CW-GA algorithms.

**Table 1.** Comparative results of CW, GA, TS, CW-GA and CW-TS.

|                | CW      |         |             | GA      |              | TS      |               | CW-GA  |             | CW-TS  |             |
|----------------|---------|---------|-------------|---------|--------------|---------|---------------|--------|-------------|--------|-------------|
|                | Best    | CW      | %           | Value   | %            | Value   | %             | Value  | %           | Value  | %           |
| Eil51          | 426     | 437     | 2.62        | 437     | 2.62         | 437     | 2.62          | 437.15 | 2.62        | 437.15 | 2.62        |
| Berlin52       | 7,542   | 8,291   | 9.93        | 7,748   | 2.73         | 8,117   | 7.63          | 7747.9 | 2.73        | 8117.4 | 7.63        |
| Eil76          | 538     | 574     | 6.73        | 595     | 10.52        | 817     | 51.82         | 574.21 | 6.73        | 570.58 | 6.06        |
| pr76           | 108,159 | 113,930 | 5.34        | 115,340 | 6.64         | 171,630 | 58.68         | 111570 | 3.15        | 112590 | 4.10        |
| kroA100        | 21,282  | 23,049  | 8.30        | 24,852  | 16.77        | 38,759  | 82.12         | 21784  | 2.36        | 22523  | 5.83        |
| kroB100        | 22,141  | 24,392  | 10.17       | 24,747  | 11.77        | 41,775  | 88.68         | 23944  | 8.14        | 23958  | 8.21        |
| kroC100        | 20,749  | 22,516  | 8.52        | 23,233  | 11.97        | 38,223  | 84.22         | 21997  | 6.01        | 22084  | 6.43        |
| kroD100        | 21,294  | 22,902  | 7.55        | 25,477  | 19.64        | 37,072  | 74.10         | 22746  | 6.82        | 22720  | 6.70        |
| kroE100        | 22,068  | 24,496  | 11.00       | 25,516  | 15.62        | 40,990  | 85.74         | 23619  | 7.03        | 23518  | 6.57        |
| Eil101         | 629     | 691     | 9.85        | 679     | 7.87         | 683     | 8.64          | 678.5  | 7.87        | 683.37 | 8.64        |
| Lin105         | 14,379  | 15,763  | 9.63        | 14,878  | 3.47         | 15,092  | 4.96          | 14878  | 3.47        | 15092  | 4.96        |
| pr107          | 44,303  | 49,157  | 10.96       | 50,245  | 13.41        | 119,580 | 169.91        | 45872  | 3.54        | 47814  | 7.92        |
| pr124          | 59,030  | 63,978  | 8.38        | 73,611  | 24.70        | 143,790 | 143.59        | 60389  | 2.30        | 62938  | 6.62        |
| Bier127        | 118,282 | 124,030 | 4.86        | 121,530 | 2.75         | 122,830 | 3.85          | 121530 | 2.75        | 122830 | 3.85        |
| Ch130          | 6,110   | 6,817   | 11.58       | 6,623   | 8.40         | 6,696   | 9.59          | 6623.1 | 8.40        | 6696   | 9.59        |
| pr136          | 96,772  | 106,200 | 9.74        | 132,010 | 36.41        | 165,780 | 71.31         | 106000 | 9.54        | 105880 | 9.41        |
| pr144          | 58,537  | 63,447  | 8.39        | 86,919  | 48.49        | 177,080 | 202.51        | 62085  | 6.06        | 62920  | 7.49        |
| Ch150          | 6,528   | 6,972   | 6.81        | 6,927   | 6.11         | 6,931   | 6.17          | 6926.9 | 6.11        | 6930.9 | 6.17        |
| kroA150        | 26,524  | 28,526  | 7.55        | 38,486  | 45.10        | 49,763  | 87.61         | 27879  | 5.11        | 27913  | 5.24        |
| kroB150        | 26,130  | 27,833  | 6.52        | 36,831  | 40.95        | 52,699  | 101.68        | 27115  | 3.77        | 27078  | 3.63        |
| pr152          | 73,682  | 78,221  | 6.16        | 101,870 | 38.26        | 270,850 | 267.59        | 77581  | 5.29        | 78068  | 5.95        |
| D198           | 15,780  | 17,704  | 12.19       | 17,086  | 8.28         | 17,312  | 9.71          | 17086  | 8.28        | 17312  | 9.71        |
| kroA200        | 29,368  | 32,115  | 9.35        | 31,377  | 6.84         | 31,641  | 7.74          | 31377  | 6.84        | 31641  | 7.74        |
| kroB200        | 29,437  | 33,059  | 12.30       | 52,559  | 78.55        | 68,518  | 132.76        | 31724  | 7.77        | 32367  | 9.95        |
| pr226          | 80,369  | 84,902  | 5.64        | 164,690 | 104.92       | 377,510 | 369.72        | 129600 | 2.33        | 129600 | 2.33        |
| pr264          | 49,135  | 53,087  | 8.04        | 124,070 | 152.51       | 213,500 | 334.52        | 82180  | 2.25        | 84317  | 4.91        |
| Ts225          | 126,643 | 129,600 | 2.33        | 315,920 | 149.46       | 338,180 | 167.03        | 52459  | 6.77        | 52658  | 7.17        |
| A280           | 2,579   | 2,851   | 10.56       | 6,951   | 169.53       | 6,643   | 157.60        | 2798.7 | 8.52        | 2811   | 9.00        |
| pr299          | 48,191  | 54,178  | 12.42       | 134,020 | 178.10       | 145,030 | 200.95        | 52160  | 8.24        | 52274  | 8.47        |
| lin318         | 42,029  | 45,484  | 8.22        | 127,190 | 202.62       | 120,730 | 187.25        | 44676  | 6.30        | 44336  | 5.49        |
| <b>Average</b> |         |         | <b>8.39</b> |         | <b>47.50</b> |         | <b>106.01</b> |        | <b>5.57</b> |        | <b>6.61</b> |

## 4 Conclusions

Performance of individual metaheuristics was variable: GA obtained an average error throughout 30 TSP instances of 47.50%. Meanwhile, TS obtained an average error of 106.01% from best known results. However, if CW is considered as the generator of initial solutions, the hybrid CW-GA metaheuristic is able to obtain an average error of 5.57%. In comparison, the hybrid CW-TS obtained an average error of 6.61%. CW obtained an average error of 8.39%.

Regarding convergence, initially TS has faster convergence than GA. However, after 400 iterations, the convergence of GA continues, achieving better results than TS.

Individual metaheuristics can provide very suitable solutions for routing problems as the TSP. However, performance may vary significantly from one metaheuristic to other. Better performance can be achieved if integration between metaheuristics is performed. In this case, GA could improve the performance of the constructive CW algorithm, and its evolutionary features were more competitive than the features of TS.

Thus, with an average error of 5.57%, the hybrid CW-GA may provide better solutions than individual metaheuristics.

**Acknowledgements.** The main author would like to thank Tecnológico Nacional de México/Instituto Tecnológico de Puebla and Consejo Nacional de Ciencia y Tecnología (CONACYT) for the scholarship to pursue a Ph.D. degree.

## References

1. Glover F., McMillan C.: The general employee scheduling problem: An integration of MS and AI. *Computers & Operations Research*, 13(5), 563–573. doi: /10.1016/0305-0548(86)90050-X (1986)
2. Holland, J. H., *Adaptation in natural and artificial systems. An introductory analysis with application to biology, control, and artificial intelligence.* Ann Arbor, MI: University of Michigan Press (1975)
3. Glover, F.: Future paths for integer programming and links to artificial intelligence. *Computers & Operations Research*, 13(5), 533–549. doi: 10.1016/0305-0548(86)90048-1 (1986)
4. Clarke, G., & Wright, J. W. Scheduling of vehicles from a central depot to a number of delivery points. *Operations Research*, 12(4), 568–581 (1964)
5. Albayrak, M., Allahverdi, N.: Development a new mutation operator to solve the traveling salesman problem by aid of genetic algorithms. *Expert Systems with Applications*, 3(38), 1313–1320 (2011)
6. Antosiewicz, M., Grzegorz, K., & Kamiński, B.: Choice of best possible metaheuristic algorithm for the travelling salesman problem with limited computational time: quality, uncertainty and speed. *Journal of Theoretical and Applied Computer Science*, 7(1), 46–55 (2013)
7. Doyuran, T., Çatay, B.: A robust enhancement to the Clarke-Wright savings algorithm. *The Journal of the Operational Research Society*, 62(1), 223–231 (2011)
8. He, Y., Qiu, Y., Liu, G., Lei, K.: A parallel adaptive tabu search approach for traveling salesman problems. In: *Natural Language Processing and Knowledge Engineering, IEEE NLP-KE'05, Proceedings of IEEE International Conference on*, 796–801 (2005)
9. Ma, J., Yang, T., Hou, Z., Tan, M., Liu, D.: Neurodynamic programming: A case study of the traveling salesman problem. *Neural Computing and Applications*, 17(4), 347–355 (2008)
10. Marinakis, Y., Magdalene, M.: A hybrid multi-swarm particle swarm optimization algorithm for the probabilistic traveling salesman problem. *Computers & Operations Research*, 37(3), 432–442 (2010)
11. Marinakis, Y., Athanasios, M., Panos, M. P.: A hybrid genetic—GRASP algorithm using Lagrangean relaxation for the traveling salesman problem. *Journal of Combinatorial Optimization*, 10(4), 311–326 (2008)
12. Yan, X., Liu, H. M., Yan, J., Wu, Q. H.: A fast evolutionary algorithm for traveling salesman problem. In: *Natural Computation, Third International Conference on IEEE*, 4, 85–90 (2007)
13. Tsubakitani, S., Evans J. R.: Optimizing Tabu List size for the Traveling Salesman Problem. *Computers & Operations Research*, 25(2), 91–97 (1998)
14. Yang, N., Ping, L., Baisha, M.: An angle-based crossover tabu search for the traveling salesman problem. In: *Natural Computation ICNC 2007, Third International Conference on, IEEE*, 4, 512–516 (2007)



# Transmission of Digital Audio with Visible Light

Sergio Sandoval-Reyes, Arturo Hernandez-Balderas

CIC, Instituto Politécnico Nacional, CDMX,  
Mexico

sersand@cic.ipn.mx, heba920908@gmail.com

**Abstract.** Communication by visual light or VLC by its acronym in English (Visual Light Communication), uses visible light from fluorescent lamps, or light from light emitting diode (LED) to transmit information. The transmission of information is done by modulating the intensity of the LED light. In the receiver the information is initially recovered through a photo-detector, which is usually connected to a device for the final recovering of the information. In this article we describe an application based on VLC, to transmit audio stored in a micro SD card using a shield mounted on an Arduino microcontroller, and several modules (called bits) of LittleBits. The use of modular components that allow simple interconnection, facilitated the development of this application.

**Keywords:** visual light communications, audio, Arduino.

## 1 Introduction

Visible Light Communication (i.e. VLC). [1, 2], transmits data by intensity modulation. It uses Light Emitter Diodes (LEDs) and light detectors at transmit and receive ends respectively. It works in the 380 nm to 780 nm optical band which is visible light and hence the name VLC [3, 4, 5].

VLC can be used as a communications medium to transmit data by visible light for ubiquitous computing, because light-producing devices (such as indoor/outdoor lamps, traffic signs, commercial displays and car headlight and taillights) are used everywhere [6].

This paper describes a VLC application to transmit and receive digital audio using an Arduino microcontroller connected to a LED, and a light sensor connected to a speaker.

The remainder of this paper is organized as follows: Section 2 presents a summary of works related to the transmission of digital audio using VLC. Section 3 describes the design of our VLC application. Section 4 shows the results of the implementation. Finally, our conclusions and future work are presented in Section 5.

## 2 Related Work

Several research works on VLC technologies have been proposed. The most important are described in the following.

## 2.1 How LED based VLC Systems Works

Typical LED based VLC systems are implemented using an intensity modulation and direct detection (IM/DD) scheme with a line-of-sight (LOS) configuration [7]. In the transmitter, IM is implemented through the modulation of the transmitted signal into the instantaneous optical power of the LED by controlling the radiant intensity with the forward current through the LED (High modulation frequencies are used to avoid flicker). In the receiver, the transmitted signal is recovered using direct detection (DD). In this simple method, a photodiode is used to convert the incident optical signal power into a proportional current. Figure 1 shows a general VLC link structure for an IM/DD based VLC system [8].

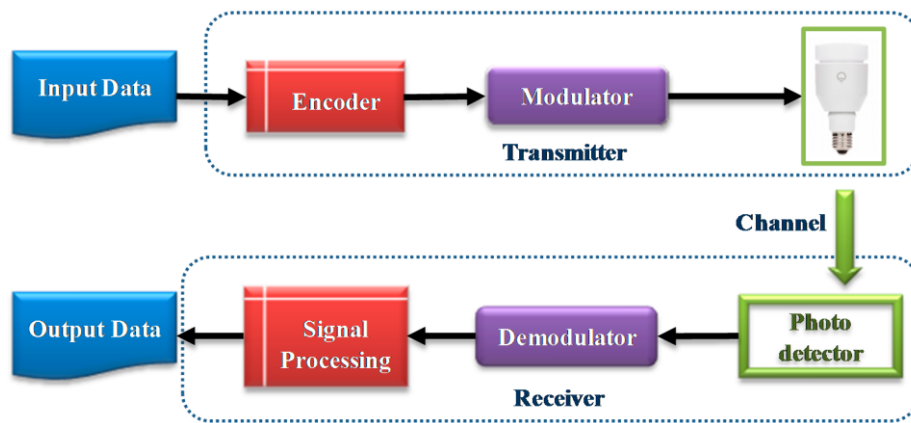


Fig. 1. A general VLC link structure.

## 2.2 VLC Transmitter

A typical LED based VLC transmitter contains a signal generator (information source), and a modulator, followed by the LED driver and the LED optics, see Figure 1 [9]. The modulation methods available for VLC, particularly for indoor applications, must support dimming and provide flicker mitigation. The modulating signals are used to switch LEDs at desired frequencies using LED drivers. These drivers rely on transconductance amplifiers to convert voltage signals to corresponding current signals to excite the light sources (LEDs) for both communication and illumination purposes.

### VLC Modulation

Although there are different modulation schemes for VLC, mainly, on-off keying (OOK), variable pulse-position modulation (VPPM), color shift keying (CSK) and orthogonal frequency division multiplexing (OFDM) [10], OOK is the most popular. OOK (On-Off-Keying) is the most commonly used IM/DD modulation scheme in VLC due to its simple implementation. In this method basically the LED intensity is

changed between two distinguishable levels corresponding to the data bits (1 or 0). See Figure 2. A modified OOK, called Variable OOK (VOOK) can provide dimming. It is achieved by changing the data duty cycle through pulse-width modulation (PWM), with only 1 bit of information carried per symbol period

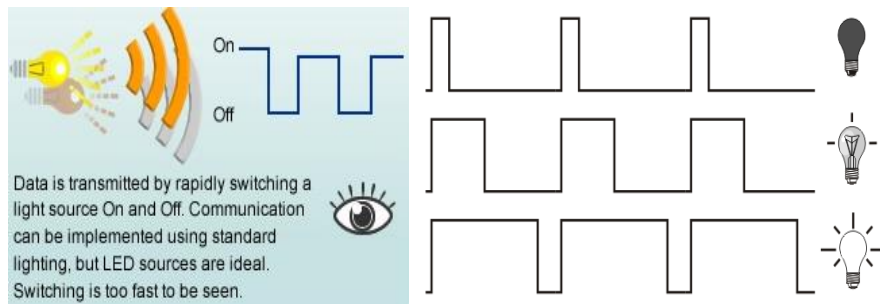


Fig. 2. On-Off Keying with PWM.

### 2.3 VLC Receiver

A typical optical receiver's front end consists of a photo detector followed by an amplifier. The photo detector can be a photo diode or a Light Detect Resistor (LDR). In both cases its impedance decreases in the presence of light and increases in its absence. See Figure 3. A simple photo detector can be used as a receiver since VLC exhibits no Doppler shift, and therefore it is not necessary a sophisticated receiver tracking algorithm.

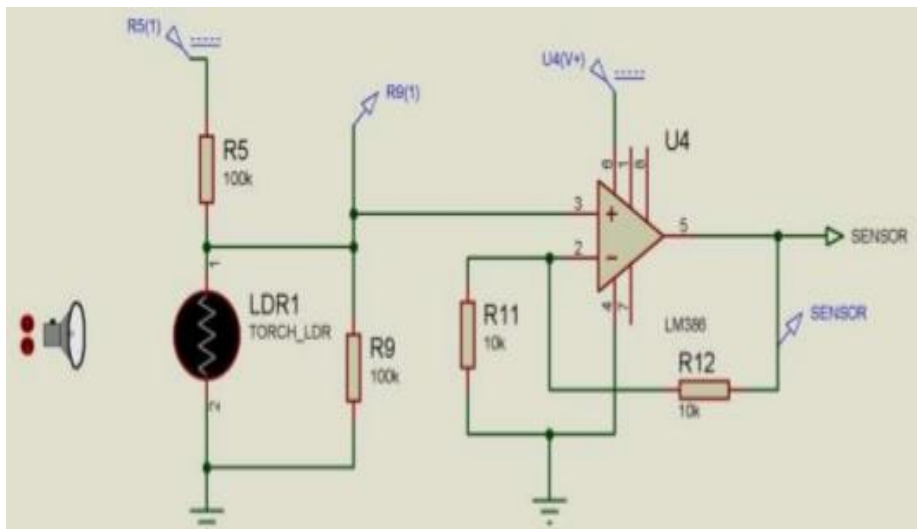


Fig. 3. A LDR photo detector followed by an amplifier.

### 3 Audio Streaming Using VLC

In the following we develop a VLC application to transmit and receive realtime audio using light from a LED in the transmitter, and a photo detector in the receiver.

In order to do that, we will use in the transmitter as a data source, an Arduino microcontroller with a SD shield 3.0 [11] containing digital music in WAV format, and two LittleBits modules [12]: A microphone/amplifier bit and a bright LED bit. See Figure 4. The Arduino output ports produce OOK-PWM output signals, whose duty cycles represent the audio intensity.

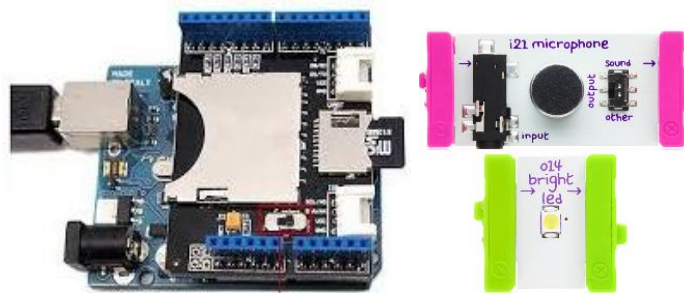


Fig. 4. An Arduino microcontroller with a SD Shield and two LittleBits modules.

While as in the receiver we will use two LittleBits components: A light sensor bit, and a speaker bit. See Figure 5.



Fig. 5. Receiver components: Light sensor and speaker.

#### 3.1 Transmitting Digital Audio via VLC

The Arduino (Master device) loads the WAV file from the micro-SD card (Slave device) in .wav format through pins d4 (CS: Chip Select), d11 (MOSI: Master Output Slave Input), d12 (MISO: Master Input Slave Output), and d13 (SCK: Signal Clock). It then generates an On-Off PWM signal and outputs it (pin 9), toward the microphone/amplifier component, which amplifies the On-Off PWM signal and feeds it to the bright LED bit component. The .wav file stored in the SD card has the following specifications: 8 bits per sample; 22050 Hz sampling rate; mono channel; and PCM unsigned 8-bit format. The Arduino code to execute the above mentioned is shown in Figure 6.

```
#include "SD.h"
#define SD_ChipSelectPin 4
#include "TMRpcm.h"
#include "SPI.h"

TMRpcm tmrpcm;

void setup(){
  tmrpcm.speakerPin = 9;
  Serial.begin(9600);
  if (!SD.begin(SD_ChipSelectPin)) {
    Serial.println("SD fail");
    return;
  }

  tmrpcm.setVolume(6);
  tmrpcm.play("REC00000.wav");
}

void loop(){ }
```

**Fig. 6.** Arduino code to play the audio .wav file stored in the SD card.

In this code (modified from [13]), the library "SD.h" allows Arduino-SD card communication; "TMRpcm" allows asynchronous playback of PCM/WAV files directly from the SD card; SPI (Serial Peripheral Interface) allows the transfer of audio data through the MISO, MOSI and SCK signals between the Arduino and the SD card.

### 3.2 Receiving Digital Audio via VLC

As it was mentioned, the streaming music sent as a LED light is received through a light sensor module which then sends it to the speaker module. This speaker module not only filters the audio signal but also amplifies it. Using these LittleBits components makes these tasks very simple. See Figure 7.

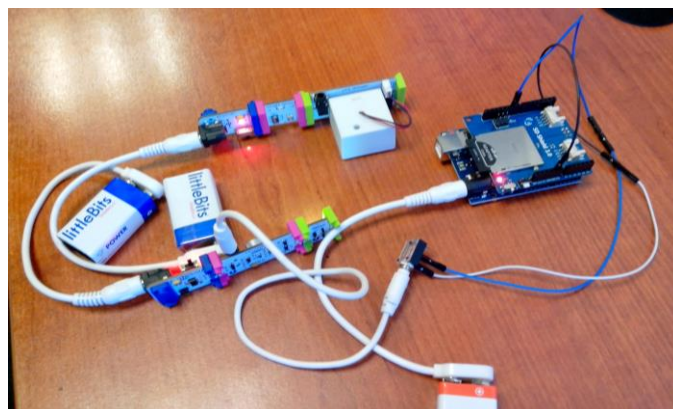


**Fig. 7.** Receiving digital audio via VLC.

## 4 Experiments and Results

For the experiments we use as was mentioned an Arduino microcontroller with a SD card and several LittleBits components. The whole setup is shown in Figure 8.

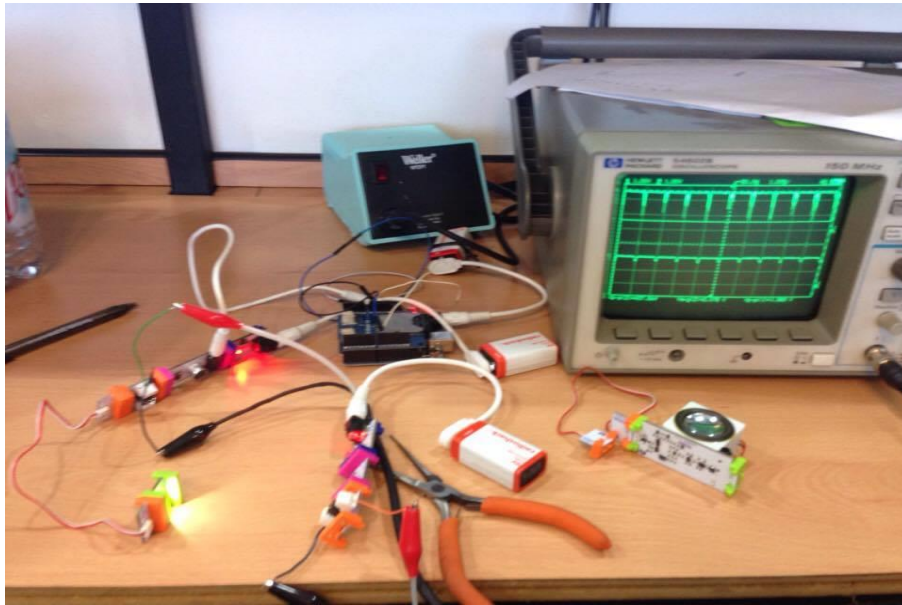


**Fig. 8.** Setup for the transmission and reception of digital audio using VLC.

Figure 8 shows the Arduino microcontroller with a SD shield. The shield contains a micro SD card which in turn contains the .wav file. The output from the Arduino is sent to the Mic-Amp-LED modules through an audio connector. Note that the audio connector has only two wires (digital audio signal and ground), because the audio has just one channel. Note also that both the Arduino and the LittleBits modules are energized with 9 V batteries.

This Figure 8 also shows the light coming from the LED and in the lower part of this figure, the backward face of the light sensor and the speaker modules. Naturally if an object blocks the light from the LED, the light sensor ceases of receiving this light and the music reproduced by the speaker, is interrupted.

### 4.1 Discussion of Results

The setup for the transmission and reception of audio using VLC worked well, although with a little noise. Naturally, this noise increases when the distance between the LED and the light sensor is greater. Also the brightness of the LED and the alignment between LED and light sensor also influence the performance.

Using an oscilloscope we could capture the transmission signal feeding to the bright LED, thus as the reception signal recovered from the light sensor. This is shown in Figure 9. It can be seen that the light sensor signal is well recovered at 3 cm.

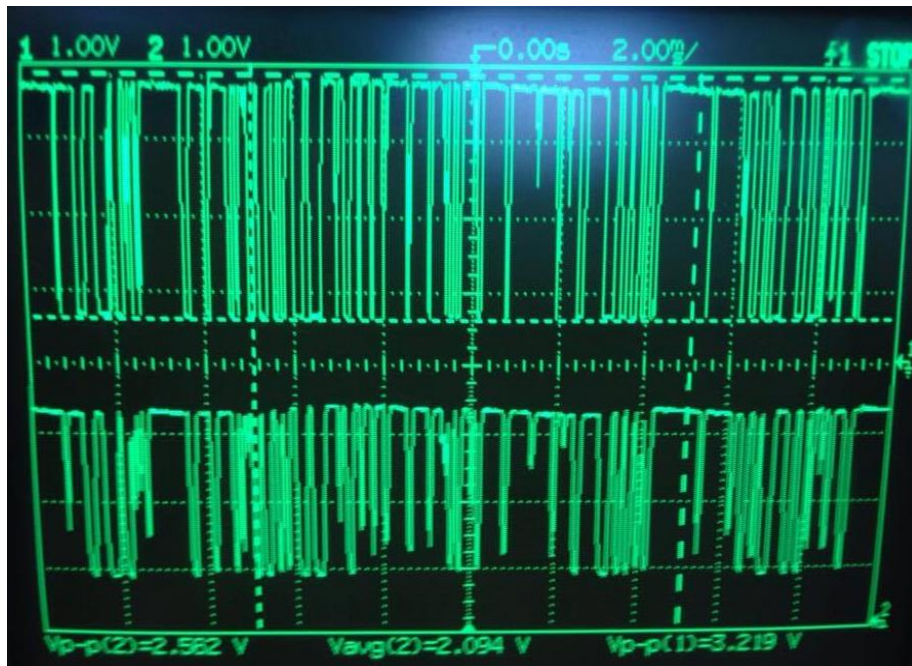


**Fig. 9.** Up: Digital transmission signal feeding the LED; Down: Received signal from the light sensor.

This work differs with respect to similar works as in [13], [14] and [15], in the following. In [13] it is required to use a specific microcontroller, in this case an "Arduino Due", which has a digital-to-analog converter at the output, to convert the audio in digital format to analog. In this work, the Arduino Due is not used, but the Arduino ONE which is more common. In [14], it is required to use two microcontrollers (one for the transmission and one for the reception), and the detection is done by biasing inversely to a LED diode (which modifies its resistance depending on the light received). In [15] an Arduino microcontroller is used for the transmission and a LDR photo sensor for reception, however no code is reported.

## 5 Conclusions

An audio transmission and reception application using VLC was developed using Arduino and LittleBits components. The application worked acceptably well although with a small presence of noise. It should be noted that this noise is also due to the fact that the wav file was recorded with only 8 bits per sample. In other words, it's not Hi-Fi.

Also, the performance of the application depends on the brightness of the emitter LED and the sensitivity of the photo sensor with respect to the light received from the LED and the surrounding light (in Figure 5 it can be seen that the light sensor has a control for graduating the sensitivity in the presence of high or low light). Additionally, the alignment between the LED and the light sensor influences the reception, and consequently the quality of the audio reproduction. This work could be improved by: 1) Increasing the emission power of the LED to increase the reception distance; and 2) Include video transmission by adding another LED light source to encode video.

**Acknowledgements.** This work was supported by the Instituto Politecnico Nacional; Project SIP 20171260.

## References

1. Haas, H.: Wireless data from every light bulb. TED Ideas worth spreading, [http://www.ted.com/talks/harald\\_haas\\_wireless\\_data\\_from\\_every\\_light\\_bulb](http://www.ted.com/talks/harald_haas_wireless_data_from_every_light_bulb) (2011)
2. Tsonev, D., Videv, S. Haas, H.: Light fidelity (Li-Fi): towards all-optical networking. In: Proc. SPIE (Broadband Access Communication Technologies VIII) 9007(2) (2013)
3. Sherman, J.: How LED Light Bulbs could replace Wi-Fi. Digital Trends. <http://www.digitaltrends.com/mobile/light-bulb-li-fi-wireless-internet/>, last accessed 2016/05/01
4. Haas, H.: High-speed wireless networking using visible light. SPIE Newsroom (2013)
5. Vincent, J.: Li-Fi revolution: internet connections using light bulbs are 250 times faster than broadband. <http://www.independent.co.uk/news/science/li-fi-revolution-internet-connections-using-light-bulbs-are-250-times-faster-than-broadband-8909320.html> (2013) (last accessed on March 2016)
6. Jovicic, A., Li, J., Richardson, T.: Visible light communication: opportunities, challenges and the path to market. IEEE Communications Magazine, 51(12), 26–32 (2013)
7. Kamsula, P.: Design and implementation of a bi-directional visible light communication testbed. University of Oulu, Department of Electrical and Information Engineering, Master's Thesis, 59 p. (2015)
8. He, Y., Ding, L., Gong, Y., Wang, Y.: Real-time audio & video transmission system based on visible light communication. Optics and Photonics Journal, 3(02), 153 (2013)
9. Lee, K., Park, H.: Modulations for visible light communications with dimming control. IEEE photonics technology letters, 23(16), 1136–1138 (2011)
10. Arduino Homepage, <https://www.arduino.cc/>, last accessed 2017/09/01
11. LittleBits Homepage, <https://littlebits.cc/> last accessed 2017/09/01
12. Banzi, M., Fitzgerald, S., Guadalupi, A.: Simple Audio Player. (2015)
13. Jpiat, J.: Arduino Simple Visible Light Communication. <https://github.com/jpiat/arduino/wiki/Arduino-Simple-Visible-Light-Communication>, last accessed 2017/09/01
14. Yıldırım, G., Özen, Ö., Yüksel, H., İnci, M.: A Low-Cost Li-Fi Communication Setup. (2017)

# Implicaciones computacionales de los aeromanipuladores

Julio Mendoza-Mendoza<sup>1</sup>, Baltazar Jiménez-Ruiz<sup>2</sup>,  
V́ctor Javier González-Villela<sup>1</sup>, Mauricio Méndez-Martínez<sup>3</sup>,  
Leonardo Fonseca-Ruiz<sup>3</sup>, Erick López Alarcón<sup>3</sup>

<sup>1</sup> Centro de Ingeniería Avanzada, Facultad de Ingeniería, UNAM,  
México

<sup>2</sup> Escuela Superior de Cómputo, Instituto Politécnico Nacional,  
México

<sup>3</sup> Unidad Profesional Interdisciplinaria en Ingeniería y Tecnologías Avanzadas,  
Instituto Politécnico Nacional,  
México

aladegabriel@hotmail.com

**Resumen.** Este documento presenta las necesidades computacionales implícitas en el diseño y operación de manipuladores de robots aéreos; para este propósito, se identifican y verifican diferentes consideraciones en el estado de la técnica actual y muy reciente. Se inicia con el cálculo requerido para las unidades UAS individuales, y continúa con la operación de estructura completa, que se divide en 4 modos de operación cíclicos: vuelo hacia el área de trabajo y transformación a manipulador; despegue de aeronaves; control en modo manipulador y finalmente aterrizaje. A lo largo del texto, hay un ejemplo de aplicación, un brazo de robot volador desarrollado por los autores.

**Palabras clave:** manipuladores aereas robóticos, diseño, operación.

## Computational Implications of Aeromanipulators

**Abstract.** This document presents the computational needs implicit in the design and operation of aerial-robot manipulators, for this purpose, different considerations are identified and verified in the current and very recent state of the art. It is started with the computation required for the individual UAS units, and continue with the full-structure operation which is divided into 4 cyclic modes of operation: flight towards the work area and transformation to manipulator; aircraft take off; control in manipulator mode and finally landing. Along the text, there is an example of application, a flying robot arm in development by the authors.

**Keywords:** aerial-robot manipulators, design, operation.

## 1. Introducción

La tecnología de aeromanipuladores como estructuras voladoras de tipo brazo robot, tanto en configuraciones seriales como paralelas (Figura 1) data de 2012 [1,2,3,4,5,6,7,8,9].

Básicamente se trata de estructuras aéreas donde los UAVs (acrónimo inglés para vehículo aéreo no tripulado) que las transportan, funcionan también como los elementos de manipulación robótica, para comprender las implicaciones computacionales relacionadas a estos mecanismos, es necesario subdividir las en las siguientes áreas: 1 consideraciones computacionales generales de los UAVs; 2 consideraciones de transformación y vuelo hacia la zona de operación del sistema de manipulación aérea conjunta; 3 implicaciones computacionales de ascenso; 4 implicaciones computacionales de control en el modo de manipulación aérea; 5 implicaciones computacionales de descenso.

En nuestra aplicación particular, cada una de estas implicaciones es satisfecha vía hardware por el sistema embebido de vuelo Pixhawk y vía software mediante las librerías APM [10,11], sin embargo, este texto resultará de utilidad para quien desee hacer su propio sistema con microprocesadores, FPGAs, DSPs, microcontroladores o tarjetas de desarrollo de altas prestaciones. Para el correspondiente modelado y condiciones de operación ver [9].

## 2. Implicaciones generales

Las implicaciones computacionales generales de los vehículo aéreo no tripulado, se recogen en [12,13,14,15].

Cada uno de los elementos descritos posee distintas frecuencias de operación por lo cual es necesario un sistema de administración RTOS (real time operating system) que dictamine la adecuada lectura, procesamiento, almacenamiento, jerarquía y ejecución, estos consisten en:

**Lectura de sensores de orientación, posición planar y altura:** La manera estándar es utilizar IMUs, magnetómetros, barómetros, acelerómetros y GPS o cámaras, todos operando en distintos protocolos de comunicación y frecuencias de muestreo, en algunos casos por construcción del sensor y en otros por prioridad de medición.

**Escritura a propelas y mecanismos de ejecución mediante servomotores:** Lo primero es el uso directo con motores generalmente brushless (sin escobillas) y lo segundo consiste en utilizar motores auxiliares, para tareas secundarias al vuelo, por ejemplo estabilizadores de cámara, alerones y mecanismos de thrust vectoring (vectorización del empuje principal) [16,17,18]. Esto es importante porque la escritura a los primeros debe ser en frecuencias mucho mayores a los segundos, básicamente porque de los primeros depende que no caiga la aeronave y están sujetos a altas vibraciones, estos por lo general deben operar a PWMs (acrónimo inglés para modulación por ancho de pulsos) de 490 Hz mientras que los secundarios a 50Hz.

**Control retroalimentado de orientación, posición planar y altura:** De manera general, se subdivide la tarea de movimiento de un UAV en estos tres

modos de ejecución, el prioritario es mantener una altura de operación también conocido como hovering; el de rango de prioridad intermedia es controlar la orientación o actitud de la aeronave y finalmente su posición planar, también conocida como steering [19,20,21,15,22].

**Procesamiento de imágenes:** Esta tarea se vuelve necesaria en aquellas condiciones donde no funcionan los sistemas de posicionamiento global satelital (por ejemplo en interiores, o zonas rocosas o boscosas).

**Comunicación interna de datos de entrada y salida:** Esta por lo general se realiza en un bus de topología serial, como se indica consiste en la forma en la cual se comparten y procesan los datos de los sensores hacia el procesador principal y a la vez el modo en el que este decide su escritura a los diversos sistemas de actuadores.

**Almacenamiento de datos de vuelo y telemetría:** Es el modo en el que el sistema almacena los datos para su uso e interacción y el modo de comunicación inalámbrica entre el mando de control autónomo principal.

**Lectura de mandos de control remoto:** Consiste en la lectura de unidades de teleoperación, las cuales establecen el vínculo entre la unidad en vuelo y la base manual en tierra, como puede verse, junto con la telemetría existen dos distintos módulos de mando inalámbrico, el reto aquí es garantizar que operen con precisión en frecuencias distintas y en múltiples canales independientes.

**Lectura de unidades analógicas y digitales tipo GPIO:** Consiste en la habilitación, interacción, lectura y escritura de los puertos analógicos o bien aquellos digitales de propósito general (general purpose input/output).

**Filtrado de señales:** La adición de ruido a los UAVs esta implícita en la vibración de los motores y su interacción eléctrica, de esta forma, es necesario un algoritmo de filtrado de señales, el cual generalmente es mediante técnicas.

**Fusión sensorial:** Cuando el medio cambia de manera constante, es necesario utilizar combinación de sensores de geolocalización, un ejemplo es entre tareas donde el dron pase de un ambiente externo a un interno y se deba también intercambiar entre la lectura de un sistema de visión artificial y un sensor GPS.

**Planificación de tareas:** Es necesario obtener datos de velocidad y aceleración para disponer de movimientos suaves, mas aun, hay autores que indican y demuestran que es necesario incluir snap (segunda derivada de aceleración) [23], como los sensores se limitan a lectura de velocidades posiciones y aceleraciones y en la mayoría de los casos es parcialmente, es necesario incluir estimadores que implican observadores, estimación neuronal, estimación difusa y a su vez algoritmos de planificación de trayectorias entre puntos, lo cual, también vuelve necesario incluir algoritmos de optimización de productos matriciales.

**Prioridad de tareas en tiempo real:** Dadas las diferentes frecuencias de operación de sensores, actuadores, sistemas y sub-lazos de control, es necesario priorizar las tareas de ejecución, las de mayor prioridad suelen ser aquellas de escritura a motores y lectura de altura; las intermedias las de lectura planar y orientacional y finalmente en menor rango las de comunicación serial, lectura de mandos remotos y almacenamiento de datos de vuelo, ahora bien dentro de las prioritarias relacionadas a escritura de motores, las jerarquía es altitud, actitud,

movimiento de plano y trayectoria espacial, el Pixhawk dispone para ello de un sistema RTOS para asignar prioridades y tiempos, sin embargo en caso de diseñar su propia controladora de vuelo, es necesario establecer un sistema de tiempo real para ejecución de eventos.

### **3. Máquina de estados del vuelo de un aeromanipulador, caso particular aerobrazo**

Antes de proseguir con las áreas de implicaciones computacionales es adecuado indicar la máquina de estados relacionada a la operación del aerobrazo [9], para ello se subdivide la operación conjunta en dos etapas: 1 traslado y transformación: es decir la operación conjunta del sistema de UAVs para llegar a la zona de operación y una vez ahí transformarse en manipulador aéreo; 2 manipulación aérea: es decir anclar su posición en la zona de operación deseada y funcionar como brazo robótico flotante:

A la izquierda de la Figura 3 se ilustra la ejecución de la máquina de estados, el lazo mas externo es la transformación entre aeronave y brazo volador el cual corresponde a la activación o desactivación de un sistema tipo clutch, cuando el clutch esta activo, los UAVS tienen un comportamiento de estructura rígida y solo contribuyen al traslado de la misma, una vez que esta desactivado el clutch, lo cual esta en función de la zona de operación donde se desea el modo de manipulador aéreo, se inicia el modo de manipulación aérea.

El modo de manipulación aérea, es decir el lazo interno de la máquina de estados, esta basado en el hecho de que se poseen dos controles remotos y puede compartirse su mando auxiliar entre ambos drones mediante protocolos alámbricos o inalámbricos Figura 2, de esta manera cada botón auxiliar tiene dos estados 1 o encendido y 0 o apagado, al ser dos mandos existen entonces 4 combinaciones (00), (01), (11) y (10), que respectivamente indicarían la secuencia de apagado, ascenso, control y descenso respectivamente, la maquina de estados deseable para nuestros propósitos es la siguiente: estando en el modo apagado (00) solo se admite trasladarse al estado de ascenso (01), cualquier otra combinación mantiene al sistema en el modo de apagado. Una vez ascendiendo (01) solo se admite el paso al modo de control de altura (11) y ángulos de hombro y codo o bien al modo de descenso (10). En el modo de control (11) solo es admisible pasar al modo de descenso (10). Del modo de descenso (10) solo es admisible cambiar al modo de apagado (00).

### **4. Implicaciones computacionales de vuelo y transformación hacia la zona de trabajo, modo aeronave**

**Coordinación y programación paralela de vuelo físicamente restringido de múltiples UAVS:** La cual puede ser centralizada si se usa un solo procesador y se ve al sistema no como un conjunto de UAVS sino como un

conjunto de hélices o bien descentralizada (multiprocesador) si cada UAV usa su respectivo procesador y se ve al sistema como un grupo coordinado de UAVs autónomos, la tarjeta Pixhawk es capaz de realizar ambos modos de operación con UAVs de hasta 4 rotores para una configuración de aerobrazo de 8 hélices (es decir 2 cuadrotoros o bien 4 coaxiales de dos hélices u ocho monocopteros). El problema de la operación centralizada es la sobrecarga de tareas de actuación y control para un solo procesador.

**Estimación de perturbaciones en vivo:** Aunque todo el vuelo posee perturbaciones, la parte crítica es aquella de larga duración, es decir en modo aeronave, donde se vuelve necesario estimar y contrarrestar los efectos del viento, la presión y temperatura, esto es computacionalmente complicado a cielo abierto pues el aire representa un flujo laminar y varía con modelos diferenciales parciales que inciden sobre variaciones de una viga (la aeronave se considera como una viga múltiplemente apoyada sobre sus hélices).

**Lectura simultánea de múltiples puntos para determinar parámetros de inercia y masa en un punto virtual:** Dicho punto virtual es el centro de gravedad o de masas el cual es virtual porque puede o no estar físicamente en el cuerpo del sistema, pero es de suma importancia para el control del mismo, como este punto dependen de la configuración de cada UAV, un buen algoritmo para determinarlo está en [24] el cual implica calcular las variaciones inerciales de cada UAV y/o punto intermedio de unión y transferirlas a una central de mando para calcular así el punto inercial equivalente, esto computacionalmente implica el envío de datos sensoriales simultáneos a una central de procesamiento donde se procesan y a su vez se devuelve el punto resultante a cada UAV para que tengan noción de la operación conjunta, ello implica envío por protocolos alámbricos o inalámbricos, generalmente seriales y a su vez métodos para asegurar la adecuada transferencia de la información (el más básico es el checksum).

**Interacción de transformación:** En este punto, es necesario un método para transformar la estructura aérea desde un modo de vuelo estándar y coordinado (por ejemplo un helicóptero o un ala volante) a uno de vuelo independiente pero igualmente coordinado (es decir un brazo volador), la implicación computacional es la conmutación de frecuencias de operación de las hélices las cuales deben apagarse y encenderse en una secuencia precisa mientras el sistema vuela (helibot patente MX/a/2016/014595) o bien [6,9], véase Figura 1.

## 5. Implicaciones computacionales de ascenso modo compartido

El ascenso es la parte más simple pero peligrosa de la operación de un sistema aéreo, esto es porque primero se debe garantizar un despegue el cual no ocurre de manera inmediata a la activación de las hélices, es decir existe un bias en el cual las hélices giran pero el sistema no consigue elevación, más aun cada hélice posee su propio bias de despegue en dependencia del adecuado centrado de todo el sistema o bien el balanceo de cada propela, la implicación computacional en esta parte consiste en monitorear un valor óptimo para la elevación conjunta sin

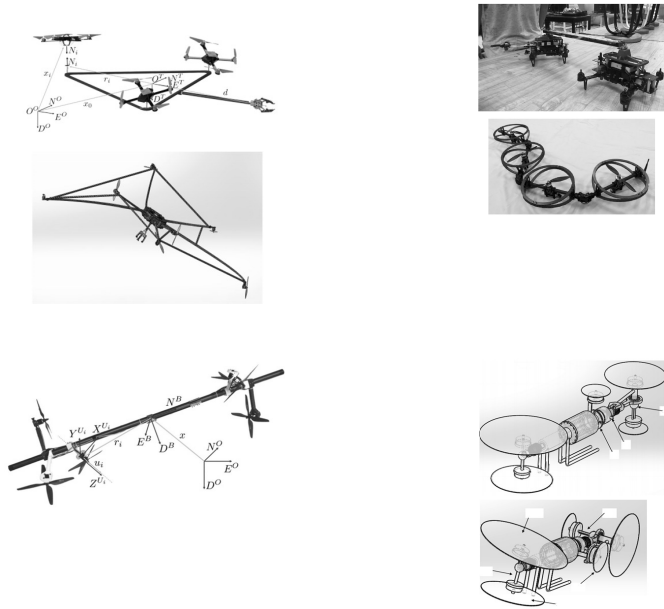


**Fig. 1.** Aeromanipuladores: De arriba a abajo y de izquierda a derecha: Hai-Nguyen 2015; Julio Mendoza 2015; Alexandros Nikou 2015; Moju Zhao 2016; Sangyul Park 2016; Mendoza MX/a/2016/014595 MX/a/2015/015160.

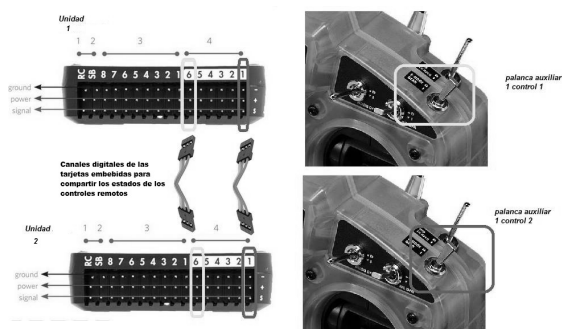


**Fig. 2.** Comunicación alámbrica entre UAVs hombro y código.

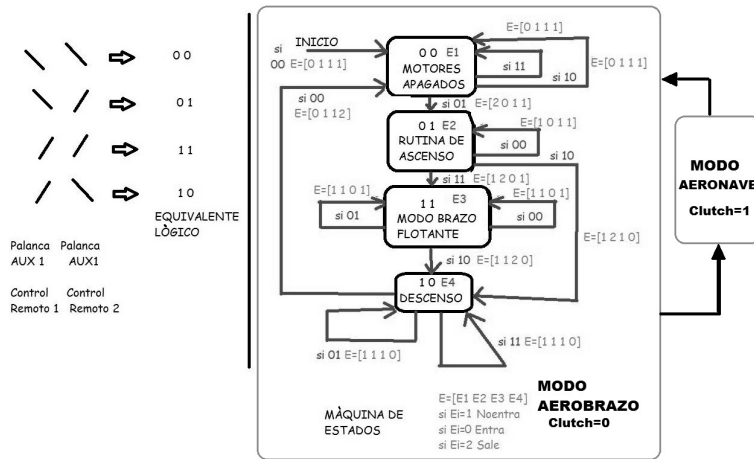


Fig. 3. Máquina de estados del aerobrazo.

llegar al nivel de apagado y también dictaminar un valor en el cual se mude al estado de control.

## 6. Implicaciones computacionales de control modo aeromanipulador

**Restricciones de giro en los motores:** Una vez activado el modo de control, surgen dos importantes implicaciones computacionales, la primera guarda relación al cambio de giro de los motores, es decir mientras el control puede alcanzar cotas positivas y negativas, algunas aeronaves como los cuadricopteros exigen que sus motores no cambien de sentido de giro (para evitar efectos de autorotación), por lo tanto se debe recurrir al problema de optimización descrito en [8,5]:

El cual simplemente expresa eso, el control aplicado a los motores debe mantenerse positivo pese a la variación del error y el control de vuelo.

Ahora bien en caso de disponer variación de sentido de giro, esta no puede realizarse arbitrariamente y sigue consignas de absorción de resultantes, una manera es agregar un motor adicional que contrarreste vectorialmente todas las variaciones negativas de la señal de control de los demás motores [3].

**Jerarquía y calculo en línea del control:** La segunda consiste en recalcular el propio control, el cual como se dijo es de tres tipos, elevación, actitud y plano y saber en que situaciones resulta adecuado dotar de mas importancia a uno respecto a otro, como se dijo el control mas importante es el de altura, pero paradójicamente en la elevación del dron, dada la desigualdad en el bias de empuje de cada motor, el mas importante es el de actitud, otro ejemplo es en las tareas acrobáticas y agresivas [25,23] en este caso se debe discernir y diseñar si

la tarea tiene prioridad por la conservación de ángulo o por la de posición planar [26].

**Optimización de sobreactuación:** Otra implicación computacional de control es la de sobreactuación (mas motores que grados de libertad): en este caso la matriz que transfiere el control cartesiano 6D (3 dimensiones de traslación y 3 de rotación), debe transformarse a control de velocidades en cada propela, si por ejemplo tenemos un sistema de 2 cuadricopteros, son 8 propelas por lo cual las matrices de transformación exigen métodos de optimización como los basados en pseudoinversas y además respetar las restricciones descritas en los párrafos precedentes.

## 7. Implicaciones computacionales de descenso modo compartido

El descenso es otra operación simple pero delicada, consiste en apagar paulatinamente los motores pero cuidando que estos se mantenga en su modo de sustentación (es decir que posean suficiente fuerza para garantizar que el sistema no se desplome), como fue dicho, los motores no tienen un bias homogéneo por lo cual el control de orientación cobra mayor prioridad en este modo de operación, tal y como es exagerado en el cine y la tv, el proceso implica escalones de encendido y apagado, cuando se nota un desplome severo, se aplica un impulso de elevación y así hasta tocar suelo, la complejidad computacional consiste en mantener operativos los sensores y actuadores en tiempos precisos que garanticen un descenso suave y además no destructivo.

## 8. Conclusiones

En este documento se muestran las implicaciones computacionales mas frecuentes encontradas en el diseño del aerobrazo y también encontradas en proyectos semejantes [3,5,6], estas se subdividen en distintas tareas y se muestran al lector como un conjunto de módulos a considerar y resolver si se pretende realizar manipulación aérea coordinada.

Asimismo se da énfasis en la necesidad de poseer sistemas RTOS desde nivel moderado hasta estricto en función de la tarea a ejecutarse, de esta forma se sugiere utilizar sistemas aéreos de navegación embebida como el Pixhawk, Erlebrain o NavIO, microcontroladores dedicados o bien FPGAs o microprocesadores y decantar opciones de tarjetas de desarrollo básicas (Arduino, Raspberry), de hecho este fue el motivo de la evolución del APM al Pixhawk, el primero basado en un Arduino y el segundo basado en un microprocesador Cortex M4F.

**Agradecimientos.** Los autores agradecen a la Secretaría de Investigación y Posgrado del Instituto Politécnico Nacional, y sus correspondientes proyectos SIP y BEIFI, asimismo a la DGAPA-UNAM y a COFAA-IPN.

## Referencias

1. Tognon, M., Franchi, A.: Control of motion and internal stresses for a chain of two underactuated aerial robots. In: Control Conference (ECC), 2015 European, IEEE (2015) 1620–1625
2. Naldi, R., Forte, F., Marconi, L.: A class of modular aerial robots. In: Decision and Control and European Control Conference (CDC-ECC), 2011 50th IEEE Conference on, IEEE (2011) 3584–3589
3. Nikou, A., Gavrilidis, G.C., Kyriakopoulos, K.J.: Mechanical design, modelling and control of a novel aerial manipulator. In: Robotics and Automation (ICRA), 2015 IEEE International Conference on, IEEE (2015) 4698–4703
4. Mellinger, D., Shomin, M., Michael, N., Kumar, V.: Cooperative grasping and transport using multiple quadrotors. In: Distributed autonomous robotic systems. Springer (2013) 545–558
5. Park, S., Her, J., Kim, J., Lee, D.: Design, modeling and control of omni-directional aerial robot. In: Intelligent Robots and Systems (IROS), 2016 IEEE/RSJ International Conference on, IEEE (2016) 1570–1575
6. Zhao, M., Kawasaki, K., Chen, X., Kakiuchi, Y., Okada, K., Inaba, M.: Transformable multirotor with two-dimensional multilinks: Modeling, control, and whole-body aerial manipulation. In: International Symposium on Experimental Robotics, Springer (2016) 515–524
7. Nguyen, H.N., Park, S., Lee, D.: Aerial tool operation system using quadrotors as rotating thrust generators. In: Intelligent Robots and Systems (IROS), 2015 IEEE/RSJ International Conference on, IEEE (2015) 1285–1291
8. Choi, F.: Modeling and control of asymmetrically coupled quadrotor uavs. Master's thesis, Seoul National University (2015)
9. Mendoza-Mendoza, J., Sepulveda-Cervantes, G., Aguilar-Ibanez, C., Mendez, M., Reyes-Larios, M., Matabuena, P., Gonzalez-Avila, J.: Air-arm: A new kind of flying manipulator. In: Research, Education and Development of Unmanned Aerial Systems (RED-UAS), 2015 Workshop on, IEEE (2015) 278–287
10. authors, S.: Pixhawk webpage. <https://pixhawk.org/> (2010) Acces 18-08-2017.
11. authors, S.: Ardupilot libraries webpage. <http://ardupilot.org/dev/docs/apmcopter-programming-libraries.html> (2010) Acces 18-08-2017.
12. Meier, L., Tanskanen, P., Fraundorfer, F., Pollefeys, M.: Pixhawk: A system for autonomous flight using onboard computer vision. In: Robotics and automation (ICRA), 2011 IEEE international conference on, IEEE (2011) 2992–2997
13. Fresk, E., Nikolakopoulos, G., Gustafsson, T.: A generalized reduced-complexity inertial navigation system for unmanned aerial vehicles. *IEEE Transactions on Control Systems Technology* **25**(1) (2017) 192–207
14. Santana, L.V., Brandao, A.S., Sarcinelli-Filho, M.: Outdoor waypoint navigation with the ar. drone quadrotor. In: Unmanned Aircraft Systems (ICUAS), 2015 International Conference on, IEEE (2015) 303–311
15. Quan, Q.: INTRODUCTION TO MULTICOPTER DESIGN AND CONTROL. Springer (2017)
16. Páscoa, J., Dumas, A., Trancossi, M., Stewart, P., Vucinic, D.: A review of thrust-vectoring in support of a v/stol non-moving mechanical propulsion system. *Open Engineering* **3**(3) (2013) 374–388
17. Rajappa, S., Ryll, M., Bühlhoff, H.H., Franchi, A.: Modeling, control and design optimization for a fully-actuated hexarotor aerial vehicle with tilted propellers. In: Robotics and Automation (ICRA), 2015 IEEE International Conference on, IEEE (2015) 4006–4013

18. Ryll, M., Bühlhoff, H.H., Giordano, P.R.: Modeling and control of a quadrotor uav with tilting propellers. In: Robotics and Automation (ICRA), 2012 IEEE International Conference on, IEEE (2012) 4606–4613
19. Carrillo, L.R.G., López, A.E.D., Lozano, R., Pégard, C.: Quad rotorcraft control: vision-based hovering and navigation. Springer Science & Business Media (2012)
20. Valavanis, K.P., Vachtsevanos, G.J.: Handbook of unmanned aerial vehicles. Springer Publishing Company, Incorporated (2014)
21. Schafroth, D., Bermes, C., Bouabdallah, S., Siegwart, R.: Micro helicopter steering: Review and design for the mufly project. In: Mechatronic and Embedded Systems and Applications, 2008. MESA 2008. IEEE/ASME International Conference on, IEEE (2008) 216–221
22. Torenbeek, E., Wittenberg, H.: Flight physics: essentials of aeronautical disciplines and technology, with historical notes. Springer Science & Business Media (2009)
23. Mellinger, D., Kumar, V.: Minimum snap trajectory generation and control for quadrotors. In: Robotics and Automation (ICRA), 2011 IEEE International Conference on, IEEE (2011) 2520–2525
24. Al-Rawashdeh, Y.M., Elshafei, M., Al-Malki, M.F.: In-flight estimation of center of gravity position using all-accelerometers. Sensors **14**(9) (2014) 17567–17585
25. Lee, T., Leoky, M., McClamroch, N.H.: Geometric tracking control of a quadrotor uav on se (3). In: Decision and Control (CDC), 2010 49th IEEE Conference on, IEEE (2010) 5420–5425
26. Mellinger, D., Michael, N., Kumar, V.: Trajectory generation and control for precise aggressive maneuvers with quadrotors. The International Journal of Robotics Research **31**(5) (2012) 664–674

# Lumped Parameter Estimation of a Stochastic Process of Second Order Using the Second Moment and Recursiveness

Romeo Urbietta Parrazales<sup>1</sup>, José de Jesús Medel Juárez<sup>1</sup>, Karen Alicia Aguilar Cruz<sup>1</sup>,  
Rosaura Palma Orozco<sup>2</sup>

<sup>1</sup> Centro de Investigación en Computación - Instituto Politécnico Nacional, CDMX,  
Mexico

<sup>2</sup> Escuela Superior de Cómputo - Instituto Politécnico Nacional, CDMX,  
Mexico

rurbietta700@gmail.com, jjmedelj@yahoo.com.mx, karen\_ali320@hotmail.com,  
rpalma@ipn.mx

**Abstract.** In this article, a stochastic algorithm is briefly presented based on the one of second moment applied to a stochastic process model of second order. The design initially consisted in formulating the state equation model and the stochastic outputs, in order to apply the second moment using the internal product of Martingale and the stochastic operators of the expectation, variance and covariance. The design results generated the formulas on: the covariances and the internal product variances to calculate the lumped estimation parameters, the error functional based on the mean quadratic error, the output variable as a function of the estimation parameters obtained. Furthermore, the recursive form was formulated in this design starting from the premise of the obtained results using the second stochastic moment. The main interest lays on the recursive form, because this is the one capable of being implemented in a digital system. In order to observe the precision and the convergence of the estimation parameters and the output variables, Matlab-based figures are shown.

**Keywords:** Linear stochastic systems, parameter estimation, second moment.

## 1 Introduction

The random input and output variables of a noisy process can be modeled by means of experimental data obtained from measurements carried out during time intervals  $T$ . These models are called Black Box Models (Fig. 1) [1, 2].

The Black Box Models are called this way, because their internal states are not known. One method to determine these unknown states starting from observable states are the so called methods of identified states based on the mean quadratic error [3].

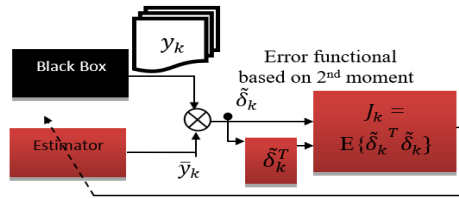


Fig. 1. Stochastic Estimation based on the second moment.

The method relies on turning the unknown or non-measurable states  $x_k$  into an identified state  $\hat{x}_k$  by means of the stochastic conditions of the observable state  $y_k$ , based on the identified error (1):

$$\tilde{\delta}_k = y_k - \bar{y}_k. \quad (1)$$

The error can lead to different methods of stochastic estimation and is hereby known as the innovation process.

The error functional from the identification error  $\tilde{\delta}_k$  using the second moment of probability, is defined as the expected value of the Euclidean norm of  $\tilde{\delta}_k$  [4, 5, 6]:

$$J_k(\tilde{\delta}_k) = E\{\tilde{\delta}_k^T \tilde{\delta}_k\} = (y_k - \bar{y}_k)^T (y_k - \bar{y}_k). \quad (2)$$

On the other hand, within the linear stochastic model, the observable state was represented by means of finite differences equations of 2<sup>nd</sup> order (3):

$$\frac{d^2 f(y)}{dy^2} \cong (f(y) - 2f(y(k-1)) + f(y(k-2))). \quad (3)$$

As it can be observed in (1) a system of this type has two delays and a negative sign in one of its parameters [7, 8, 9, 10, 11].

As we mentioned before, based on a second order state and a quadratic mean of second moment, the main purposes of this work are to design the estimation state based on this second moment, further on, to identify the stochastic output variable and finally, to determine the precision by means of the error functional. Additionally, the parameters and the variables of interest will be plotted.

This article was structured in the following manner: abstract, second moment, stochastic recursive algorithm, quadratic mean error functional, experiment, conclusions and bibliography.

## 2 Simplified Stochastic Output Model.

Like it was said in this introduction, a stochastic system based on noisy output and input measurements taken during a certain number of time intervals  $T$ , can adopt the following linear model in differences like the state equation (4) with stochastic output (5) [9, 10]:

$$x_{k+1} = a_1 x_k + a_2 x_{k-1} + b w_k, \quad (4)$$

$$y_k = c x_k + d v_k. \quad (5)$$

Delaying (4) and (5) we have (6) and (7) respectively

$$x_k = a_1 x_{k-1} + a_2 x_{k-2} + b w_{k-1}, \quad (6)$$

$$y_{k-1} = c x_{k-1} + d v_{k-1}. \quad (7)$$

Now, solving for the delayed state from (7) yields (8), and delaying (8) gives (9):

$$x_{k-1} = c^{-1} y_{k-1} - d c^{-1} v_{k-1}, \quad (8)$$

$$x_{k-2} = c^{-1} y_{k-2} - d c^{-1} v_{k-2}. \quad (9)$$

Substituting (8) and (9) in (6) gives (10). Besides, substituting (10) in (5) yields (11):

$$x_k = a_1 c^{-1} y_{k-1} + a_2 c^{-1} y_{k-2} - a_1 d c^{-1} v_{k-1} - a_2 d c^{-1} v_{k-2} + b w_{k-1}, \quad (10)$$

$$y_k = a_1 y_{k-1} + a_2 y_{k-2} - a_1 d v_{k-1} - a_2 d v_{k-2} + b c w_{k-1} + d v_k. \quad (11)$$

And from (11) the noise is (12) leading to the simplified stochastic output (13):

$$V_k = -a_1 d v_{k-1} - a_2 d v_{k-2} + b c w_{k-1} + d v_k, \quad (12)$$

$$\bar{y}_k = a_1 y_{k-1} + a_2 y_{k-2} + V_k. \quad (13)$$

### 3 Stochastic Algorithm Based on the Second Moment

The second moment is a technique used in probability theory to demonstrate that a random variable (RV) has a positive probability. Generally, the method consists in delimiting the probability that a RV fluctuates away from its mean. The method involves a comparison of the second moment of the RV and the square of the first moment. Hence:  $\mu_2 = E((Y - \mu)^2)$ , where Y is the RV and  $\mu$  is the mean [12].

From (13), we can obtain (14), that is (15), where  $\bar{a} = [a_1 \ a_2]$ , and  $\bar{z}_{k-1} = [y_{k-1}; y_{k-2}]^T$ :

$$y_k = \bar{a} \bar{z}_{k-1} + V_k, \quad (14)$$

$$y_k = [a_1 \ a_2] [y_{k-1} \ y_{k-2}]^T + V_k, \quad (15)$$

Taking the second moment of probability from (14) for the variable  $z_{k-1}^T$  [13, 14], we have (16), that once solved gives (17):

$$E\{y_k \bar{z}_{k-1}^T\} = \bar{a} E\{\bar{z}_{k-1} \bar{z}_{k-1}^T\} + E\{V_k \bar{z}_{k-1}^T\}, \quad (16)$$

$$E\{y_k \bar{z}_{k-1}^T\} - E\{V_k \bar{z}_{k-1}^T\} = \bar{a} E\{\bar{z}_{k-1} \bar{z}_{k-1}^T\}. \quad (17)$$

Here is the estimated parameter based on the second moment (18):

$$\bar{a}_k = (E\{y_k \bar{z}_{k-1}^T\} - E\{V_k \bar{z}_{k-1}^T\})(E\{\bar{z}_{k-1} \bar{z}_{k-1}^T\})^+. \quad (18)$$

From (18), the stochastic estimated parameter is defined as a direct function to the covariance  $p_k$ , and inverse to the covariance  $q_k$  as indicated in (19):

$$\bar{a}_k \triangleq \frac{p_k}{q_k}, \quad (19)$$

where,  $\bar{a}_k$ ,  $p_k$ , and  $q_k$  are vectors of 1x2, 1x2 and 2x2 dimensions, respectively.

To calculate the covariances  $p_k$  and  $q_k$ , the stochastic covariance is represented by the expectation of the internal products of the output variable, which is convoluted with the same output, but now with a delay, (20) [11]:

$$[\bar{p}_{1,k} \quad \bar{p}_{2,k}] = E(\{y_k \bar{z}_{k-1}^T\} - \{V_k \bar{z}_{k-1}^T\}). \quad (20)$$

The stochastic expectation comes represented as a sequence from zero to k samples and is expressed by means of a sum [15] as it can be seen in (21):

$$[\bar{p}_{1,k} \quad \bar{p}_{2,k}] = \frac{1}{k} [\sum_{i=0}^k ([y_i y_{i-1} \quad y_i y_{i-2}] - [V_i y_{i-1} \quad V_i y_{i-2}])]. \quad (21)$$

Solving the sums from 0 to k samples, the two vectors of the covariances [13]  $p_{1,k}$  and  $p_{2,k}$ , are obtained as in (22):

$$[\bar{p}_{1,k} \quad \bar{p}_{2,k}] = \frac{1}{k^2} [y_k y_{k-1} - V_k y_{k-1} + (k-1)^2 \bar{p}_{1,k-1} \quad y_k y_{k-2} - V_k y_{k-2} + (k-1)^2 \bar{p}_{2,k-1}]. \quad (22)$$

While the covariance  $q_k$  comes expressed as a quadratic matrix of 2x2 (23), in this case, the matrix turns out to be singular yielding into a pseudoinverse matrix.

$$\begin{aligned} & \begin{bmatrix} \bar{q}_{11,k} & \bar{q}_{12,k} \\ \bar{q}_{21,k} & \bar{q}_{22,k} \end{bmatrix} = E\{\bar{z}_{k-1} \bar{z}_{k-1}^T\} \\ & = E \left\{ \begin{bmatrix} y_{k-1} \\ y_{k-2} \end{bmatrix} \begin{bmatrix} y_{k-1} & y_{k-2} \end{bmatrix} \right\} = E \begin{bmatrix} y_{k-1}^2 & y_{k-1} y_{k-2} \\ y_{k-2} y_{k-1} & y_{k-2}^2 \end{bmatrix}. \end{aligned} \quad (23)$$

Solving for the expectation operator over the internal product, the covariances matrix  $q_k$  is obtained in (24):

$$\begin{bmatrix} q_{11,k} & q_{12,k} \\ q_{21,k} & q_{22,k} \end{bmatrix} = \frac{1}{k^2} \sum_{i=0}^k \begin{bmatrix} y_{i-1}^2 & y_{i-1} y_{i-2} \\ y_{i-2} y_{i-1} & y_{i-2}^2 \end{bmatrix}. \quad (24)$$

Now, by inserting the sums into each one of the terms within the pseudoinverse matrix, the result is (25).

Developing the samples in each one of the sums from 0 to k samples leads to obtain the sequential form of each one of the components of the pseudoinverse matrix (26) of the covariance  $q_k$ .

$$\begin{bmatrix} \bar{q}_{11,k} & \bar{q}_{12,k} \\ \bar{q}_{21,k} & \bar{q}_{22,k} \end{bmatrix} = \frac{1}{k^2} \begin{pmatrix} \sum_{i=0}^k y_{i-1}^2 & \sum_{i=0}^k y_{i-2}y_{i-1} \\ \sum_{i=0}^k y_{i-1}y_{i-2} & \sum_{i=0}^k y_{i-2}^2 \end{pmatrix}, \quad (25)$$

$$\begin{bmatrix} \bar{q}_{11,k} & \bar{q}_{12,k} \\ \bar{q}_{21,k} & \bar{q}_{22,k} \end{bmatrix} = \frac{1}{k^2} \begin{pmatrix} q_{11,k} & q_{12,k} \\ q_{21,k} & q_{22,k} \end{pmatrix}, \quad (26)$$

where the components of the pseudoinverse matrix are (27):

$$q_{11,k} = y_{k-1}^2 + (k-1)^2 q_{11,k-1}; \quad q_{12,k} = y_{k-2}y_{k-1} + (k-1)^2 q_{12,k-1}, \quad (27)$$

$$q_{21,k} = y_{k-1}y_{k-2} + (k-1)^2 q_{21,k-1}; \quad q_{22,k} = y_{k-2}^2 + (k-1)^2 q_{22,k-1}.$$

The equation (25) can be divided into two components as in (28):

$$\left(\frac{1}{k^2}\right) \begin{pmatrix} y_{k-1}^2 & y_{k-1}y_{k-2} \\ y_{k-1}y_{k-2} & y_{k-2}^2 \end{pmatrix} + (k-1)^2 \begin{bmatrix} \bar{q}_{11,k-1} & \bar{q}_{12,k-1} \\ \bar{q}_{21,k-1} & \bar{q}_{22,k-1} \end{bmatrix}. \quad (28)$$

The estimated parameter using the second moment expressed in (18), (21) and (26) is presented in (29):

$$\bar{a}_k = [\bar{a}_{1,k} \quad \bar{a}_{2,k}] = [\bar{p}_{1,k} \quad \bar{p}_{2,k}] \begin{bmatrix} \bar{q}_{11,k} & \bar{q}_{12,k} \\ \bar{q}_{21,k} & \bar{q}_{22,k} \end{bmatrix}^+, \quad (29)$$

where  $\bar{a}_k$  and  $p_k$ , are matrices of dimensions: 1x2, while  $q_k$  is a matrix of dimension: 2x2, and is also a pseudoinverse [16]. Then, the simplified stochastic output  $\hat{y}_k$  of (13) respect to the estimation parameter of second moment  $\bar{a}_k$  ends up being (30):

$$\bar{y}_k = \bar{a}_1 y_{k-1} + \bar{a}_2 y_{k-2} + \bar{V}_k. \quad (30)$$

#### 4 Recursive Stochastic Estimation Algorithm

From (19), the covariance  $p_k$  can be obtained as the matrix (31) of 1x2 being a function of the covariance  $q_k$ .

$$\begin{aligned} [\hat{p}_{1,k} \quad \hat{p}_{2,k}] &= \frac{1}{k} ( y_k y_{k-1} - V_k y_{k-1} \quad y_k y_{k-2} - V_k y_{k-2} \\ &+ (k-1) [\bar{q}_{1,k-1} \bar{a}_{1,k-1} \quad \bar{q}_{2,k-1} \bar{a}_{2,k-1}] ). \end{aligned} \quad (31)$$

Using (18) to calculate the estimation parameter, together with (22) and (25) we get (32), then, the stochastic output based on the recursive second moment is (33).

$$\hat{a}_k = [\hat{a}_{1,k} \quad \hat{a}_{2,k}] = [\hat{p}_{1,k} \quad \hat{p}_{2,k}] \begin{bmatrix} \bar{q}_{11,k} & \bar{q}_{12,k} \\ \bar{q}_{21,k} & \bar{q}_{22,k} \end{bmatrix}^+, \quad (32)$$

$$\hat{y}_k = \hat{a}_1 y_{k-1} + \hat{a}_2 y_{k-2} + \hat{V}_k. \quad (33)$$

## 5 Functional of Mean Quadratic Error

The mean quadratic error functional is a measurement to accurately know about the estimation parameter convergence by means of the errors between the normal parameter and the one from the second stochastic moment [18]. Considering the parametric error 1 (34), parametric error 2 (35), error functional 1 (36), and error functional 2 (37):

$$\bar{e}_{1,k} = a_{1,k} - \bar{a}_{1,k}, \quad (34)$$

$$\bar{e}_{2,k} = a_{2,k} - \bar{a}_{2,k}, \quad (35)$$

$$\bar{J}_{1,k} = \left(\frac{1}{k^2}\right) [\bar{e}_{1,k}^2 + (k-1)^2 \bar{J}_{1,k-1}], \quad (36)$$

$$\bar{J}_{2,k} = \left(\frac{1}{k^2}\right) [\bar{e}_{2,k}^2 + (k-1)^2 \bar{J}_{2,k-1}]. \quad (37)$$

The recursive form has utmost importance, because it generally gives proof of precision between the stochastic estimation parameters and the ones based on the second moment, which are meant to be implemented in a digital system. Considering parametric error 1(38), parametric error 2 (39), error functional 1 (40), error functional 2 (41).

$$\hat{e}_{1,k} = a_{1,k} - \hat{a}_{1,k}, \quad (38)$$

$$\hat{e}_{2,k} = a_{2,k} - \hat{a}_{2,k}, \quad (39)$$

$$\hat{J}_{1,k} = E\{\hat{e}_{1,k}^2\} = \left(\frac{1}{k^2}\right) [\hat{e}_{1,k}^2 + (k-1)^2 \hat{J}_{1,k-1}], \quad (40)$$

$$\hat{J}_{2,k} = E\{\hat{e}_{2,k}^2\} = \left(\frac{1}{k^2}\right) [\hat{e}_{2,k}^2 + (k-1)^2 \hat{J}_{2,k-1}]. \quad (41)$$

## 6 Experiment

The stochastic estimation algorithm based on the second moment is meant to be placed as an example.

For the stochastic process the considered parameters are  $a1=0.1+i0.05i$ ;  $a2=-0.1+0.05$ ;  $b=0.002$ ;  $c=1$ ;  $d=0.003$ .

The identification of the system variable is presented by means of the Fig. 2 and Fig. 3. Where the first fifteen samples of the output responses are matched and hence, tend to be confused with each other. For the recursive case, the identification of the output variables is achieved more quickly. The graphs of the experiment were carried out using Matlab [19, 20].

For a second stage the initial conditions of the recursive stochastic estimation algorithm, for (26) and (27) are:  $pr1(2)=0.003$ ;  $pr2(2)=0.001$ ;  $anr1(2)=0.05$ ;  $anr2(2)=0.05$ . Implementing this values, the result for the parameter estimation is seen in Fig. 4.

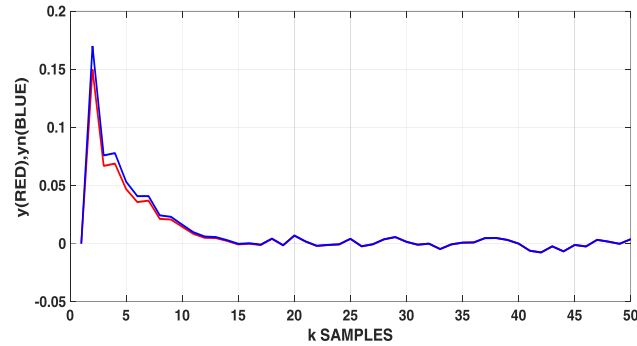


Fig. 2. Stochastic simplified output variable identification.

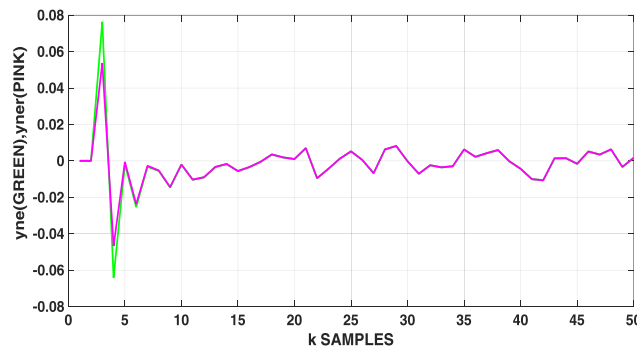


Fig. 3. Stochastic recursive outputs variable identification.

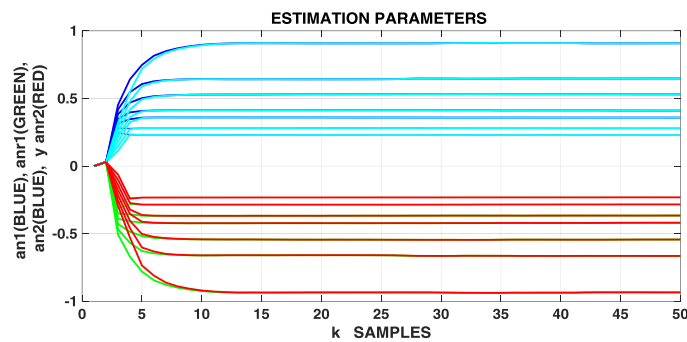
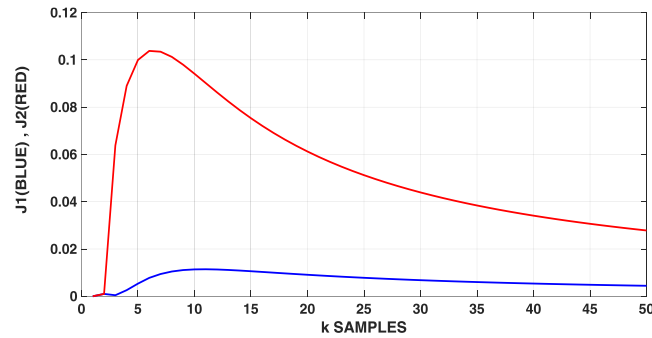


Fig. 4. Estimated stochastic parameters based on the second moment  $\bar{a}_1$  and  $\bar{a}_2$  from Eq. (29) and recursive stochastic calculated parameters  $\hat{a}_1$  and  $\hat{a}_2$  from Eq. (32).

To have a better idea of the convergence we use the error functional to measure the convergence level for both estimated parameters. The initial conditions for the mean quadratic error functional based on the second moment and the recursiveness, Eqs. (30) and (31) together with (34) and (35), respectively are the following: second mo-

ment:  $J1(2)=0.0004$ ;  $J2(2)=0.0004$  and recursiveness:  $Jr1(2)=0.0004$ ;  $Jr2(2)=0.0004$ . Results are shown in Fig. 5 and Fig. 6.



**Fig. 5.** Graph 6. Error functional of second moment  $\bar{J}_1$  in blue colour and  $\bar{J}_2$  in red colour. Remark: Here we deal with a Super Martingale.

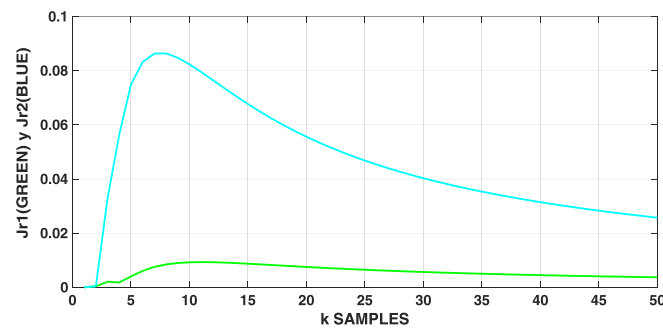


**Fig. 6.** Graph 7. Error functional of second moment  $\bar{J}_1$  in green colour and  $\bar{J}_2$  in sky-blue colour. Remark: Here we deal again with a Super Martingale.

## 7 Conclusions

The main objective of making the convergence of the two estimation parameters of states  $\bar{a}_k$ , based on the estimation algorithm using the second moment, into the value lost by the parameters of the linearly modelled stochastic states was fulfilled.

The found estimation parameters for the second moment were only able to locate the convergence, when they were subjected to a sign inversion, just as it is described in (1). The convergence range of the estimation parameters did work only within  $0 < \bar{a}_k < 1$ . The paths of the estimation parameters were always of the Super Martingale form.

The fireproof took place, when the estimation parameters of this proposed algorithm were replaced at the output variable and it was noticed that the experimentally measurable random data was perfectly compared with the *a priori* data.

Due to the previous acknowledgements, we come up with the conclusion that the estimation algorithm based on the second moment applied to a random experimental model and represented by a linear stochastic second order model worked out properly.

Also, it was possible to design and simulated experiment with a recursive estimator model  $\hat{a}_k$ , starting with the estimator based on the second moment, whose objective in the future is to be placed at the disposal of whomever wants to implement it on a digital system by only having experimental data of random systems.

**Acknowledgments.** The authors would like to thank the Instituto Politécnico Nacional, through projects SIP20171418, SIP20170227, and CONACYT, for the support given to carry out this project.

## References

1. Abonyi, J.: Fuzzy Model Identification for Control. Editorial Birhauser, pp. 1–21 (2003)
2. Rivals, I., Personnaz, L.: Black Box Modeling with State Space Neural Networks. (1995)
3. Sinha, A.: Optimal and Robust Control. CRC Press, pp. 179–228 (2007)
4. Lewis, F. L., Xie, L., Popa, D.: Optimal Estimation, Optimal and Robust Estimation. CRC Press, pp. 3–50 (2008)
5. Medel, J., García, C.V.: Estimación de Parámetros Usando la deconvolución y la Pseudo-inversa: Descripción e Implementación Recursiva. Revista de Física 56 (1) 54–60 (2009)
6. Aguado, A., Martínez, M.: Identificación y Control Adaptivo. Cap 2. Prentice Hall (2003)
7. Schiavi, E., Muñoz, A. I.: Métodos en Diferencias Finitas para para la Resolución de Problemas de Contorno. (2007)
8. Rivero, R.: Identificación de Sistemas de Segundo Orden.
9. Elliot, R. J., Aggoun, L., Moore, J. B.: Hidden Markov Models. Estimation and Control. p. 19, Springer (2008)
10. Alavez, J.: Estimación de Parámetros en Ecuaciones Diferenciales Ordinarias. Cap. 1, pp. 1–34.
11. Heij, C., Ran A., van Schagen, F.: Introduction to Mathematical System Theory. In: Linear Systems, Identification and Control, p. 75. Birkhauser Verlag (2007)
12. Hoel, P. G., Port, S. C., Stone, C. J.: Introduction to Probability Theory. Chapter 4, pp. 92–95. Houghton Mifflin Company (1971)
13. Domínguez, J. A., González-Farías, G., Rodríguez-Dagnino, R. M.: Un procedimiento práctico para estimar el parámetro de forma de la distribución Gaussiana Generalizada. p. 6, Centro de Investigación de Matemáticas.
14. Wilfredo Domínguez C. Convergencia Aleatoria en Espacios de Hilbert. PESQUIMAT. Revista de la F.C.M. de la Universidad mayor de San Marcos. Vol. II, No. 1, pp. 69–70. Lima-Perú (Agosto 1999)
15. Debnath, L., Mikusinski, P.: Hilbert Spaces with Applications. Chap. 3, pp 93–135. Elsevier Academy Press (2005)
16. Medel Juárez, J.J., Zagaceta Álvarez, M.T.: Estimación-Identificación como Filtro Digital Integrado: Descripción e Implementación Recursiva. Revista Mexicana de Física 56 (1) 1–8 (Feb. 2010)
17. Rengifo, C. F.: Una Herramienta para Identificación Recursiva de Sistemas Dinámicos. pp. 1–12 (2004)

*Romeo Urbietta Parrazales, José de Jesús Medel Juárez, Karen Alicia Aguilar Cruz, et al.*

18. Santo Orcero, D.: La Matriz Fundamental y la Matriz esencial. Conceptos y aplicaciones. (2002)
19. Lewis, F.L., Xie, L., Popa, D.: Optimal Estimation. In: Optimal and Robust Estimation. Chapter 9, pp. 423–442. CRC Press (2008)
20. Rodríguez del Río, R.: Gráficas con MatLab. Madrid, España.
21. Dukupatti, R.: Analysis and Design of Control Systems Using Matlab. New Age International (2006)
22. Lagunas, M.A.: Procesos Estocásticos y Estimación de Parámetros. Cap. II (2007)
23. Stroock, D.W.: Probability Theory: An Analytic View. Chapter 4. Cambridge University Press (1994)

# A Survey on Computer Science Techniques in the FOREX Market: Models and Applications

Diego Aguilar, Ildar Batyrshin, Oleksiy Pogrebnyak

Centro de Investigación en Computación, Instituto Politécnico Nacional,  
CDMX, México

diego.aguilar.m15@gmail.com, batyr1@cic.ipn.mx, olek@cic.ipn.mx

**Abstract.** In this paper a survey on computer science techniques such as natural language processing, machine learning, data mining, association rules, etc. which are applied on the FOREX market is presented. The main objective of investing in FOREX market is to maximize the profits given a certain period of time. This survey can be useful to researchers in this area, in order to compare and extend previous works.

**Keywords:** time series, Forex, data mining, natural language processing.

## 1 Introduction

### 1.1 Foreign Exchange Market

The Foreign Exchange (FOREX)<sup>1</sup> market is one of the biggest and most liquid<sup>2</sup> markets for investors, trading in average \$5.1 trillion dollars per day in April 2016 [1]. It trades in pairs of currencies, the first coin of the pair is called base currency and is the one that an investor can sell or buy. The second coin is called reference currency and it means the money that an investor is willing to pay or to receive for the base currency.

FOREX is a decentralized market, also know as an Over the Counter (OTC) market. OTC markets are not controlled by any government nor have a physical location, all transactions are made by computer, phone and email orders. OTC trades a great number of listed securities, such as currencies, bonds, and shares of companies that does not meet the requirements to be listed on exchanges such as the New York Stock Exchange (NYSE) or the Bolsa Mexicana de Valores (BMV) exchange in Mexico. There are mainly two forms of trades, one where a dealer trade with institutions or corporations and other intermediate trades between different dealers.

Modeling the economic markets and currency pair market is a difficult task as stated by Rey [2], who published a paper in which the role of a vehicle currency

<sup>1</sup> Some sources also use the FX abbreviation.

<sup>2</sup> A liquid asset is described as one that can be easily exchanged for money, i.e. currencies, shares, bonds, etc.

is studied in order to explore the rise and fall of currencies through the evolution of trades patterns between countries.

## 1.2 The Risk on OTC Markets

OTC markets such as FOREX are considered to have more risk implied on the transactions, due to little or non existent regulations, which make OTC markets less transparent; for this reason many advisors do not recommend this type of market for small and unexperienced investors.

## 1.3 Mexico in the FOREX Market

According to the results given by Bank of Mexico (Banxico), in 2016 the Mexican peso (MXN) was the tenth currency with most trade in the world, and the second one in the list of emerging countries<sup>3</sup>, only behind the Chinese renminbi.

It is recognizing patters using fuzzy logical also important to notice that most of the transactions made with the MXN currency are realized outside of Mexico, besides the US dollar (USD) is the main currency that is traded against the MXN [3].

## 1.4 Trading in FOREX

To make transactions in the FOREX market it is necessary to have an account with a brokerage company; as the OTC market works on networks, it is possible to open an account from other country, but it is recommended to use the most trusty broker one can find, i.e. a broker with the biggest capital liquidity.

## 1.5 Spread

The spread is one of the main subjects in FOREX trading, it is described as the difference between the bid and ask price of a currency<sup>4</sup>, is common to find it in practice as the Bid-Ask Spread. Currency pairs usually have the lowest spread, movements around \$0.0001<sup>5</sup> also known as Pip<sup>6</sup>.

Because there are no commissions on the FOREX transactions, brokers use the spread as a way of making profit, this means the tighter a spread is, the better profit an investor can make. The competition between FOREX brokers is fierce, it is recommendable to shop around for the best prices in currencies<sup>7</sup>.

<sup>3</sup> An emerging market economy is described as one who is progressing into becoming an advanced economy, i.e: Mexico, Brazil, Russia, India, Turkey and China.

<sup>4</sup> The ask price is the money that a seller is asking to receive for a security, conversely the bid price is the money a buyer is willing to pay for a security.

<sup>5</sup> Some currencies trade at movements of \$0.01

<sup>6</sup> A Pip is the equivalent of 1/100 of 1%.

<sup>7</sup> Many variables can affect the spread of a currency pair, such as volatility, high or low demand and also affects the political issues on the base currency country.

## **1.6 Making a Profit on the FOREX Market**

### **1.7 Two Strategies for Trading**

There are mainly two strategies for trading in currencies, shares, bonds, etc. The long and the short position.

#### **Long Position**

The long position is the most common among investors in markets, it follows the principle “Buy low, sell high”, in the FOREX market is the same as buying a currency which an investor thinks is going to appreciate in the future (in FOREX changes may occur in relatively small intervals of time, such as minutes), if the currency price rise then the investor will sell it obtaining a profit from the operation. On the other hand if the currency loss its value the investor could sell it at lower price taking losses.

#### **Short Selling**

The short selling is a strategy in which an investor predicts the value of an asset, such as currency, will drop in the future. In practice an investor could “borrow currencies” from a margin account<sup>8</sup>, the short investor exchange the currency pair, if the prediction is true and the value of the base currency drops such investor could buy the same currency at a lower cost, finally returning it to broker in the margin account.

Short selling is seen as a highly risky strategy, because the maximum profit can be achieved when a base currency drops down to near zero; however, the maximum losses tend to infinity since there is no limit for a currency to appreciate. Thus this strategy is recommended only for experienced investor. The main idea behind short selling is to bet against a security.

## **2 Previous Related Surveys**

In this section, previous survey related to FOREX and financial markets using computer science techniques are described.

Most recently, Kumar et al. [4] performed a survey on applications of text mining in financial domain; it categorized the applications into FOREX rate prediction, stock market prediction, customer relationship management (CRM) and cyber security which were published in the period of 2000-2016. They divide the text mining task into four categories, namely classification, clustering, summarization, topic identification and association rule mining. The survey concluded that more efficient techniques are needed to handle and predict a significant amount of data, also the most frequently used text mining task is classification followed by prediction: one of the purposes is to standardize the performance metrics to compare various works.

<sup>8</sup> Brokerage firms offer margin accounts in which they lend money to investors in order to purchase securities.

Batyrshin et al. [5] presented a survey paper on perception based patterns in time series. They discussed the importance of recognizing patterns using fuzzy logic on time series in order to support decision making processes. In this study they found that most of the decision making procedures in problems on financial and economics are based on human decisions supported by statistics, data mining or data processing software.

The main contributions are the applications that uses fuzzy logic for the description of patterns such as sign derivatives, scaling trends, linguistic interpretations of patterns as result of clustering, relationship between patterns, etc.

This survey includes studies which use financial data, i.e stock prices, news, indicators as well as non-financial data, i.e climate conditions. They conclude that time series data mining along with natural language computation and computing with word and perceptions is an opportunity field for researchers to explore new method and publish new techniques.

Soft computing techniques applied on the stock market where reviewed by Atsalakis et al. [6]. In this research they stated that soft computing techniques are candidate to capture stock market nonlinear relations returning significant forecasting results, the methods included in the survey are mainly neural networks and neuro-fuzzy models with several types of training. The results were compared against conventional models such as artificial neural networks, linear and multi-linear regression, ARIMA models, genetic algorithms, random walk, buy and hold, etc.

Data mining techniques with applications in the stock markets were surveyed by Hajizadeh et al. [7], they stated that data mining techniques in the financial domain are gaining interest from the researchers. One of the most important problems is finding efficient ways to summarize and visualize the stock market data in order to give useful information for investment decisions.

The survey categorized six data mining techniques and its applications on the stock market, namely decision tree, neural networks, clustering, association rules, factor analysis and time series. They conclude that the use of data mining techniques in the financial domains has reached good results and they expect the number of studies in this field increase.

### **3 Review of Computer Science Techniques for the FOREX market**

This survey highlights some applications of computer science which have an application in the FOREX market. These applications are categorized mainly into FOREX rate forecast, up-down movements, trend analysis.

The FOREX rate predictions attempts to give an accurate price of a currency pair in the future, using available data, such as past values of bid/ask quotes.

Due to space limitations most of the mathematical framework of the studies will not be presented.

Nassirtoussi et al. [8] published a research in 2015, in which they classified the future of a currency pair; a binary classification was used, namely POS if a

currency pair will appreciate or NEG if the bid/ask price will drop. The study included a novel system that used text mining, natural language processing, statistical pattern recognition as well as sentiment analysis that predicts the directional movement on currency pairs in the FOREX market on the words used in news headlines in previous hours. The forecast horizon for this study is 1-2 hours as they were working with intra-day trading data, news headlines were obtained from a financial news web page via web service and data from EUR/USD currency pair.

Before the research of Nassirtoussi the idea of forecasting the FOREX rates from news headlines was revised by Peramunetilleke and Wong [9], in their study they proposed that the information contained in news was better in contrast to numeric time series, because they not only contain the effect, but also the possible cause of the event that affects the FOREX rates.

They implemented a new technique that relies on natural language processing, which automatically evaluated the news. The system receives as an input news headlines from Reuters and the output is a categorical forecast divided in three: the dollar moves up, remains steady or goes down within the next one, two or three hours.

The system generates weights for keywords on headlines, then it creates rules that can handle continuous attributes, rather than boolean expressions, to create the rules they use two methods, namely *TFxIDF* which consist in term frequency, discrimination factor and normalization and the *TFxCDF* method which uses category frequencies.

The results they obtained showed that the *TFxCDF* method reaches better results than other methods, it was also compared to a conventional time series analysis tool and two different neural network approaches and outperformed them.

Idvall et al. [10] in their master thesis investigated the use of Markov chains in hidden Markov models with two implemented extensions: a Gaussian mixture model (GMM) and an exponentially weighted expectation maximization (EWEM) in order to create a new way of algorithmic trading which main objective is to increase the profit of the alpha returns on intra-day trading.

They concluded that the use of hidden Markov models on the FOREX markets is still an area of opportunity for researchers. Their model in some settings was able to obtain significance profit, whereas other settings the predictor looked close to a random generator, this was attributed to the great quantity of factors that have to be considered when setting up a model.

They propose that a different machine learning method and improving the initial estimates of the parameters would produce better results. As for the model itself it could be expanded in order to diversify the portfolio of HMM, including different currency pairs, since each pair might depend on different causes thus have different patterns, also the usage of leverage could be advantageous to enhance the profits.

Regarding the machine learning (ML) area, Baasher and Fakhr [11] published an article in which they used ML techniques to forecast the High exchange rate

daily trend; They represented the forecast problem as a binary classification task with the two possible outcomes being uptrend and downtrend. This article used four major currencies, namely USD/YEN, USD/EGP, EUR/EGP, EUR/SAR.

The ML algorithms used for classification were radial basis function (RBF), multilayer perceptron neural network (MLP) and support vector machines (SVM). The results for forecasting of the generalized autoregressive conditional heteroscedasticity (GARCH) were used as part of the feature set, along with other classical technical analysis techniques for time series i.e momentum. Feature selection and extraction method were applied in order to optimize the results given by the ML algorithms. For the comparison analysis, they used the percentage classification performance and a novel function called percentage normalized profit (PNP), which represents the ratio between accumulated profits using the predicted trends versus the accumulated profit using perfect predictions during a test period.

The study concludes that a good feature selection along with regularization on the ML techniques can provide good results, making a profit in the FOREX market.

Karuzzman and Sarker [12,13] published a research on predictions of foreign currencies rates using neural networks with three different learning algorithms, namely Standard Backpropagation (SBP), Scaled Conjugate Gradient (SCG) and Backpropagation with Bayesian Regulation (BPR). They concluded that the SCG learning algorithm outperformed the other models.

In their tests they used moving averaged values to feed the neural network to predict the following week, comparing six currencies against the Australian dollar (AUD), in terms of performance measure the SCG model achieves very close prediction in terms of NMSE and MAE metrics. The Figure 1 shows the results obtained.

Batyrshin et al. [14] proposed a novel definition for a non-statistical measure of time series comovement called “local trend association measure” (*lta*), which is based on an early work the “moving approximation transform” (*mat*) [15]. The *lta* measures positive and negative shape associations between time series.

They conclude that the correlation coefficient is not an useful tool in the analysis of time series shape similarity and shape associations. They realized a comparative analysis between exchange rates with data from Google Finance [16], Figure 2 shows the initial points where the local trends change sign and this can be associated with business events. Also using the approach of “pair of stocks” (or currencies), one can associate pairs which move asynchronous (positively associated) or with inverse movements.

García et al. [17] proposed a method to choose a better sliding window in the moving approximation transform (MAT) [15]. This new method uses the length of a pattern instead of the *cos* function to measure the positive or negative similarity between time series; they also presented a new method to visualize the associations between time series which is easier to understand than the one used in [15,14].

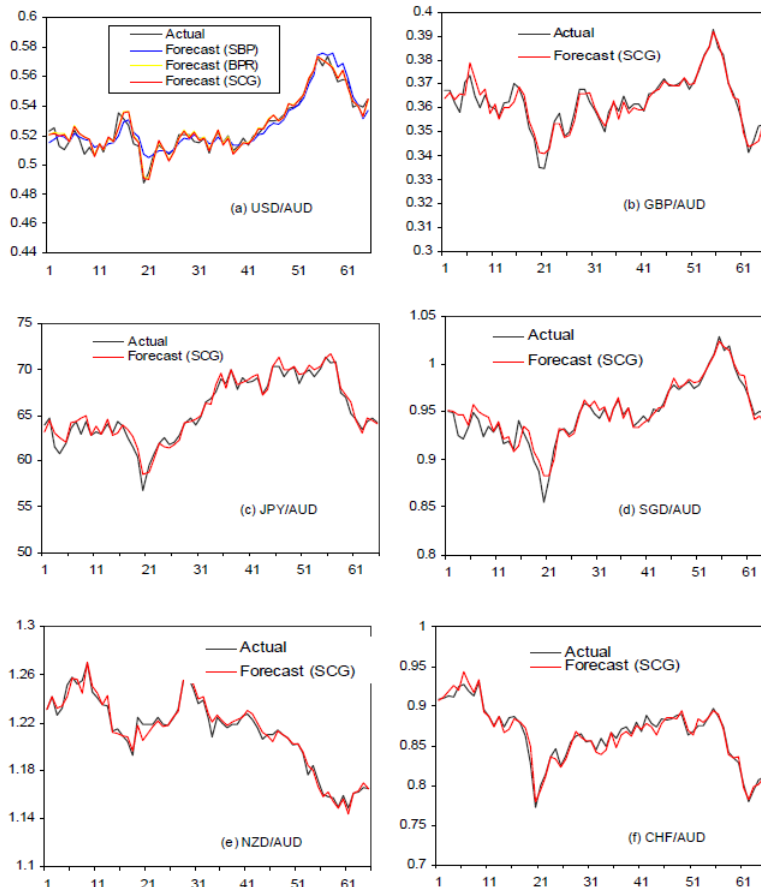


Fig. 1: Forecasting of different currencies by SCG based neural network model over 65 weeks.

Kayacan et al. [18] used gray systems theory-based approaches to predict FOREX rates, because gray systems are more robust with respect to noise which make them ideal to treat the non stationary, and nonlinear time series of FOREX rates.

They used six models in this study, namely GM(1,1), modified GM(1,1) model using modeling errors and Fourier series (EFGM), modified GM(1,1) model at time domain using Fourier series (TFGM), Grey Verhulst model using modeling errors and Fourier series (EFGVM) and Grey Verhulst model at time domain using Fourier series (TFGVM).

The results they obtained were that GM(1,1) models are better on both interpolation and extrapolation when compared to GVM model without using a filter. On the other hand, using a moving average filter (MAF), the performances

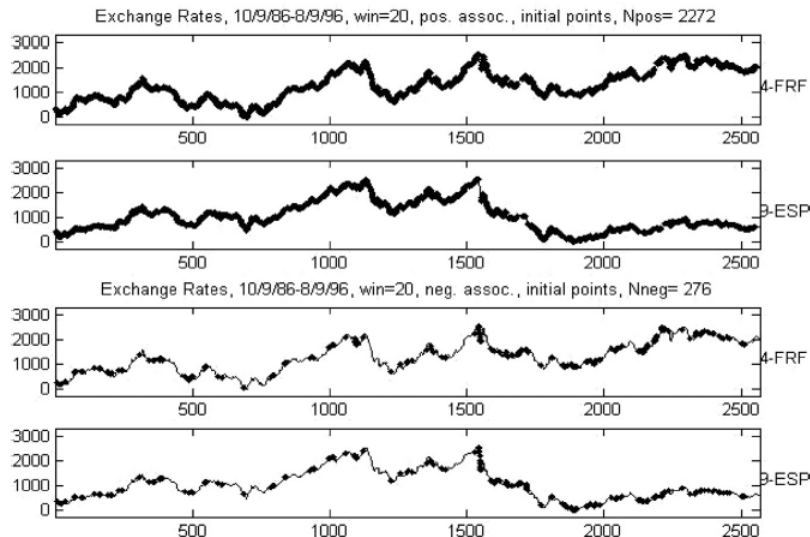


Fig.2: The initial points of positively associated (at the top) and negatively associated (on the bottom) of moving approximations (shown by bold) in sliding window of size 20 of time series 4-FRF and 9-ESP.

of GVM models were increased and the performance of the GM(1,1) model was decreased.

They conclude that the modified GM(1,1) using Fourier series in time domain is the best model fitting and forecasting.

Nieh and Lee [19] revised dynamic relationship between stock prices and exchange rates of the G7 countries. They found that there is no long-run significant relationship between them, on the short-run significant relationship was found for one day in some of G7 countries.

In their research they found that some studies have encountered limited success in identifying a significant correlation between stock prices and currency's fluctuations. The authors implemented various test to explore the dynamic relationships, such as Engle-Granger (EG) and Johansen maximum likelihood cointegration; they applied the vector error correction model (VECM) as an appropriate framework to assess both the short-run inter-temporal co-movement and their long-run equilibrium relationship.

The data they used consisted in stock prices and foreign exchange rates for the G7 countries, namely Canada, France, Germany, Italy, Japan, UK and the US. They concluded that these two financial variables do not have predictive capabilities for more than two consecutive trading days; they stated that from a practical view the investors believed that stock prices and exchange rates can serve as instruments to predict the future of each other, but the VECM only shows that one day prediction power of these two financial assets for certain

G7 countries. Moreover, the significant long-run outlook implies that these two assets share no common trends in their economy system.

A study in 2011 by Li, Bin et al. [20] showed the existence of seasonality in the FOREX market, they studied eight currency, namely the Canadian dollar, EUR, Japanese yen, Swiss franc, Swedish krona, British pound, Australian dollar and New Zealand dollar; which are traded against the USD. They used statically test to measure the returns month by month of the currencies in the years from 1972 to 2010.

The researchers found that five currencies exhibit significantly higher returns in the month of December and a significant reversal in January, this is maybe due to the effect of the “January effect”; this is a commonly know effect in the stock market but this study also detects its presence in the FOREX market.

The study only used hard data and statistics to obtain these results, as for the source of this seasonality effect in the months of December and January is remarked as an open opportunity for other researchers to provide new findings.

## 4 Conclusions

This survey presents a review of computer science techniques for the FOREX market from the year 2000 up to date. The presented applications are mainly focused to rates forecast using a diverse variety of techniques, from natural language processing and statistical models to machine learning algorithms. In our study we found that:

- Since 2000 many researchers have been gaining interest in analyzing the FOREX market in order to obtain better profits.
- Due to the FOREX market being an OTC market the studies we found uses different databases, which makes difficult to compare results between them, so we propose to standardize the data used for benchmark, or even create a public repository of FOREX rates and news in order to have a comparison of results.
- The foreign exchanges rates are moistly noisy, non-stationary and chaotic, for this reason many researchers have choose to use machine learning and data mining techniques.
- The main task in FOREX market is to forecast the exchange values in order to generate a bigger profit, but since there are no official benchmarks is difficult to compare results between studies.

## References

1. Bank of International Settlement: Triennial Central Bank Survey - Foreign exchange turnover in April 2016, Monetary and Economic Department (2016)
2. Rey, H.: International trade and currency exchange. *The Review of Economic Studies* 68(2):443–464 (2001)

3. Banco de México: Resultados de la encuesta realizada por el Banco de Pagos Internacionales (BIS) sobre volúmenes de operación en los mercados cambiarios y de derivados durante abril de 2016 (2016)
4. Shravan, K., Ravi, V.: A survey of the applications of text mining in financial domain. *Knowledge-Based Systems* 114. pp. 128–147 (2016)
5. Batyrshin, I. Z., Sheremetov, L., Herrera-Avelar, R.: Perception based patterns in time series data mining. *Perception-based Data Mining and Decision Making in Economics and Finance*. pp. 85–118 (2007)
6. Atsalakis, G.S., Kimon P. V.: Surveying stock market forecasting techniques Part II: Soft computing methods. *Expert Systems with Applications* 36(3):5932–5941 (2009)
7. Hajizadeh, E., Ardakani, H. D., Shahrabi, J.: Application of data mining techniques in stock markets: A survey. *Journal of Economics and International Finance* 2(7) (2010)
8. Nassirtoussi, A. K.: Text mining of news-headlines for FOREX market prediction: A Multi-layer Dimension Reduction Algorithm with semantics and sentiment. *Expert Systems with Applications* 42(1):306–324 (2015)
9. Peramunetilleke, D., Wong. R.: Currency exchange rate forecasting from news headlines. *Australian Computer Science Communications* 24(2):131–139 (2002)
10. Idvall, P., Jonsson, C.: Algorithmic trading: Hidden Markov models on foreign exchange data. Master Thesis, Department of Mathematics, Linkopings Universitet (2008)
11. Baasher, A., Fakhr, M. W.: Forex daily trend prediction using machine learning techniques. In: 11th WSEAS Int. Conf. on Applied Computer Science (2011)
12. Kamruzzaman, J., Sarker, R.A.: ANN-based forecasting of foreign currency exchange rates. *Neural Information Processing-Letters and Reviews* 3(2):49–58 (2004)
13. Kamruzzaman, J., Sarker R. A.: Forecasting of currency exchange rates using ANN: A case study. In: *Neural Networks and Signal Processing, Proceedings of the 2003 International Conference on*. Vol. 1. IEEE (2003)
14. Batyrshin, I. Z., Solovyev V., Ivanov V.: Time series shape association measures and local trend association patterns. *Neurocomputing* 175, pp. 924–934 (2016)
15. Batyrshin, I. Z.: Moving approximation transform and local trend associations in time series data bases. In: *Perception-based Data Mining and Decision Making in Economics and Finance*. Springer Berlin Heidelberg, pp. 55–83 (2007)
16. <https://www.google.com/finance>
17. Garcia-Lopez, F. J., Batyrshin I. Z., Gelbukh, A. F.: Similitud de series de tiempo basada en longitud de patrones de la transformada por aproximación móvil. *Research in Computing Science* 115. pp. 79–92 (2016)
18. Kayacan, E., Ulutas, B., Kaynak, O.: Grey system theory-based models in time series prediction. *Expert systems with applications* 37(2):1784–1789 (2010)
19. Nieh, C., Lee, C.: Dynamic relationship between stock prices and exchange rates for G-7 countries. *The Quarterly Review of Economics and Finance* 41(4):477–490 (2002)
20. Li, B.: Monthly seasonality in currency returns. *JASSA* 3, pp. 1972–2010 (2011)

# Armagedroid, APKs Static Analyzer Software

Luis Enrique Héctor Almaraz García, Eleazar Aguirre Anaya,  
Ponciano Jorge Escamilla Ambrosio, Raúl Acosta Bermejo

Instituto Politécnico Nacional, Centro de Investigación en Computación, CDMX,  
Mexico

lalmarazg1400@alumno.ipn.mx, eaguirre@cic.ipn.mx,  
pescamilla@cic.ipn.mx, racostab@ipn.mx

**Abstract.** Armagedroid, a software for static analysis of Android APKs, arises with the objective of assisting in the decision making by the user analyst, who must evaluate, thanks to the metadata obtained by the program, if it is a reliable package or a possible malware application, automating the procedures involved in this type of analysis. Consistent phases of the Armagedroid analysis consider the APK structure, its contents, its manifest file to extract the package, permissions and archive activities using action modules. The result obtained with the use of the tool is the gathered information from each module applied to a benign APK and one with malware, which, once compared, distinguish that the malicious package requests more permissions than the trusted APK and with just having an activity. The contributions of Armagedroid in comparison with other programs of static analysis are: the validation that the file loaded in memory is really an APK, checking its size, obtaining its content and generating the analysis report of the APK which consists of the information of the metadata obtained from the APK: the name, size in bytes, integrity checksums, which are MD5, SHA1 and SHA256, APK content, information of the files it contains, the name of the package, the list of activities and permissions of the APK in order to make the results known to the user.

**Keywords:** APKs, Android, mobiles, applications, static analysis, malware, software.

## 1 Introduction

The rise of the Internet and recently the Internet of Things, it is estimated that there are about 19 billion digital devices connected to it [1], has led to the growth of malware development by cybercriminals, to pursue certain purposes, mainly: data theft, cybercrime, espionage and hacktivism. Each quarter of 2016 found 600 million new samples of malware [2]. Currently, there is malware for all operating systems of personal computers like Windows, Linux and MacOS, to mention a few examples, but also malware has been developed for operating systems of mobile devices, the most attacked are Android and iOS [3].

Malware analysts on different platforms employ 2 types of malware analysis, static analysis and dynamic analysis. Static analysis identifies cryptographic hashes, fingerprints and metadata for a malware, while in the dynamic analysis malware execution is performed to study its behavior [4].

Android has become the operating system mostly used by smartphones, tablets, watches, smart TVs and even some vehicles, so it has caught the attention of malicious attackers to develop malware and take advantage of its users. A new Android application with malware is discovered every 10 seconds [5], it is estimated that by the end of this year 2017, the number of malware for this operating system will reach 3,500,000 samples [5]. These applications are formed by a variant of the Java JAR format, which is called APK [6]. An APK file contains the necessary resources for the installation of APPS, specifically: the manifest file (AndroidManifest.xml), the executable code (classes.dex) the compiled resources of the application (resources.arsc) and the directories of the application.

This paper describes a new approach called Armagedroid that performs the functions of a static analysis, obtaining: package name, size in bytes, integrity check sums, the hash functions MD5, SHA1 and SHA256, APK content, the files it contains, such as comments on them, last modified date, operating system in which they were created, ZIP version used to compress them, their size once they have been compressed and decompressed, the list of activities and permissions of the APK. The development of Armagedroid allows a user to automate the tasks of performing the static analysis of Android APKs that comprises the process of decompilation of the APK, the extraction of its metadata, its directories and files.

The remaining of this document is organized as follows: Section 2 defines the main concepts related to APKs: Android manifest file, package name, permissions, and packaging activities. The existing related works about static analysis of APKs are described in section 3, the phases of the software they developed and the results obtained. The description of the modules of Armagedroid static analysis are presented in section 4, which range from loading the APK, validating it, calculating its integrity checksums, obtaining its contents, decompiling its resources, reading the file of the packaging and the generation of the static analysis report. In section 5 the tests and results obtained by applying the developed software on a benign application and on a malicious APK are presented. Section 6 presents the conclusions reached in the implementation and use of the software, as well as the future scope regarding the improvement of the tool.

## **2 Android Application Packages**

Applications are distributed and installed in the form of packaged application files, called APKs. They are containers that include the code and the resources of the application, as well as the manifest file (containing the permissions of the app).

APK is an extension of the JAVA JAR format, which in turn is an extension of the ZIP format. The contents of an APK are presented in Table 1 [7].

**Table 1.** Contents of an APK and its description.

| Content of an APK   | Description  |
|---------------------|--|
| AndroidManifest.xml | Declares the name of the application package, its version, activities, services, message receivers and content providers that integrate it [8].  |
| Classes.dex         | Contains the executable code of the application in Dalvik VM format which is the file with extension .dex.   |
| Resources.arsc      | It has compiled application resources such as strings and styles.  |
| Assets directory    | It stores unprocessed resources, i.e. those that at the time of generating the APK retain their name and characteristics,  |
| Lib directory       | This directory is present in applications that use native libraries via JNI (Java Native Interface).   |
| Res directory       | Group resources that are directly referenced from the Android code, either directly using the android.content.res.Resources class or indirectly through the high-level APIs, they are split into separate subdirectories for each type of resource (animations, images, menu definitions, etc.). |
| META-INF dir.       | It hosts the package manifest file and signature code.   |

## 2.1 Package that Contains the Android Application

It is the file that works as a unique identifier for the application and contains the classes that implement a specific function once the APK is installed [9]. The example of announcing a package is shown in Fig. 1, see that it begins with the `<manifest package = tag and the name of the package in quotation marks with its tag close >`.

|  |
|--|
| 1. <code>&lt;manifest package="com.example.project"&gt;</code> |
| 2. <code>...</code>  |
| 3. <code>&lt;/manifest&gt;</code>                              |

**Fig. 1.** Declaration of a package in an APK.

## 2.2 Permissions on Android for APKs

They define the access rights of the apps to the resources of the device to perform an action, they can be used to access the hardware, to obtain connectivity to the Internet, to use data of the user or the services of security, memory and processes. Once installed the apps request these permissions through the file [10]. The declaration of a permission is shown in Fig. 2, it should be noted that, in its construction, they start with the label `<uses-permission android: name =` followed by the name of the permission to which the app must access, finally the label is closed with `>`.

```
1. <manifest
xmlns:android="http://schemas.android.com/apk/res
/android"
2.   package="com.android.app.myapplication" >
3.   <uses-permission
android:name="android.permission.RECEIVE_SMS" />
4.   ...
5. </manifest>
```

Fig. 2. Declaration of a permit in an APK.

### 2.3 Activities of an APK

An activity is a component of the application that contains the screens that are presented to the user to interact and perform an action on it, thanks to the methods it implements. The APK developer encodes an activity for each window that is shown to the user.

All activities are declared in the AndroidManifest.xml file to be accessed by the application [11]. Fig. 3 shows the declaration of an activity is done by adding an element *<activity Android: name plus the name of the activity in quotation marks and the closing of the element with >*.

```
1. <manifest ...>
2.   <application ...>
3.     <activity android:name=".ExampleActivity"/>
4.     ...
5.   </application>
6.   ...
7. </manifest>
```

Fig. 3. Declaration of an activity in an APK.

## 3 Works Related to Static Analysis APKs

There have been several publications related to using computational tools to perform static analysis and dynamic analysis in the APKs, however, the focus of this document and the Armagedroid software takes only static analysis as a reference.

A program that performs static analysis extracting the most relevant features of an Android application [12] is performed by means of 4 stages: The first one involves obtaining the APK and decompressing it through APKTool, stage 2 is responsible for extracting the characteristics of the application through the manifest file (AndroidManifest.xml), taking into consideration the actions That request other actions of the different components of the application and also in the categories which contain additional information on the type of component that action must handle, in addition the software considers the permissions of the application, it is assigned a

category to the APK Analyzed in stage 3, according to a classification that the authors previously made with the largest number of permissions present in several applications and in stage 4 the user gives an assessment on the characteristics obtained on the APK and the category that will be assigned. The results that they obtained after analyzing several APKs were a list of categories: communications, games, social networks, utilities, education, multimedia, widgets and trips.

At the University of Technology, they developed a framework that detects malware in Android applications. They use the concept of machine-learning monitoring the permissions of the application and events, in this way, the machine-learning classifier is fed through 4 phases, the first is responsible for extracting the permissions requested by the APK, the second uses the clustering algorithm K-Means to provide information to the classifier, with the permits obtained before, the third phase applies decision tree algorithms to determine if the APK is malware or is benign and in the fourth phase evaluates the accuracy and accuracy of classification by means of true positive, false positive, true negative, false negative, and general accuracy formulas. They obtained 2 sets of data that differentiate between a malware APK and a benign one, the database was composed of a total of 500 malware APK features, which were extracted [13].

At the University of Luxembourg, authors used a set of 50,000 Android applications to feed a machine-learning that classifies a group of features for malware detection [14]. Firstly, the classifier is fed to the classifier with 2 types of sets, the set of APKs obtained from Google Play with a module of the program that is responsible for downloading them and the set of APKs with malware. They take the APK to analyze from which their permissions are obtained, a prediction is obtained thanks to the algorithms of RandomForest, J48, JRip and LibSVM, which, with the support of the characteristics of the machine-learning information, informs if the APK is malware or benign, together with the support of VirusTotal. As results obtained a classification accuracy radius with mean values of 0.94, this implies a better probability to differentiate between benign and malignant APKs.

## **4 Armagedroid System Modules**

This section details the construction and operation of Armagedroid modules. The overview of its components can be seen in Fig. 4 which describes that the software currently has 7 modules of static analysis, which range from loading the APK into memory, validating it, calculating checksums integrity, obtaining information from its contents, Table 1, decompiling, reading the file AndroidManifest.xml and generating the static analysis report.

**a) Module of loading APK in memory:** It is the first phase of the analysis, the user selects the APK between their files; this is possible with the module of loading APK in memory.

**b) Module of validating APK:** A feature that Armagedroid has before executing the following phases of static analysis is to ensure that the selected file, in the previous

phase, is really an APK, for this, it observes the structure of the same and within its content looks for the magic number of the packaging. The magic number of a file is a numeric value that identifies it and associates it with a certain format. In the case of APKs, the magic number is the value represented in hexadecimal as "PK \ x3 \ x4", see the structure of an APK in Fig. 5. If the file does not contain this value, then Armagedroid stops the analysis informing the user that the file is not APK, otherwise, proceed to calculate the size of the it and the condition at this time to continue with the analysis is to calculate its size in bytes, if it turns out to be 0 bytes, the analysis stops and the user is told that the APK size does not allow the analysis.

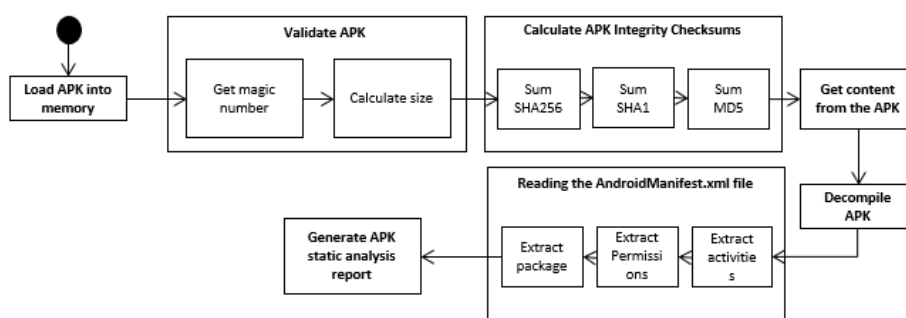


Fig. 4. Modules of Armagedroid analysis.

**c) Module of APK Integrity Checksum Calculation:** As shown in Fig. 4, the system determines 3 integrity check sums of the APK: MD5, SHA1, and SHA256 using the Integrity Checksum calculation module, it uses methods of the Python language, in its version 3, with which the system was implemented, included in the hashlib library, these are: hashlib.md5(), hashlib.sha1() and hashlib.256() respectively, each one receives as input the byte set of the APK, Fig. 5, outputting a 128-bit alphanumeric string for MD5, 160 bits for SHA1 and 256 bits for SHA256.

**d) Module of obtaining the content of the APK:** This module obtains the contents of the same one, the packaging contains the files of the Table 1 and of each one of them are extracted: comments on the same, its last date of modification, operating system in which they were created, version of the used ZIP to compress them, their size once they have been compressed and decompressed. Armagedroid takes this data informing the user analyst what the content of the APK, thus favoring the execution of the module of obtaining its content without the need to add a decompression function of it.

**e) Module of APK decompilation:** It uses the APKTool component for the APK decompilation task, reading the decoded AndroidManifest.xml and obtaining the name of the package, the permissions and activities corresponding to it, in the later stages of the analysis. It results in a directory with the name of the APK and the decompiled files in Table 1, if APKTool is not used, the files would not be readable.

**f) Module of AndroidManifest.xml file reading:** Reading module is responsible for reading the Android manifest file, previously decoded, extracting the package name from the APK, also gets the permissions and activities that compose it. The software uses regular expressions to find the format in which the 3 elements are found before the determination and thus their values, in the figures 1, 2 and 3 the declarations of a package, a permission and an activity are described respectively.

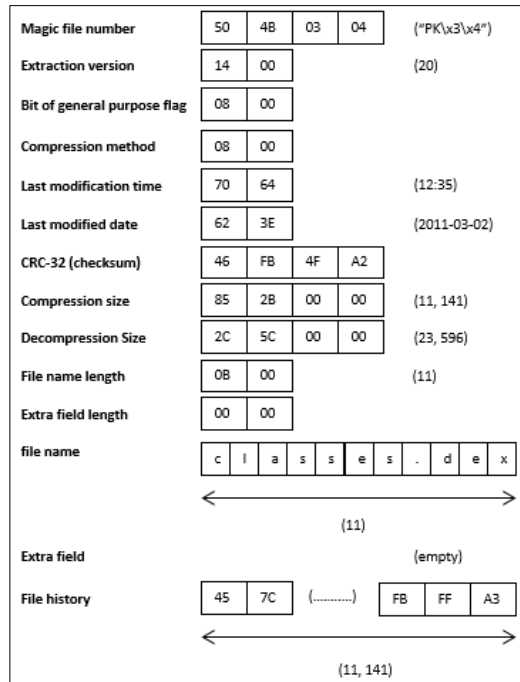


**Fig. 5.** Structure of an APK.

**g) Module of APK static analysis report generation:** In its last execution, Armagedroid performs a report in .txt file format containing the metadata obtained from the APK: the name, size in bytes, checksum integrity checksums, which are MD5, SHA1 and SHA256, APK content, information of the files it contains, such as comments on them, last modified date, operating system in which they were created, ZIP version used to compress them, their size once they have been compressed and decompressed, also included name the package, the list of activities and permissions of the APK, this task is performed by the module of generation of the report of static analysis of the APK.

## 5 Tests and Results

Armagedroid software was tested with 2 APKs, one of which corresponds to a video game of ships that destroy asteroids called *Asteroides.apk* and the second one is malware, with the name *badapk.apk*, the purpose of analyzing these 2 APKs is to

know the scope that would have each one in the device once installed. Table 2 shows the hardware and software features used for running Armagedroid.

**Table 2.** Hardware and software features used for running Armagedroid.

| <b>Software</b>             |  |
|-----------------------------|--|
| <b>Operating System</b>     | Kali Linux 2017.1                            |
| <b>Architecture</b>         | 32 bits                                      |
| <b>Programming language</b> | Python 3                                     |
| <b>Hardware</b>             |  |
| <b>RAM memory</b>           | 3.8 Gb                                       |
| <b>Processor</b>            | Intel® Pentium(R) CPU N3520 @<br>2.16GHz × 4 |
| <b>HDD</b>                  | 26.1 GB                                      |

|   |                 |
|---|-----------------|
| 1. <code>android.permission.WRITE_EXTERNAL_STORAGE</code> | 1. Asteroides   |
| 2. <code>android.permission.INTERNET</code>               | 2. AcercaDe     |
|   | 3. Preferencias |
|   | 4. Puntuaciones |
|   | 5. Juego        |

**Fig. 6.** Permissions and activities from the APK Asteroides.apk.

|  |                 |
|--|-----------------|
| 1. <code>android.permission.INTERNET</code>                | 1. MainActivity |
| 2. <code>android.permission.ACCESS_WIFI_STATE</code>       |                 |
| 3. <code>android.permission.CHANGE_WIFI_STATE</code>       |                 |
| 4. <code>android.permission.ACCESS_NETWORK_STATE</code>    |                 |
| 5. <code>android.permission.ACCESS_COARSE_LOCATION</code>  |                 |
| 6. <code>android.permission.ACCESS_FINE_LOCATION</code>    |                 |
| 7. <code>android.permission.READ_PHONE_STATE</code>        |                 |
| 8. <code>android.permission.SEND_SMS</code>                |                 |
| 9. <code>android.permission.RECEIVE_SMS</code>             |                 |
| 10. <code>android.permission.RECORD_AUDIO</code>           |                 |
| 11. <code>android.permission.CALL_PHONE</code>             |                 |
| 12. <code>android.permission.READ_CONTACTS</code>          |                 |
| 13. <code>android.permission.WRITE_CONTACTS</code>         |                 |
| 14. <code>android.permission.RECORD_AUDIO</code>           |                 |
| 15. <code>android.permission.WRITE_SETTINGS</code>         |                 |
| 16. <code>android.permission.CAMERA</code>                 |                 |
| 17. <code>android.permission.READ_SMS</code>               |                 |
| 18. <code>android.permission.WRITE_EXTERNAL_STORAGE</code> |                 |
| 19. <code>android.permission.RECEIVE_BOOT_COMPLETED</code> |                 |
| 20. <code>android.permission.SET_WALLPAPER</code>          |                 |
| 21. <code>android.permission.READ_CALL_LOG</code>          |                 |
| 22. <code>android.permission.WRITE_CALL_LOG</code>         |                 |
| 23. <code>android.permission.WAKE_LOCK</code>              |                 |

**Fig. 7.** Permissions and activities from the APK badapk.apk.

As seen in Fig. 6, the permissions of the APK *Asteroides.apk* request access to information storage and Internet access, are the permissions of a video game that writes the scores obtained in the memory of the device and that has the capacity to

access the Internet. Also, in Fig. 6, provides an overview of the activities that the user will see on the screen.

In the case of APK with malware, Armagedroid extracted the permissions of Fig. 7, in total there are 23, ranging from the request for Internet access, Wi-Fi network state settings, user location, reading of your contacts, control over the sending and receipt of both messages and phone calls, access to the camera and the microphone, to change the background image of the device and write to memory. The software detected a single activity, represented in Fig. 7, suggesting to the user that the APK is analyzed, that it is a main activity that runs in the background avoiding raising suspicions about their work.

## **6 Conclusions and future scope**

Thanks to the implementation of Armagedroid, it was possible to create a tool that automates the task of decompiling the APK, to extract its metadata, its directories and files, procedures proper to a static analysis, the results of comparing a benign APK with a malware resulted in a large difference in the permissions requested by the malicious application as it requested a set of permissions on the configuration of the wireless network, as well as the Internet, access to calls, messages and contacts on the phone, also to write information in memory, manipulate the device's camera and microphone, all give full scope to the tasks of the Android operating system and give access to a cybercriminal to manipulate it.

As for benign APK, only two permissions were written in memory and Internet access, which gives an idea that the application is what it claims to be, a video game. An important point to say is that the tool does not yet predict probabilistically if the APK is malware or benign, but only assists in the decision making, through the obtained metadata, to the analyst user.

To get the APK valuation task, Armagedroid will be attached to the Garmdroid web application, developed in the Cyber Security laboratory of the Computer Research Center, which informs the user if the APK it analyzes is malware or benign. Due to this interaction with the web platform, a communication component will be created between both softwares, both Armagedroid and Garmdroid. In future tests Armagedroid will be applied to a malware database of APKs to know the characteristics that it obtains from them.

**Acknowledgements.** We thank the Instituto Politécnico Nacional and CONACyT who have made possible the development of the Armagedroid project, both in support of the necessary resources and in the provision of facilities for the realization of it.

## **References**

1. Neely L.: Exploits at the Endpoint: SANS 2016 Threat Landscape Survey. (2016)

2. Universidad Internacional de Valencia: Ciberseguridad: Tendencias 2017. Jun 6, 2011, from Universidad Internacional from Valencia (2011)
3. Case A., Golden R.: Advancing Mac OS X Rootkit Detection. In: Digital Forensic Research Conference (2015)
4. Dunham K., Hartman S., Morales J., Quintans M., Strazzere T.: Android Malware and Analysis. E.U.: Auerbach Publications, pp. 7, 51, 52, 91, 92 (2014)
5. Lueg, C.: 8,400 new Android malware samples every day. April 27, 2017, from G DATA. <https://www.gdatasoftware.com/blog/2017/04/29712-8-400-new-android-malware-samples-every-day>, last accessed 2017/08/14 (2017)
6. Elenkov N.: Android Security Internals: An In-Depth Guide to Android's Security Architecture. San Francisco, No Starch Press, pp. 51–52 (2014)
7. Elenkov N.: Android Security Internals: An In-Depth Guide to Android's Security Architecture. San Francisco, No Starch Press, pp. 51–52 (2014)
8. Developers Android: App Manifest, Developers Android. <https://developer.android.com/guide/topics/manifest/manifest-intro.html>, last accessed 2017/08/14
9. Developers Android: Package, Developers Android, <https://developer.android.com/reference/java/lang/Package.html>, last accessed 2017/08/14
10. Elenkov N.: Android Security Internals: An In-Depth Guide to Android's Security Architecture. San Francisco, No Starch Press, pp. 21–26 (2014)
11. Developers Android: Activities. December 4, 2016, <https://developer.android.com/guide/components/activities.html>, last accessed 2017/08/14
12. Zuhair, M., Nisar, A., Ullah, H.: Automatic Feature Extraction, Categorization and Detection of Malicious Code in Android Applications. Institute of Advanced Engineering and Science (2013)
13. Aung, Z., Zaw, W.: Permission-Based Android Malware Detection. March 3, 2013, from International Journal of Scientific & Technology Research (2013)
14. Allix K, Bissyandé T, Jérôme Q, Klein J, State R, Le Traon Y. Large-Scale Machine Learning-based Malware Detection: Confronting the 10-Fold Cross Validation Scheme with Reality. University of Luxembourg (2014)

# Experimental Comparison of Bioinspired Segmentation Algorithms Applied to Segmentation of Digital Mammographies

David González-Patiño<sup>1</sup>, Yenny Villuendas-Rey<sup>2</sup>, Amadeo J. Argüelles-Cruz<sup>1</sup>

<sup>1</sup> Centro de Investigación en Computación, Instituto Politécnico Nacional,  
Ciudad de México, Mexico

<sup>2</sup> Centro de Innovación y Desarrollo Tecnológico en Cómputo, Instituto Politécnico Nacional,  
Ciudad de México, Mexico

davidglezp-92@hotmail.com, yenny.villuendas@gmail.com, aarguelles@ipn.mx

**Abstract.** Breast cancer has affected people worldwide despite of age or economic condition. In this paper, we explore the possibility of using bioinspired algorithms, mainly designed for optimization, for segmentation of mammographies, which showed good performances in this task. The results showed useful methods with promising results to segment digital mammographies using bioinspired algorithms.

**Keywords:** breast cancer, bioinspired algorithm, comparison, segmentation optimization.

## 1 Introduction

Breast cancer is one of the main causes of death in women all over the world [1]. This is the main reason why researchers have been trying to detect breast cancer in early phases using non-invasive techniques instead of invasive ones such as biopsies.

Mammographies studies are a useful tool for medics in order to diagnose breast cancer in early phases since it allows them to get a digital image of the breast using a low dose of x-rays. These studies are recommended to be done for women older than 26 years once a year [1].

A mammography is a digital image produced by a mammographic study and typically, these images are gray scales which allows to differentiate the lesion in the breast due to the texture and color [2]. To perform this task, the medic needs to segment the region of interest (lesion) in order to split lesion and background and diagnose accurately.

The bioinspired algorithm are inspired, as referred by their name, in natural and biological processes and they have been used to solve optimization problems [3]; however this has not been the unique approach where they have been used.

In this paper, we perform an experimental comparison using bioinspired algorithms to segment mammography images and comparing the results with other algorithms used for segmentation.

The paper is organized as follows. Section 2 is a review of some of the previous works in automatic or semi-automatic segmentation processes in breast cancer mammographies. In section 3, there is a little explanation of the algorithms used in this work. Section 4 presents the results of the experiments got by the algorithms using them in segmentation of mammography images and finally in Section 5, the conclusions and future work is presented.

## **2 Previous Works**

Mammographies are not the unique tool to help the expert medic to diagnose breast cancer; however it has been the most commonly used technique.

Segmentation is a commonly used process after the mammography is taken, since it allows to split the digital image into groups of pixels which are easier to analyze [4].

Although, there are many segmentation algorithms, which have showed good performances; there is not a perfect algorithm for segmentation since many approaches have been developed according to the necessities of each problem.

Some algorithms have been used for automatic diagnosis of breast cancer such as the model proposed by Pena-Reyes and Sipper in 1999 [5] or the algorithm proposed by Yan et al. in 2003 [6], which uses local entropy to segment images.

Timp and Karssemeijer [7], proposed in 2004 a segmentation method based on dynamic programming to segment mammographies; this method showed to be statistically significant between that method and other existing methods.

Cascio et al. [8] proposed an algorithm for mammogram segmentation using neural networks. This algorithm also uses feature selection based on linear discriminating analysis to choose the features which are able to distinguish lesions.

In 2012 [9], a method to split a mammographic image in lesion and background was proposed; this algorithm was based on a maximum likelihood active contour which showed good performances.

Later on, in 2016 [10], Dubrovina et al. presented a method using deep neural networks for segment mammographies and in the same year, Sargent and Park [11] implemented a method to segment mammographies using side-by-side comparisons.

Most of the works only focus on comparisons between classic algorithms, and, bioinspired algorithms have not been compared with classic algorithms to segment, this is why we addressed this problem in this paper.

## **3 Segmentation Algorithms**

In this work, three algorithms were tested, a classic algorithm named Otsu method, which is very used in segmentation tasks. The remaining two algorithms are genetic algorithms and simulated annealing inspired in two different processes.

Otsu method [12] is a thresholding method based on selecting the optimal limit to segment images into two regions. This method has been widely used in many segmentation problems showing good performances. Even so, this method have problems when one of the regions is significantly bigger, however this problem has been solved in newer implementations of this method.

Genetic algorithms (GA) are a subclass of evolutionary algorithms which are heuristics inspired on natural selection theory [13]. These algorithms generate random populations at the beginning and improve their individuals each generation through crossover and mutation in order to keep the best population according to a fitness function.

Simulated Annealing (SA) [14] is a technique used to find the global optimum which relies on the principle of annealing in metallurgy which involves heating and control the cooling phase in order to reduce the defects.

Since most of the bioinspired algorithms are focused for optimization problems, in this work there was a necessity to change the approach.

For this task, the Dunn index was used [15]; this index allows to evaluate clustering algorithms, so, the higher the Dunn index, the better the clustering.

To represent a possible solution for the bioinspired algorithms in this work, we used the representation of the individuals showed in figure 1.



Fig. 1. Representation of an individual.

This representation shows an individual with 3 components, which components are represented as gray levels in the gray scale.

Table 1. Description of variables for equations 1 and 2.

| Variable  | Description   |
|-----------|---|
| $N$       | Number of regions   |
| $S_j$     | Quantity of pixels in region $j$                          |
| $SI$      | Area of the image   |
| $N(b)$    | Number of regions with exactly an area equal to $b$ units |
| $e_j^2$   | Squared color error of region $j$                         |
| $Cx(p)$   | Value of component $x$ for pixel $p$                      |
| $Cx(R_j)$ | Average value of component $x$ in the region $j$          |

To evaluate the segmentation done by each algorithm, we used the error measures presented by Hui Zhang et al. in 2007 [16]. These measures were presented for image segmentations using unsupervised methods. The two measures used were Average squared color error, defined as  $F$  (equation 1) and  $F'$  (equation 2), which is an improved version of  $F$  which penalizes segmentations which contains lots of small regions:

$$F = \sqrt{N} \sum_{j=1}^N \frac{e_j^2}{\sqrt{S_j}}, \quad (1)$$

$$F' = \frac{1}{1000 * SI} \sqrt{\sum_{b=1}^{MaxArea} N(b)^{1+\frac{1}{b}} \sum_{j=1}^N \frac{e_j^2}{\sqrt{S_j}}}. \quad (2)$$

The variables for each equation are defined in table 1.

## 4 Experiments

The images used in this work were provided by the Faculty of Medicine of the University of Porto, Portugal in the dataset named Breast Cancer Digital Repository [17], which is a repository that contains 200 lesions of 190 Portuguese women, corresponding to 362 segmentations of mammographies identified by expert radiologists.

The images are described by 38 attributes, representing several characteristics of the lesions, such as clinical data, descriptors of the intensity of the lesion contour, descriptors of the lesion texture and descriptors of location and shape of the lesion. In addition, each image has associated the corresponding class (malign, benign). These classes were corroborated by biopsy analysis, that is, we are certain about the classification of each lesion.

The dataset contains some missing values (represented by NaN, Not a Number), which were substituted by the attribute mean.

The three algorithms presented in this work processed all the images, and the error measures were calculated for each image. The results are presented in this section.

Tables 2-4 show the segmentation of three lesions, as an example. In these tables, we show the original image carried out by an expert radiologist, the lesion segmented by the radiologist (Region of Interest, ROI), the ROI overlapped with the mammography image, and then, the segmentation obtained by Otsu method, Genetic Algorithm (GA) and Simulated Annealing (SA), respectively.

As shown, the algorithm that got the best segmentation was genetic algorithms, eventhough the region of interest is not covered as much as in the other images, the region which does not belong to the region of interest is not as much as in the other two algorithms.

In the images is observed that Otsu method segmented the region of interest with a bigger area compared to the other segmented images. This is relevant since the other algorithms got a lower area and they had a bigger similarity to the original segmented image carried out by an expert radiologist.

Genetic algorithms got a better segmentation comparing the produced image with the original image carried out by an expert radiologist since the area in the image is similar to the original segmented image carried out by an expert radiologist.

In this experiment can be observed that the three segmented images are visually similar to the original segmented image carried out by an expert radiologist. Eventhough the error measures in this image could be similar, the values for all the images need to be calculated in order to obtain correct conclusions.

**Table 2.** (a) Original image, (b) ROI segmented by expert radiologist, (c) Overlap of the ROI over original image, (d) Image segmented by Otsu method, (e) Image segmented by GA, (f) Image segmented by SA.

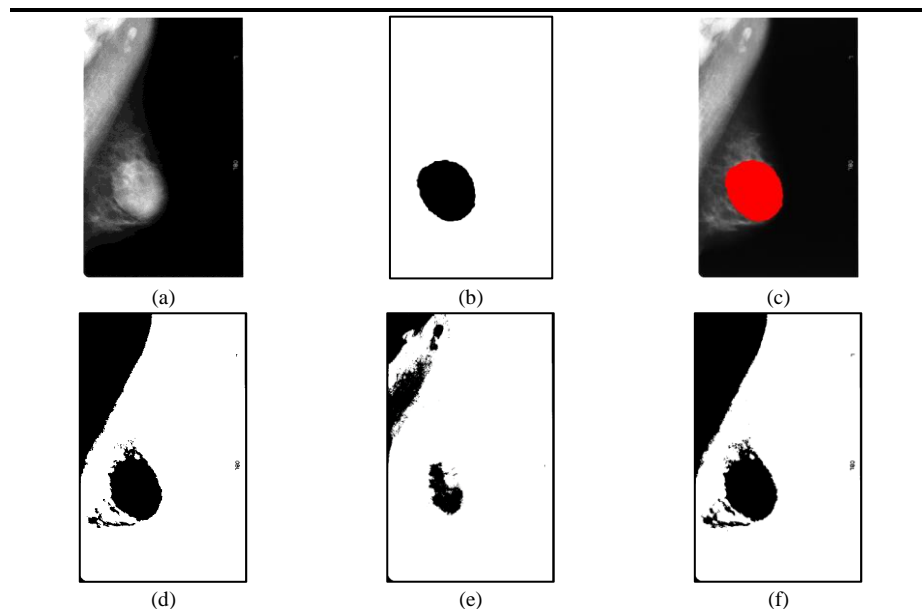


**Table 3.** (a) Original image, (b) ROI segmented by expert radiologist, (c) Overlap of the ROI over original image, (d) Image segmented by Otsu method, (e) Image segmented by GA, (f) Image segmented by SA.

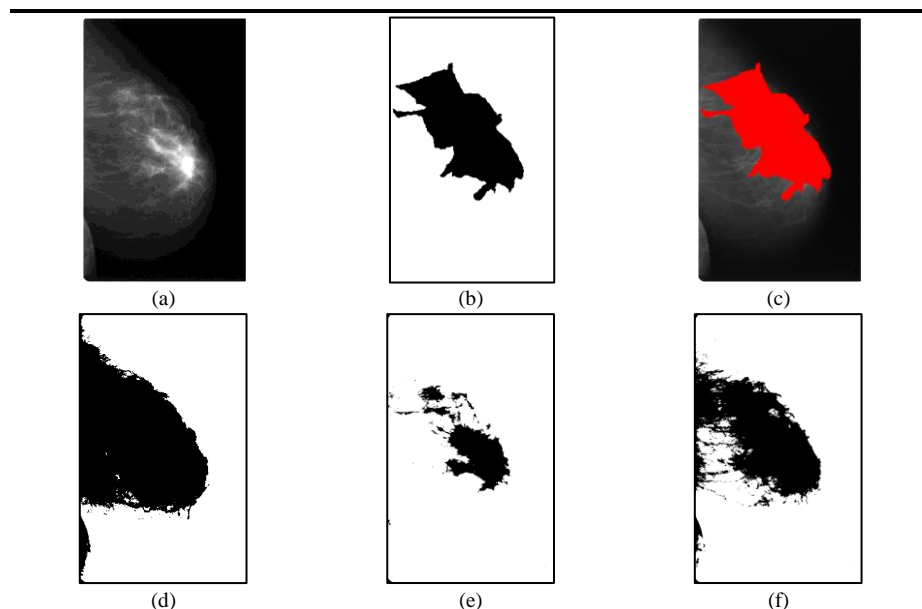
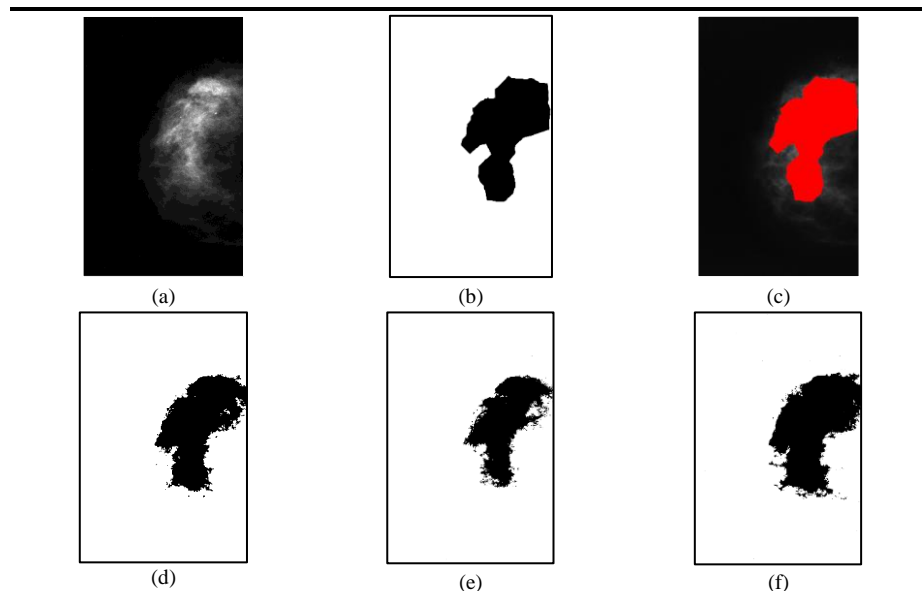


**Table 4.** (a) Original image, (b) ROI segmented by expert radiologist, (c) Overlap of the ROI over original image, (d) Image segmented by Otsu method, (e) Image segmented by GA, (f) Image segmented by SA.



All the 362 images were processed and the error measures were calculated for each image by equations 1 and 2. The table 5 shows the measures calculated.

**Table 5.** Mean of the errors calculated for the segmentation of the 362 mammographies.

| Algorithm           | F mean               | F' mean                 |
|---------------------|----------------------|-------------------------|
| Otsu method         | $15.324 \times 10^6$ | $12.880 \times 10^{-3}$ |
| Genetic Algorithm   | $9.888 \times 10^6$  | $8.313 \times 10^{-3}$  |
| Simulated annealing | $14.88 \times 10^6$  | $12.519 \times 10^{-3}$ |

In addition, a comparison in running time was done for the 3 algorithms and the results of the mean times are presented in table 6.

**Table 6.** Times calculated for the segmentation of the 362 mammographies.

| Algorithm           | Mean time (secs.) | Minimum time (secs.) | Max. time (secs.) |
|---------------------|-------------------|----------------------|-------------------|
| Otsu method         | 0.0515            | 0.022                | 0.590             |
| Genetic Algorithm   | 170.830           | 126                  | 278               |
| Simulated annealing | 130.406           | 97                   | 211               |

As shown in tables 5 and 6, the algorithm having the best segmentation was Genetic algorithm since the mean error calculated was lower compared to the other algorithms.

This could be due to the exploration and the capabilities of the algorithm for finding better solutions which produce better segmentations.

Simulated annealing got a higher error compared with genetic algorithm, however the error presented in Simulated annealing is lower than the one calculated for Otsu method.

With respect to computational cost Otsu method showed a very lower time compared to the other algorithms, which showed to be a good implementation and a fast method to produce binary images with the possibility to segment the region of interest.

## 5 Conclusions

The bioinspired algorithms tested in this work showed lower errors comparing them to Otsu method, which is a very used method for thresholding. Although the genetic algorithm got a lower error and Otsu got the highest error, in the running time test, the genetic algorithm got the highest running times while the Otsu method got very little running times.

This could be due to the implementation of the Otsu method in Matlab since this algorithm is implemented and optimized in order to execute faster operations.

According to the error measures calculated, Genetic algorithms got a lower error when segmenting the mammography images, this can be visually observed in the segmented images since the regions of the segmented images are smaller and cover a better portion of the original segmented image carried out by an expert radiologist.

In this comparison the best algorithm applied for segmentation was Genetic algorithms according to the error measures, although Otsu got the lowest running time.

**Acknowledgements.** The authors would like to thank the Instituto Politécnico Nacional (Secretaría Académica, Comisión de Operación y Fomento de Actividades Académicas, Secretaría de Investigación y Posgrado, Centro de Investigación en Computación, and Centro de Innovación y Desarrollo Tecnológico en Cómputo), the Consejo Nacional de Ciencia y Tecnología (Conacyt), and Sistema Nacional de Investigadores in México for their economical support to develop this work. Also thanks to the support provided by the SIP project 20170362, for the economic support and related work.

## References

1. Ferlay, J., Héry, C., Autier, P., Sankaranarayanan, R.: Global burden of breast cancer. In: Breast cancer epidemiology. pp. 1–19. Springer (2010)
2. Yaffe, M.J.: Digital mammography. In: PACS. pp. 363–371 (2006)
3. Yang, X.-S., Hossein Gandomi, A.: Bat algorithm: a novel approach for global engineering optimization. *Eng. Comput.* 29, 464–483 (2012)
4. Pham, D.L., Xu, C., Prince, J.L.: Current methods in medical image segmentation 1. *Annu. Rev. Biomed. Eng.* 2, 315–337 (2000)

5. Pena-Reyes, C.A., Sipper, M.: A fuzzy-genetic approach to breast cancer diagnosis. *Artif. Intell. Med.* 17, 131–155 (1999)
6. Yan, C., Sang, N., Zhang, T.: Local entropy-based transition region extraction and thresholding. *Pattern Recognit. Lett.* 24, 2935–2941 (2003)
7. Timp, S., Karssemeijer, N.: A new 2D segmentation method based on dynamic programming applied to computer aided detection in mammography. *Med. Phys.* 31, 958–971 (2004)
8. Cascio, D., Fauci, F., Magro, R., Raso, G., Bellotti, R., De Carlo, F., Tangaro, S., De Nunzio, G., Quarta, M., Forni, G., others: Mammogram segmentation by contour searching and mass lesions classification with neural network. *IEEE Trans. Nucl. Sci.* 53, 2827–2833 (2006)
9. Rahmati, P., Adler, A., Hamarneh, G.: Mammography segmentation with maximum likelihood active contours. *Med. Image Anal.* 16, 1167–1186 (2012)
10. Dubrovina, A., Kisilev, P., Ginsburg, B., Hashoul, S., Kimmel, R.: Computational mammography using deep neural networks. *Comput. Methods Biomech. Biomed. Eng. Imaging Vis.* 1–5 (2016)
11. Sargent, D., Park, S.Y.: Automatic segmentation of mammogram and tomosynthesis images. In: *SPIE Medical Imaging*. (2016)
12. Otsu, N.: A threshold selection method from gray-level histograms. *Automatica* 11, 23–27 (1975)
13. Banzhaf, W., Nordin, P., Keller, R.E., Francone, F.D.: *Genetic programming: an introduction*. Morgan Kaufmann San Francisco (1998)
14. Khachatryan, A.G., Semenovskaya, S. V, Vainstein, B.: A statistical-thermodynamic approach to determination of structure amplitude phases. *Sov. Phys. Crystallogr.* 24, 519–524 (1979)
15. Dunn, J.C.: A fuzzy relative of the ISODATA process and its use in detecting compact well-separated clusters. (1973)
16. Zhang, H., Fritts, J.E., Goldman, S.A.: Image segmentation evaluation: A survey of unsupervised methods. *Comput. Vis. image Underst.* 110, 260–280 (2008)
17. Moura, D.C., López, M.A.G.: An evaluation of image descriptors combined with clinical data for breast cancer diagnosis. *Int. J. Comput. Assist. Radiol. Surg.* 8, 561–574 (2013)

# Sequence Prediction with Hyperdimensional Computing

Job Isaias Quiroz Mercado, Ricardo Barrón Fernández,  
Marco Antonio Ramírez Salinas

Instituto Politécnico Nacional (IPN), Centro de Investigación en Computación,  
Mexico City, Mexico

jobquiroz@hotmail.com, barron2131@gmail.com, marco.a.ramirez.s@gmail.com

**Abstract.** Hyperdimensional Computing is an emergent model of computation where all objects are represented in high-dimensional vectors. This model includes a well-defined set of arithmetic operations that produce new high-dimensional vectors, which, in addition to represent basic entities, can also represent more complex data structures such as sets, relations and sequences. This paper presents a method for sequence prediction using Hyperdimensional Computing and the Sparse Distributed Memory model. The proposed method is based on the encoding, storage and retrieval of *sequence vectors*, which store the  $k$  consecutive vectors of a sequence. The next element of a sequence is selected by taking into account the current, as well as the  $k$  immediate preceding elements of the sequence. Each vector is associated to a sequence vector that is stored in memory; the way in which each vector is associated to its sequence vectors is the main contribution of this paper. We present experimental results for the encoding and prediction of randomly generated sequences and the results indicate that the method performs correct predictions.

**Keywords:** hyperdimensional computing, prediction methods, sequence representation, sparse distributed memory.

## 1 Introduction

Sequence learning is essential to human intelligence, sequences are everywhere, going from low-level sensory-motor behavior up to high-level problem solving and reasoning. Sequential processes can also be found in fields such as robotics, finances, language processing, etc.

Hyperdimensional Computing is an emergent model of computation. It is based on the manipulation of high-dimensional vectors which are used not only to represent variables and values, but also to represent relations, sets and sequences [2].

In this work, we use a Hyperdimensional Computing approach for sequence prediction. We present the main idea behind the use of high-dimensional vectors as a representation scheme, describe the operations used to manipulate these vectors and propose a method for storage and prediction of sequences.

The rest of the paper is organized as follows: Section 2 summarizes several works related to the use of HD Computing for sequence representation. Section 3 explains the main properties and operations used in HD Computing. In Section 4 we describe a new method for storage and prediction of sequences, Section 5 presents the experimental results and finally, Section 6 draws the conclusions and future work.

## **2 Related Work**

### **2.1 Hyperdimensional Computing**

The main difference between hyperdimensional computing (HD computing) and traditional computing relies on the type of elements used for computation. In HD computing information is encoded in high-dimensional vectors (typically between 1,000 and 10,000 bits long). These vectors have no dedicated fields, information is distributed along all vector.

Kanerva [6] summarizes the main properties of HD Computing and explains three applications where it can be used: language processing, learning from example and analogy-making.

Hyperdimensional spaces can be binary, real or complex, in [9] Rahimi et al. give a brief review of several frameworks for HD Computing, each framework having its own set of symbols and operations. They also describe a hardware architecture for operating high dimensional vectors.

HD Computing has been applied in different domains, such as visual character recognition [3], cognitive software agents [14], robotics [5], biosignal processing [10], and sequence prediction [1, 13].

### **2.2 Sequence Prediction with Hyperdimensional Computing**

One of the first applications conceived for the Sparse Distributed Memory [7] was to store and retrieve sequences, in order to learn a sequence the memory can be operated in heteroassociative mode, where each location stores the next value of the sequence, forming a chain of pointers. Even though this approach has several flaws, it was the first idea to develop a prediction system based on HD Computing.

Kanerva proposed the use of several Sparse Distributed Memories for storing sequences, where each memory could store higher order sequential structures [7]. The main limitation of this approach was the need of a very large memory system. This type of learning has been applied in the modeling of service robot movement [22]. Bose et al. [1] proposed a framework for online sequence learning based on an associative memory model. In their approach, the prediction value is obtained as a result of the sum of a set of history vectors.

In [13] Snaider and Franklin proposed a modification to the SDM model that allows a more efficient way to store and retrieve sequences. These sequences are encoded using hyperdimensional operations (sums and permutations). Räsänen and Saarinen propose a predictor based on HD Computing where, unlike the two previous

approaches, there is no need of a special memory, “the idea is to represent the previously observed history of each possible sequence state using a single vector of very large dimensionality” [12].

In this work we propose a prediction model based on HD Computing operators and the original SDM model, without the need of increasing the size of the memory.

### 3 Hyperdimensional Computing Background

One of the most relevant properties of the high-dimensional spaces is that most of the space is nearly orthogonal to any given point. This means that if two random vectors are generated, it is highly probable (more than 99.999%) that they are mutually orthogonal. These properties were exploited in the SDM model developed by Kanerva in 1988 [7]. However, the properties of high-dimensional spaces can also be used to perform other type computations, for which is necessary to define a set of HD computing operators.

#### 3.1 HD Computing Operations

HD Computing is based on three operations: addition, multiplication and permutation. In this paper we use binary vectors, but these three operations can be defined for other types of vectors [9]. A more detailed explanation of HD Computing operations can be found in [6].

##### Addition

Addition is an element-wise binary average. The sum vector  $X_s = \sum_{k=1}^n x_k$  is computed by adding each component  $i$  of each vector  $x_k$  and then using the threshold function  $\Theta$  to maintain the values as 0 or 1:

$$X_{s,i} = \Theta \left( \frac{1}{n} \sum_{k=1}^n x_{k,i} \right), \quad (1)$$

where

$$\Theta(u) = \{1 \text{ for } u > 0.5, 0 \text{ for } u < 0.5, \text{random otherwise.}$$

The components of the sum vector can be computed independently, which means that it can be easily parallelized. The result vector  $X_s$  is the concatenation of all the corresponding components.

The sum vector has the property of being similar to the vectors added together; therefore the addition operation is used to encode sets of vectors. The elements of the sum are ‘visible’ in the representation of the set.

##### Multiplication

For binary vectors, multiplication is realized with an element-wise exclusive-or

(XOR); the resulting vector is dissimilar to the original ones. Multiplication is a reversible operation; in fact, the XOR operator is its own inverse.

Multiplication is a mapping of points in space. Given two vectors A and B, it is possible to generate C, and later retrieve either A or B.

$$C = A * B \quad \Rightarrow \quad A = C * B \quad \Rightarrow \quad B = C * A. \quad (2)$$

Another interesting property of multiplication is that preserves distance,  $d(A, B) = d(A * X, B * X)$ , “it is like moving a constellation of points bodily into a different part of the space while maintaining the relations (distances) between them” [6].

### Permutation

Permutation randomly reorders the components of the original vector, and just as multiplication, the resulting vector is dissimilar to the original one. Permutation is invertible and it also maintains distance:  $d(A, B) = d(\Pi A, \Pi B)$ .

$$B = \Pi A \quad \Rightarrow \quad A = \Pi^{-1} B. \quad (3)$$

Unlike the two previous operations, permutation is not explicitly defined; it is possible to permute a vector by changing all its components to a different place, or only some of them. An easy way to permute a vector is by performing a circular shift operation, which will change all the components and can easily be inverted. In this work we implemented permutation as a shift right logical operation and the inverse permutation as a shift left logical operation.

### 3.2 Clean-Up Memory

All previous operators allow us to encode, map and retrieve hyperdimensional patterns, but in most cases the retrieval is not going to be exact. For example,  $X = X_1 * A + X_2 * B$  is storing the association of A with  $X_1$  and B with  $X_2$ . In order to retrieve A we can multiply X by  $X_1$ :

$$\begin{aligned} X * X_1 &= (X_1 * A + X_2 * B) * X_1 \\ \Rightarrow X * X_1 &= A + X_1 * X_2 * B. \end{aligned} \quad (4)$$

The resulting vector contains the sum of the desired value (A) and an unknown vector ( $X_1 * X_2 * B$ ). In order to discriminate this last vector we can use an auto-associative memory that approximates  $X * X_1$  to A.

This auto-associative memory is called clean-up memory [8], its function is store all the items that the system should recognize. When a noisy version of an item is given as input, the memory must either output the most similar item or indicate that the input is not close enough to any of the stored items.

In the previous example it is possible to obtain A by performing a read operation from memory.

$$A \cong \text{Read}(X * X_1) = \text{Read}(A + \text{noise}). \quad (5)$$

Every time a pattern becomes meaningful it can be recorded in memory, which becomes in “a catalog of meaningful patterns”.

In this work we use the Sparse Distributed Memory [7] as clean-up memory. The SDM is an architecture that can store high dimensional binary vectors and retrieve them based on partial matches. The storing of patterns is distributed, meaning that a single pattern is stored in many physical locations (called Hard Addresses).

### 3.3 Sequence Representation

A sequence is a complex structure that represents events that occur in certain order. The ability to store and recall sequences is very important in a system that pretends to have an intelligent behavior. There are several ways to represent sequences with HD Computing [6], in this work we focus in the representation of sequences by permuting sums.

The addition operation allow us to represent a set of vectors without a particular order, this may not be useful to store sequences, unless the order of each vector is somewhat codified. Permutations can be used for this purpose.

Since permutation generates a vector dissimilar from the original one, the order of the vector can be encoded as the number of permutations performed to the vector before the sum. For example, the sequence  $ABC$ , can be encoded as:

$$S = A + \Pi B + \Pi\Pi C. \quad (6)$$

In order to retrieve each element we have to perform inverse permutations and use the clean-up memory. Since all the permuted vectors are not stored in memory, they are considered noise:

$$\begin{aligned} A &\cong \text{Read}(S) = \text{Read}(A + \text{noise}), \\ B &\cong \text{Read}(\Pi^{-1}S) = \text{Read}(B + \text{noise}), \\ C &\cong \text{Read}(\Pi^{-1}\Pi^{-1}S) = \text{Read}(C + \text{noise}). \end{aligned} \quad (7)$$

The amount of vectors that can be encoded with this method mainly is limited by its dimensionality. For dimensions near 1,000 the limits is close to 4 to 5 vectors.

## 4 Prediction Model

The sequence prediction problem consists in that given  $x_{n-k+1}, \dots, x_{n-1}, x_n$ , we want to predict  $x_{n+1}$ . In this section we describe a prediction model based on HD Computing. The model is divided in two: a storage phase, where a set of sequences is stored in memory, and a prediction phase, where the model provide the next value for a given sequence.

#### 4.1 Encoding and Storage of Sequences

The first step is to associate each value of a sequence  $x_i$  to a random binary vector  $X_i$ . Due to the properties of high dimensional spaces, we can assume that all vectors  $X_i$  are not only different, but also mutually orthogonal. All vectors  $X$  are then stored in memory in auto-associative mode.

Each vector  $X_i$  must be associated with a sequence vector  $S_i$ , which encodes the  $k$  future vectors  $X_{i+1}, \dots, X_{i+k}$ .

$$S_i = X_{i+1} + \Pi X_{i+1} + \dots + \Pi^k X_{i+k}. \quad (8)$$

Since  $X_i$  has already been used as an address to memory, it is not possible to associate the value  $X_i$  to  $S_i$  in a direct way. But we can map the address  $X_i$  to another part of the space where the association of  $X_i$  and  $S_i$  could take place. One way to implement such mapping is by multiply  $X_i$  by a known random binary vector  $M$ . The resulting vector  $X_i * M$  is used as an address to store  $S_i$ :

$$\text{Write}(M * X_i) = S_i. \quad (9)$$

In this prediction model the memory is not only used as a clean-up system (auto-associative mode), but also as a way to associate symbols (hetero-associative mode). Once that all  $X_i$  vectors have been stored and mapped to its corresponding sequence vectors, the storage phase is finished.

#### 4.2 Prediction of Sequences

In order to predict the next value of a sequence, the systems needs to have as an input at least  $k$  consecutive elements of the sequence:  $x_{j-k+1}, \dots, x_j$ . The system approximates each value  $x_j$  to a known value  $x_i$  and then associates a vector  $X_j$  to each  $x_j$ .

Each vector  $X_{j-k+1}, \dots, X_j$  is associated with a sequence vector  $S_{j-k+1}, \dots, S_j$  which can be read from memory as follows:

$$\begin{aligned} S_{j-k+1} &= \text{Read}(X_{j-k+1} * M), \\ &\dots \\ S_j &= \text{Read}(X_j * M). \end{aligned} \quad (10)$$

Since each sequence vector has encoded a vector  $X_{j+1}^k$ , the last step is to extract each of these values in order to generate the final prediction vector  $X_{j+1}$  from which is possible to obtain the prediction value  $x_{j+1}$ , Fig 1.

$$\begin{aligned} X_{j+1}^1 &= \text{Read}(\Pi^{-k} S_{j-k+1}), \\ &\dots \\ X_{j+1}^k &= \text{Read}(S_{j-k+1}), \end{aligned} \quad (11)$$

$$X_{j+1} = \sum_{r=1}^k X_{j+1}^r \rightarrow x_{j+1}.$$

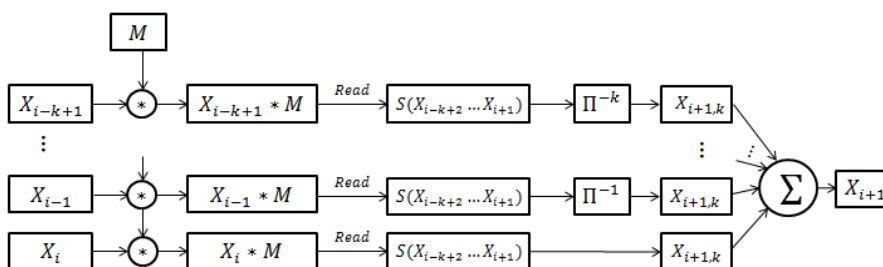


Fig. 1. Prediction model with Hyperdimensional Computing.

### 5 Experimental Results

We performed several simulations to test how the proposed method is able to store and predict sequences. As stated before, we use binary vectors with length of 1,000 dimensions, these vectors have 50% ones and 50% zeros randomly distributed. We also use the original Sparse Distributed Memory model.

For each simulation we vary the number of Hard Addresses of the memory to see how the capacity of the memory increases. We also increment the value of  $k$  which represents the number of vectors taken into account to form the sequence vector and to make a prediction (see section 4.2).

Table 1. Prediction Rate for different values of  $k$  and  $N = 50$  sequences

| Hard Addresses | N = 50 sequences |        |        |        |
|----------------|------------------|--------|--------|--------|
|                | k = 1            | k = 2  | k = 3  | k = 4  |
| 100,000        | 41.28%           | 26.40% | 58.89% | 33.25% |
| 250,000        | 60.17%           | 51.36% | 70.12% | 51.12% |
| 500,000        | 71.50%           | 59.85% | 79.85% | 70.78% |
| 1,000,000      | 74.80%           | 64.98% | 91.24% | 74.98% |

At the beginning of the experiment we generate random sequences, which are then encoded and stored into memory. Then we take  $k$  consecutive points of each sequence and try to predict the entire sequence. Each sequence consists of 20 points and we consider a prediction to be successful if it has at most 5% of error. The number of points and the criteria for a successful prediction was taken as in [13], so we can compare the results. Table 1 summarizes the results from the experiments.

In the SDM model all the data is distributed along several physical locations, if the capacity of the memory increases then the number of sequences that can be success-

fully predicted also increases. Unlike the system in [13] we do not modify the architecture of the memory, which results in a smaller size of memory, however, in this method each element of each sequence takes two addresses, one for storing itself (auto-associative mode) and one for storing its sequence vector (hetero-associative mode).

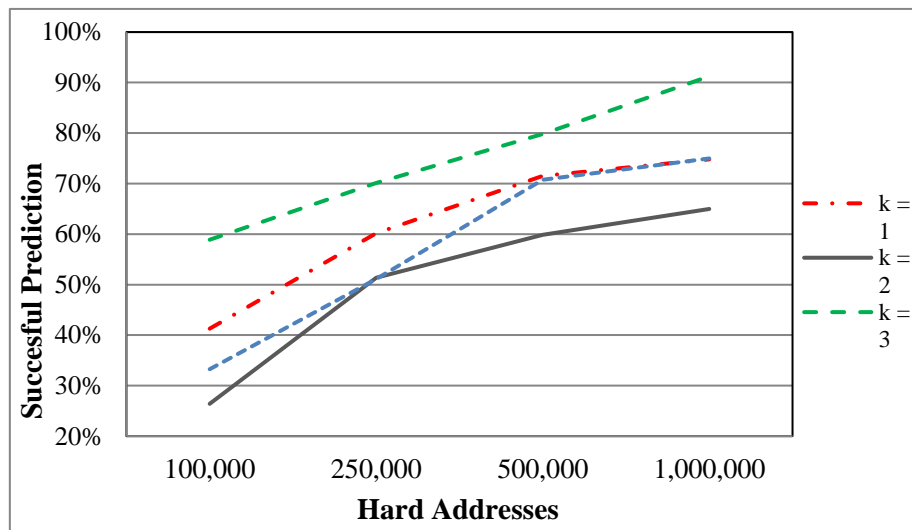


Fig. 2. Percentage of successfully predicted sequences for different values of  $k$ .

The rate of successful predictions do not increase linearly with respect to the value of  $k$  (Fig. 2), which might seem counterintuitive, because as the number of preceding points increases the prediction is expected to get better. But one of the downsides of the sum operation is that when the number of added vectors increases, the interference between them increases as well. This interference mainly depends on the dimensionality of the vectors, for vectors with length 1,000 starts to be noticeable at approximately 4 to 5 vectors.

The results presented in [13] show that their system was capable of successfully retrieve up to 49 sequences out of 50, but when the number of sequences increased to 100 none of the sequences could be restored. In this case the capacity of the memory system was the limiting factor, since they only implemented 200,000 Hard Addresses.

Another interesting behavior from Fig. 2 is that the prediction rate for  $k = 1$  is better than for  $k = 2$ . As seen in Section 3.1, the sum operation returns a random value when the sum of the components is equal to 0.5 (which prevents the sum vector to be constantly filled with ones or zeros) and when  $k = 2$  the probabilities for this to happen are much greater that when  $k = 1$  or  $k = 3$ . This behavior was also observed in [13].

## 6 Conclusions and Future Work

This work presented some highlights of Hyperdimensional Computing, which is an emergent model of computation based on the storage and manipulation of high-dimensional vectors. This type of computation allows us to encode from single concepts up to more complex data structures such as sequences.

We proposed a method for the encoding and prediction of sequences, based on arithmetical operations and a Sparse Distributed Memory system. The main feature of this method is the use of the multiplication operation as a way of mapping vectors in space, in this particular case: mapping a vector to a *sequence vector* which allows us to make predictions.

We presented experimental results for the prediction method and explain some of its limitations, such as the restriction in the number of vectors to be added into a single vector. One of the goals for future implementations is to increase the dimensionality of the vectors in order to reduce the interference, not only in sums, but in all three operations.

Another future modification is to develop a hierarchical model which allows us, not only to predict single points, but also to predict sequences and other complex structures, such as relations between concepts and sets.

## References

1. Bose, J., Furber S., Shapiro, J.: An associative memory for the on-line recognition and prediction of temporal sequences. In: Proc. IEEE International Joint Conference on Neural Networks, Montreal, Canada, 1223–1228 (Jul./Aug. 2005)
2. Gallant, S., Okaywe T.: Representing Objects, Relations and Sequences. *Neural Computation* 25(8), 2038–2078 (2013)
3. Hong, Y., Chen S.: Character recognition in a Sparse Distributed Memory. *IEEE Transactions on Systems, Man and Cybernetics*, 21(3), 674–678 (1991)
4. Jockel, S.: Crossmodal learning and prediction of autobiographical episodic experiences using a Sparse Distributed Memory. Doctoral Thesis, University of Hamburg, Department of Informatics (2010)
5. Jockel, S., Mendes, M., Zhang, J., Coimbra, P., Crisóstomo, M.: Robot navigation and manipulation based on a predictive associative memory. In: Proceedings IEEE 8<sup>th</sup> International Conference on Development and Learning, Shanghai, China (June 2009)
6. Kanerva, P.: Hyperdimensional Computing: An Introduction to Computing in Distributed Representation with High Dimensional Random Vectors. *Cognitive Computation* 1(2), 139–159 (2009)
7. Kanerva, P.: *Sparse Distributed Memory*. Cambridge, MA: Bradford/MIT Press (1988)
8. Plate, T.: *Holographic reduced representation: distributed representation of cognitive structure*. Stanfor: CSLI (2003)
9. Rahimi, A., Datta, S., Kleyko, D., Paxon, E., Olshausen, B., Kanerva, P., Rabaey, J.: High-Dimensional Computing as a Nanoscalable Paradigm. *IEEE Transactions on Circuits and Systems: Regular Papers* PP(99), 1–14 (2017)
10. Rahimi, A., Benatti, S., Kanerva, P., Benini, L., Rabaey, J.: Hyperdimensional Biosignal Processing: A Case Study for EMG-based Hand Gesture Recognition. In: Proceedings of

- the International Conference on Rebooting Computing, San Diego, CA, USE, pp. 1–8 (Oct. 2016)
11. Rao, R., Fuentes, O.: Hierarchical Learning of Navigational Behaviors in an Autonomous Robot using a Predictive Sparse Distributed memory. *Autonomous Robots* 5(3–4), 297–316 (1998)
  12. Räsänen, O., Saarinen, J.: Sequence Prediction with Sparse Distributed Hyperdimensional Coding Applied to the Analysis of Mobile Phone Use Patterns. *IEEE Transactions on Neural Networks and Learning Systems* 27(9), 1878–1889 (2016)
  13. Snaider, J., Franklin, S.: Extended Sparse Distributed Memory and Sequence Storage. *Cognitive Computation* 4(2), 172–180 (2012)
  14. Snaider, J., Franklin, S.: Vector LIDA. *Procedia Computer Science* 41, 188–203 (2004)

# Designing New CAPTCHA Models Based on the Cognitive Abilities of Artificial Agents

Edgar D. García-Serrano, Salvador Godoy-Calderón, Edgardo M. Felipe-Riverón

Centro de Investigación en Computación, Instituto Politécnico Nacional, CDMX,  
Mexico

edserrano18@outlook.com, sgodoyc@cic.ipn.mx, edgardo@cic.ipn.mx

**Abstract.** A CAPTCHA is a program that allows or denies access to services by generating and grading test that humans can pass but current computer programs cannot. Captchas are generally used to protect free web services from automated programs. Also, they can provide an idea of which fields in artificial intelligence are the most explored and which could be researched in the near future. Most of the tests that are based on text recognition have been broken by optical character recognition (OCR) techniques while those based on images are vulnerable to machine learning attacks. Humans make use of cognitive abilities to carry out tasks in daily life, even if they are not conscious which ones or how they use them. The current state of technology is still not enough to reproduce some human cognitive abilities, and the identification of those abilities is the basis for the design of new CAPTCHA models. In this paper we introduce seven new models of CAPTCHA to test some cognitive abilities that are supposed to be beyond the capabilities of artificial agents. We use some APIs to proof that images used in the proposals are extremely difficult to be recognized by artificial agents.

**Keywords:** CAPTCHA, human interaction proofs, Turing test, cognitive abilities.

## 1 Introduction

CAPTCHA is acronym for Completely Automated Turing Test to Tell Computers and Humans Apart [1], term that was introduced first time in the year 2000.

A CAPTCHA is a program that automatically generates a task or test that most humans can solve but artificial agents cannot. Captchas are based on a Turing test [2], which is a question-answer game with a human judge and two participants; a human and a computer program. The judge does not know which of the participants the computer is, and by means of a question series the judge has to identify the computer while both participants try to convince the judge that they are humans. In captchas, the judge is a computer program, and instead of a question series, it generates a task. If the task is completed successfully, the user is considered to be human, otherwise

the user is considered an artificial agent. If a computer program correctly solves a CAPTCHA, it is considered that the CAPTCHA model has been compromised or *broken*. Some uses for these tests are: online poll protection, web services registration protection, dictionary attacks prevention, blog spam comment avoidance, and many more.

Generally, captchas are used as a security measure known as question-answer authentication, and its algorithms are totally public. For this reason, breaking a CAPTCHA is an interesting artificial intelligence problem. In other words, it would be difficult to make a program able to solve CAPTCHA even if it is known how it works exactly. According to [1], a CAPTCHA is a win-win situation. On one side, if the CAPTCHA is not broken, then we keep a way to differentiate humans from computers. On the other side, if the CAPTCHA is broken, then a useful AI problem is solved.

Since its creation, captchas have motivated multiple researches in AI fields, from OCR techniques as in [3], breaking classic text captchas or machine learning with deep learning methods [4] to break semantic image captchas. In this research we left out the security context and we use the CAPTCHA as an opportunity for some cognitive computing researches. In this way, we consider some principles and features of the set human cognitive abilities for designing seven new captcha models. The tests present in these captchas are based on capabilities present in humans and which computers cannot emulate yet. Furthermore, since these are new captcha models there is no an artificial agent trained to solve them. Instead, we separately tested Google, Microsoft and IBM's agents with the abstract images included in the proposed captcha models.

## 2 Related Work

Given the wide variety of captchas currently around internet, it is possible to set a taxonomy [5, 6] in which we can identify two main groups: visual captchas and audio captchas.

Within the visual captchas class, we can find text-based captchas which are characterized by displaying a set of characters with some transformations and distortions; the user must input the characters that he can recognize. Text-based captchas are vulnerable to OCR and some examples are the classic CAPTCHA and ReCAPTCHA models [7]. Other kind of visual CAPTCHA are those based on images; it is generally a test in which the user must identify some animals or objects and select them correctly according to the instructions. An example of this is the ASIRRA captcha model [8] that is a simple image categorization test. Another captcha model is based on videos, known as video-captchas, where the task is to recognize and input the red characters, part of the banner that crosses the screen in some direction. The NuCaptcha model [9] was a pioneer in these tests, although it is vulnerable to more sophisticated OCR. The next captcha models are mathematical in nature, this is to say, the user must solve a basic arithmetic problem to get access. Finally, in the puzzle-captcha, like its name suggest, it is necessary to complete a simple puzzle to complete the task. The last two

types of captchas are often difficult for humans, but they are even more difficult for artificial agents.

Audio captchas, as an alternative for the existing captchas models, strictly require only some eye-sighting abilities to pass the test. Visually handicapped persons generally fail the test and so they are denied the corresponding services that the CAPTCHA was guarding. For this reason, it seems necessary to draw on other elements to design captchas models, for example, sound. Audio captchas make use of sound to present the instructions and the task to be solved. They consist in a fragment of audio in which a person pronounces letters or numbers and the user must type the symbols listened.

So far, webservers only use two of the CAPTCHA types above, most common are the text-based ones (already broken by OCR techniques) and image based (broken by deep learning algorithms). As they have been broken, a way of make them stronger is searched. However, this leads to a more complex task even for humans. So this search for stronger captcha models tend to create new tests to be implemented and that require the use of different types of cognitive abilities, for which artificial agents are faced with bigger challenges.

Emotion identification requires an intense use of certain cognitive abilities, for that reason a 2-layer CAPTCHA was proposed [10] where the first layer consists in a puzzle of an image describing an emotion. The second layer asks the user to select from a menu, the word that better describes the presented image. The cognitive abilities required for solving this type of CAPTCHA are mainly visual processing.

To support the fact that human cognition plays an important role while solving captchas, in [11] an experiment developed which faces many users with image based captchas in varying difficulty levels. The author observes that a captcha modeling design process that adapts models based on some cognitive factors could effectively improve results.

In [12] the human ability of humor understanding is used; according to the author, humor understanding is the most advanced cognitive ability of a human being. He proposes a captcha model where the user is presented with four images that represent different stages of some funny story, and the user has to sort these images in the proper order.

There are some researches where the design of new tasks in captcha models is strongly based on psychological principles. Such is the case of [13], where constructivist theory and mental models are the base for such design. The main consideration is that our brains do not perceive images pixel by pixel, instead, they are built with models that sum up what the senses perceive (Gestalt laws). Captchas proposed in this work are based on Gestalt laws and Geon's theory of pattern recognition. Memory and context play an important role in how humans visually interpret objects.

The captcha models proposed in our research are based on tasks that are still difficult for artificial agents to solve. For example: abstraction ability, common sense reasoning, visual perception (Gestalt laws), and attention. Background knowledge also plays an important role in the development of what we call Cognitive Captchas (C-Captchas).

### **3 Proposed Captcha Models**

CAPTCHA models herein proposed are based in human cognition, conceived as the set of all processes by which sensory input is collected, transformed, reduced, elaborated, stored and used [14]. To identify exactly all of those processes is a difficult task in which even psychologists have not come to an agreement. Following is the list of human cognitive abilities required to solve these tasks in those captcha models:

- Attention.
- Short-term memory retention.
- Visual/spatial processing.
- Natural language understanding.
- Fine grained motor skills.
- Executive functions.
- Common sense reasoning.

Even when there is not a formal definition of cognitive abilities for artificial agents, certain techniques or algorithms exist that emulate some human abilities. Here we list the artificial agents' abilities that correspondingly take part in the knowledge acquirement:

- Pattern recognition
- Natural Language processing.
- Graphical interface interaction.
- Machine Learning.
- Associative binding.

We focus on those abilities where the artificial agents face greater problems than humans. State of the art techniques in digital image processing are insufficient for adequately emulating human perception abilities. Pattern recognition and machine learning algorithms suitable for solving this kind of tasks usually require large amounts of input data. For that reason, we selected a set of images that we identify as abstract, because of their lack of textures, colors and closed outlines. All these images show objects or characters in an indirect way, either with cartoons or suggested by blurred strokes. Humans are usually able to recognize these images even with insufficient or simplified information thanks to a combination of perception, visual processing, and background knowledge processing. We refer to this combination of abilities as abstraction.

Another ability useful during the design process was common sense reasoning. It is well known that artificial agents possess strong logical reasoning but not common sense. Common sense is a set of knowledge that is acquired through experiences. Research in this kind of reasoning has been carried out [15] but it is complex and difficult to formalize; it is necessary to study the simplest cases to focus on the problems that we want to solve.

A set of minimum features is established for all captchas to keep a certain level of difficulty. These features are:

- Every CAPTCHA has three graphical regions: instructions, challenge and solution.
- Instructions in natural language must present a common sense challenge.
- All images must be abstract.
- The user has just one chance to solve the CAPTCHA.

### **3.1 Model 1: Story Completion**

This model contains two challenges. Firstly, the natural language challenge where a simple instruction is provided to complete a story that entangles a random word representing an emotion (keyword). There are three rows (see Fig. 1) with two abstract images and an empty frame; every row represents a different story. The goal is to relate the keyword from natural language challenge with one of the three stories, select the ending frame from the solution region and complete the sequence by dragging the chosen image to the empty frame of the corresponding story. This constitutes the common sense reasoning challenge.

### **3.2 Model 2: Object-environment Association**

The instructions in this captcha model simply tell the user to make proper associations in each case but do not refer to specific objects nor they give more information. In the challenge region three abstract images of animals are presented (drawn by line patterns). In the solution region several abstract images representing places or environments can be found. The user is asked to use markers with specific shape to relate each animal with its usual environment (see Fig. 1). Abstraction and background knowledge processing are required in order to solve this captcha model.

### **3.3 Model 3: Differentiating Feature Identification**

This captcha model is defined as a semantic classification challenge according to the features of several animals presented in nine independent and abstract images (see Fig. 1). All but one of the animal images share a specific feature and the remaining image does not. The user is asked to select the image that does not share the common feature and drag it to the solution region option that represents the feature in question. In this case abstraction, natural language processing, pattern recognition and background knowledge processing are required.

### **3.4 Model 4: Foreground and Background Image Composition**

The goal is to identify the foreground and background parts of a provided image, select them among the images in the challenge region and drag them into the solution region. The conceptual composition of the selected foreground element and background element images should result in the provided images (see Fig. 1). The images that represent the foreground and background elements in the challenge region are not

exactly the same as the one provided even though the image conceptually. A high level of abstraction is required for the resolution of this captcha model.

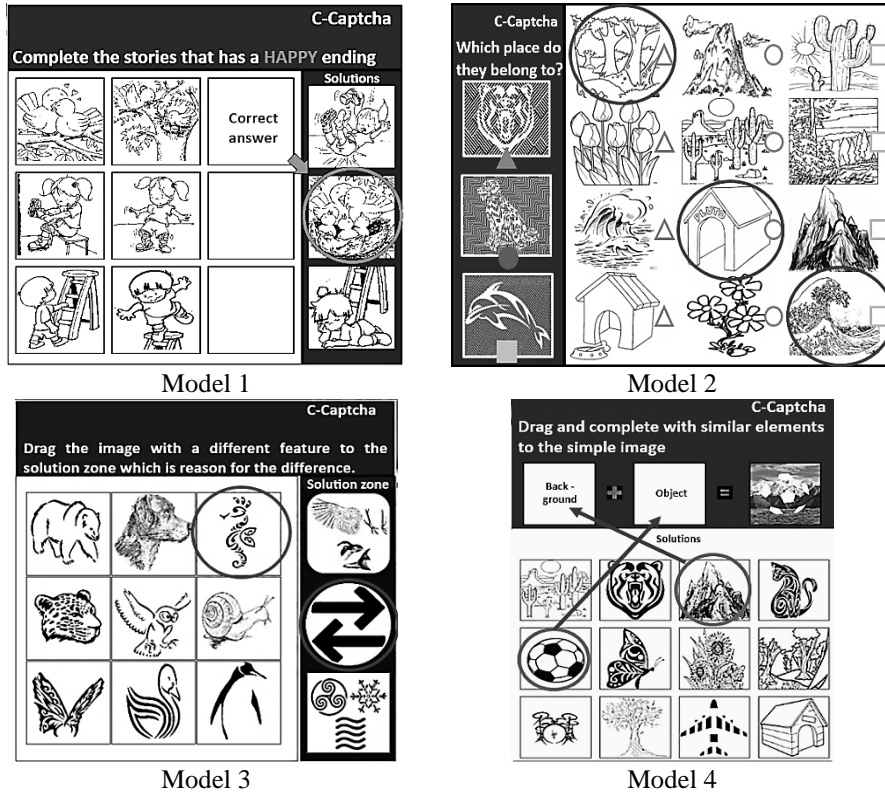


Fig. 1. Captchas from model 1 to model 4 showing the correct solutions and the correct places.

### 3.5 Model 5: Shared Features Identification

Abstraction is tested in this captcha model, a simple task in which the user needs to drag and drop the answers that match with the feature mentioned in the instructions region (see Fig. 2). The challenge region presents twelve images; from which the user has to select three images whose associated entities share the common feature. Natural language processing, abstraction, common sense reasoning and background knowledge processing are required for this challenge.

### 3.6 Model 6: Size Based Sorting

The goal is to sort, from smallest to biggest, four abstract images representing different sized objects (see Fig. 2). After recognizing each abstract image, the size sorting can only be performed by associating each image semantics with background knowledge about its represented object size.

### 3.7 Model 7: Suggested and Explicit Object Relation

The abilities needed to complete this CAPTCHA are: pattern recognition, common sense reasoning and abstraction. It is a simple test in which the user must drag the abstract image from the challenge region that corresponds with the suggested object shown in the solution region (see Fig. 2).

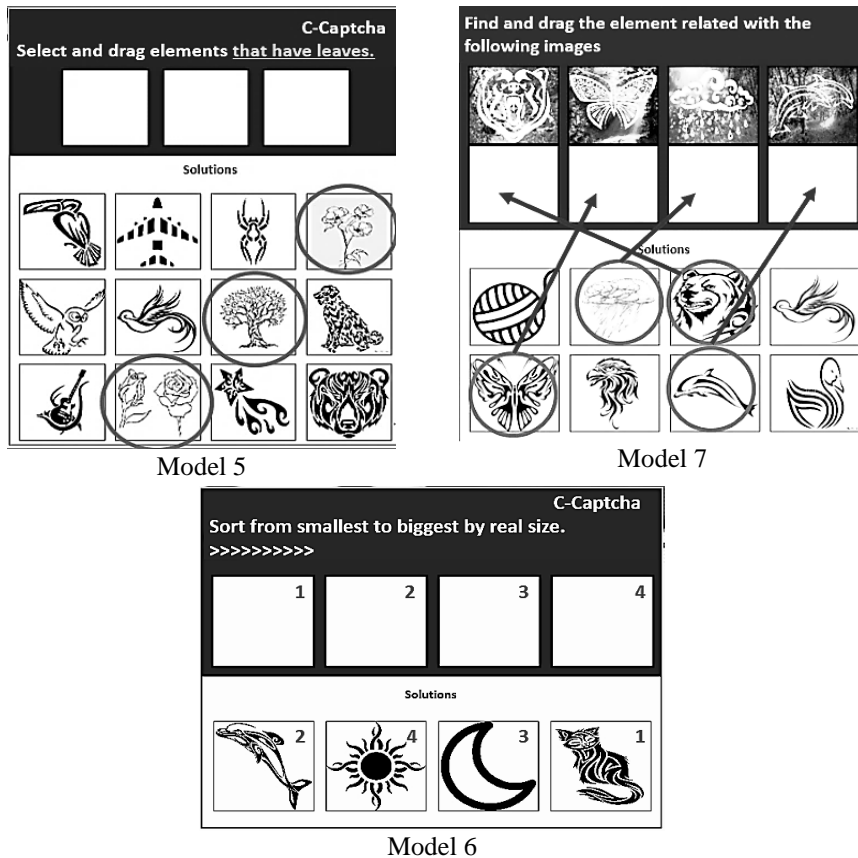
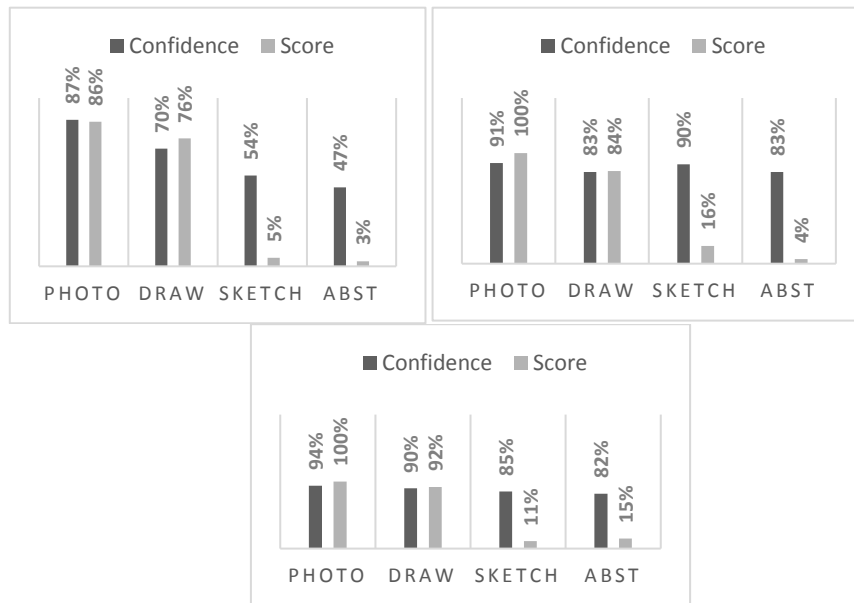


Fig. 2. CAPTCHA models 5 to 7 showing the correct solutions and their corresponding places.

## 4 Testing Artificial Agents

Since proposed captcha models are new there are no current artificial agents trained to solve them. Therefore, the only possible test is to present the abstract images for recognition to specialized cognitive agents. In order to make a comparison between humans and artificial agents, some experiments were carried out using four types of images: photography, realistic drawings, sketches and abstract images. The selected agents were: Microsoft's Computer Vision [16], IBM's Visual Recognition API [17],

and Google’s Vision API [18]. Each agent is trained to input and image and processes it to provide some information as the content, colors, size and semantics.



**Fig. 3.** Results of image recognition test: Microsoft’s API (up left), IBM’s API (up right) and Google’s API (below).

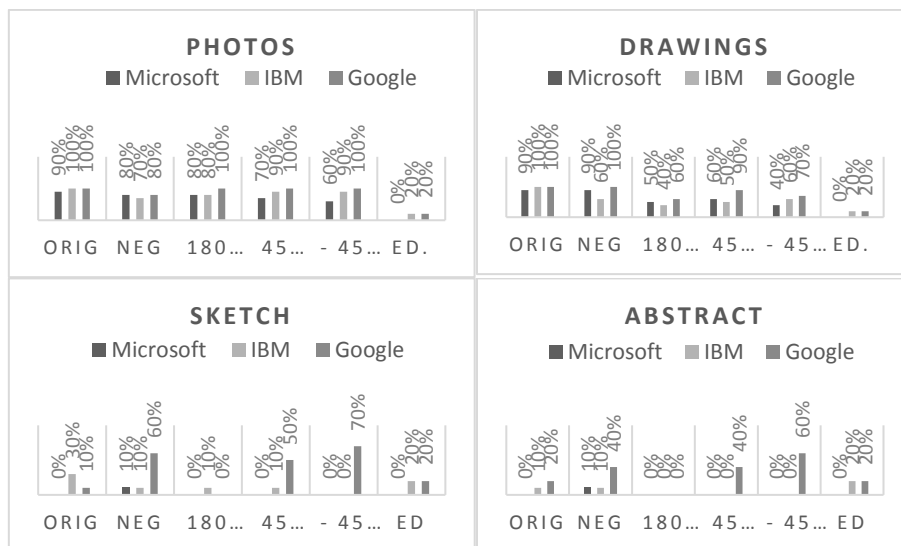


**Fig. 4.** Score comparison for each kind of images and its transformations

The first experiment used a corpus of 400 images, 100 images of every kind of image above mentioned. The results in image recognition for each agent are shown in

Fig. 3. The graphics show the number of correct classifications and the confidence level; the latter is a mark that each agent provides assessing its own classification. All agents can classify the photos and drawings with high confidence, but as the abstraction level increases the score gets reduced. When sketches and abstract images as those used in C-Captchas are presented to the selected agents, the score gets lower even when they show a high confidence.

In the second test, we took 10 images of each type and four transformations were applied to them. The transformations were: inverted colors and rotations to  $45^\circ$ ,  $-45^\circ$  and  $180^\circ$ . Also, 10 photos were modified with Photoshop to make them look like abstract images; the resulting images were added to the experiment. The agents were tested with a total of a 170 images. The results were compared among them to support the idea that abstractions and transformations make the task more difficult in case of artificial agents (see Fig 4).

As it was expected, the transformed images were more difficult to recognize than the original ones. In the case of abstract images, transformed images were almost never correctly classified by agents. Strangely Google's agent better classifies sketches and abstract images if they are in negative colors or with rotations of  $45^\circ$ . This phenomenon could probably be explained with the image that Google's team used as the training set for the agent. It should be mentioned that Google's agent had the best performance when classifying the images, but it is still low with abstractions.

So we conclude that abstract images used in the proposed captcha models represent great challenges to artificial agents as they have low rate of success in this experiment. If an artificial agent tries to break this captchas, first it must understand the instructions, recognize the images, and finally devise a solution to the test. Now, an artificial agent that has low rate of success recognizing abstract images is expected to have even a lower rate of success passing the whole test.

## 5 Conclusions

Advances in artificial intelligence have allowed traditional captchas to be broken, motivating some research to improve currently used captcha techniques. To introduce more sophisticated aspects of some cognitive abilities into captchas. Those abilities include common sense reasoning, abstraction, and visual processing as explained by Gestalt's laws. For the moment it seems not possible to replicate those cognitive abilities with artificial agents.

Abstract images, by themselves, represent a big problem for artificial agents, even for those specialized in image recognition. Enterprises like Google, Microsoft or IBM cannot handle high levels of abstraction yet.

If abstract images are added to a captcha model based on common sense and requiring natural language processing or having a specific given context, the difficulty in recognizing images increases. A future goal is to determine which areas of AI could constitute new sources for future solutions, in order to create new captchas principles that be easy for human beings and complex for artificial agents.

## References

1. Von Ahn, L., Blum, M., Langford, J.: Telling humans and computers apart automatically. *Communications of the ACM*, 47(2), 56–60 (2004)
2. Turing, A. M.: Computing machinery and intelligence. *Mind*, 59(236), 433–460 (1950)
3. Baecher, P., B üscher, N., Fischlin, M., Milde, B.: Breaking reCAPTCHA: a holistic approach via shape recognition. *Future challenges in security and privacy for academia and industry*, 56–67 (2011)
4. Sivakorn, S., Polakis, I., Keromytis, A. D.: I am robot: (deep) learning to break semantic image captchas. In: *Security and Privacy (EuroS&P), 2016 IEEE European Symposium*, pp. 388–403. IEEE (2016)
5. Sheheryar, M. A., Mishra, P. K., Sahoo, A. K.: A review on Captcha generation and evaluation techniques. *ARNP Journal of Engineering and Applied Sciences*, 11(9), 5800–5811 (2006)
6. Kaur, K., Behal, S.: Captcha and Its Techniques: A Review. *International Journal of Computer Science and Information Technologies*, 5(5), 6341–6344 (2014)
7. CAPTCHA Homepage, <http://www.captcha.net>, last accessed 2017/06/25.
8. Elson, J., Douceur, J. R., Howell, J., Saul, J.: Asirra: a CAPTCHA that exploits interest-aligned manual image categorization. In: *ACM Conference on Computer and Communications Security*. (Vol. 7), 366–374 (2007)
9. Nu Captcha Homepage, <http://www.nucaptcha.com>, last accessed 2016/04/18.
10. Tanvee, M. M., Nayeem, M. T., Rafee, M. M. H.: Move & select: 2-layer CAPTCHA based on cognitive psychology for securing web services. *International Journal of Video & Image Processing and Network Security*, 11(5), 9–17 (2011)
11. Belk, M., Germanakos, P., Fidas, C., Holzinger, A., Samaras, G.: Towards the personalization of CAPTCHA mechanisms based on individual differences in cognitive processing. In: *Human Factors in Computing and Informatics*, 409–426 (2013)
12. Yamamoto, T., Suzuki, T., & Nishigaki, M.: A proposal of four-panel cartoon CAPTCHA. In: *Advanced Information Networking and Applications, 2011 IEEE International Conference*, 159–166. IEEE (2011)
13. Rusu, A., Docimo, R.: Securing the web using human perception and visual object interpretation. In: *Information Visualisation, 13th International Conference*, 613–618. IEEE (2009)
14. Neisser, U.: *Cognitive psychology: Classic Edition*. Psychology Press, New York (2014)
15. Davis, E., Morgenstern, L.: Introduction: Progress in formal commonsense reasoning. *Artificial Intelligence*, 153(1–2), 1–12 (2004)
16. Computer Vision API Homepage, <https://azure.microsoft.com/es-mx/services/cognitive-services/computer-vision/>, last accessed 2017/05/17.
17. IBM Watson Developer Cloud, <https://visual-recognition-demo.mybluemix.net/>, last accessed 2017/05/22.
18. Google Cloud Platform, <https://cloud.google.com/vision/>, last accessed 2017/05/22.

# Estimation and Identification Process Using an Exponential Forgetting Factor

Karen Alicia Aguilar Cruz <sup>1</sup>, José de Jesús Medel Juárez<sup>1</sup>,  
Romeo Urbieto Parrazales<sup>1</sup>, María Teresa Zagaceta Álvarez<sup>2</sup>

<sup>1</sup> Centro de Investigación en Computación - Instituto Politécnico Nacional, CDMX,  
Mexico

<sup>2</sup> Escuela Superior de Ingeniería Mecánica y Eléctrica Unidad Azcapotzalco,  
Instituto Politécnico Nacional, CDMX,  
Mexico

karen\_ali320@hotmail.com, jjmedelj@yahoo.com.mx, rurbieta700@gmail.com,  
mtza79@yahoo.com.mx

**Abstract.** System identification and parameter estimation are important to obtain information from systems which are difficult to model and that are usually presented as Black- Box models. This work presents a point to point parameter estimation of a generalized non-deterministic system, whose results are variable through time, by using an exponential Forgetting Factor (FF). An average approximation is used as base to add an exponential FF to modify and improve the average results, without increasing the computational cost considerably. A comparison of the results applying the Least Square Method (LSM), the Recursive Least Square (RLS) and FF is presented using a signal for tracking a simple trajectory to prove the performance of the proposed method. As conclusion, it is obtained an online estimation for a non-deterministic signal without needing a previous training or Knowledge Base (KB).

**Keywords:** parameter estimation, system identification, exponential forgetting factor, least square method.

## 1 Introduction

A system is an arrangement of different elements interacting together to accomplish an objective [1, 2]. There are, for example, biological, physical, chemical systems or the combination of them. For their analysis, representative models are created, whose complexity depends on the number of considered details. To begin an analysis is necessary to identify the known characteristics, which generally are the inputs and outputs seen through measurable signals. Finally, a mathematical expression could be determined based on the description of the behavior and the relation between the variables and parameters.

Models created considering the involved physical phenomena are difficult to obtain because it is necessary to know what happens in the system, how it interacts with its environment and what its boundaries are. A Black-Box (BB) description, shown in Fig.1, is useful when only the input and output signals are known, and then the internal dynamic is obtained by parameter estimation techniques [3, 4, 5, 6].

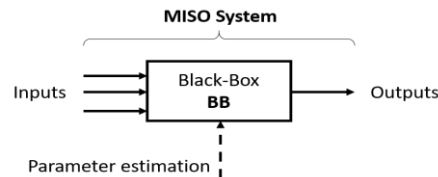


**Fig. 1.** Black-Box (BB) model for a Multiple Input Single Output (MISO) system.

System Identification (SI) and Parameter Estimation (PE) are related process, due to the first one depends on the second. First it is necessary to determine, according to the known signals, the parameters that describe the dynamic system. These parameters will allow to identify, from an input signal, an output identified signal; which is supposed to describe a reference system in an approximated form.

Different techniques have been developed and studied, such as a Fuzzy Logic (FL), Lyapunov, Sliding Modes (SM) and Intelligent Systems (IS) or their combinations integrating Hybrid Estimation- Identification (HE-I) systems.

According to [7] and [8], hybrid methods not only require a high number of operations but also of computing time. In order to reduce these magnitudes, the mathematical expectation is used. Nevertheless, a non-stationary system requiring a point to point approximations will not be modeled adequately considering only an average estimation because new parameters are necessary for each variation in the reference, and for these cases the statistical information is not useful. So that, a Forgetting Factor (FF) must be used in any method to reduce the convergence error between the reference and the identification results deleting unnecessary past information.

Within the state of the art, FF has been represented through constant coefficients, linear functions, and exponential functions considering the Euler number, by intervals or with a specific sample time [9]; in almost all cases the FF is used to improve another algorithm [10, 11, 12]. In [13] is mentioned that FF must be between 0 and 1, where close to 0 values discard the information faster than those closer to 1.

In fact, real systems are variable, meaning their characteristic parameters too, creating the necessity developing algorithms that allow the calculation of parameters under non-constant conditions within time restrictions. Thus, for variable systems, it is necessary to determine also a variable FF to obtain an adaptive response.

In the present paper the effectiveness of an Exponential Forgetting Factor (EFF) applied to an average estimation is proved by implementing following steps: first, an equivalent Multiple Input Single Output (MISO) system seen as a BB with variable parameters; then, it is used a recursive description to obtain an online estimation, after that, the error between the input and output is used to determine the necessary convergence to reach a reference using the magnitude and sign properties as arguments in the

last estimation stage and finally, obtaining values are applied into BB model to complete the system identification process. The method is implemented in a signal tracking problem and is compared to the Least Square Method (LSM) and the Recursive Least Square (RLS) to identify their advantages.

## 2 Average Estimation

Considering an Autoregressive Moving Average (ARMA) of first order with a single delay, due to the characteristics and description presented in [14], it is possible to estimate the unknown parameters  $\hat{A}_t$  from the reference signal  $y_t$  and the inputs of a system  $x_t$ , as shown in Fig. 2, using the average expected value as in (1), where  $T$  and  $+$  are the transpose and inverse operations, respectively. Then, the identified signal is obtained using the estimated parameters as in (2).

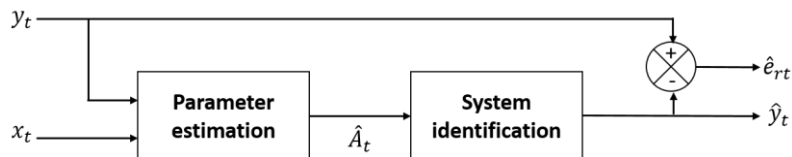


Fig. 2. Parameter estimation and system identification from a first order ARMA model.

$$\hat{A}_t = E\{y_t x_t^T\} (E\{x_t x_t^T\})^+, \quad (1)$$

$$\hat{y}_t = \hat{A}_t x_t. \quad (2)$$

Comparing the reference and the identified signals obtaining the identification error  $\hat{e}_{rt} = \hat{y}_t - y_t$ . Based on its functional  $J_{et}$  an average parameter estimation gave a zero error only in the infinite point in which the estimation is considered optimal [15].

## 3 Recursive Parameters Estimation

When using the concept of Functional Error (FE), the recursive description (3) of the estimated parameters is obtained.

$$\hat{A}_t = t^{-1} y_t x_t^T Q_t^+ + t^{-1} (t - 1) \hat{A}_{t-1} Q_{t-1}^+ Q_t^+, \quad (3)$$

where  $Q_t = t^{-1} x_t x_t^T + t^{-1} (t - 1) Q_{t-1}$  and then applying (3) in (2) the recursive description of the identified signal is obtained. An explained description of (2) is presented in [14].

At this point, an average estimation, useful for systems with small parameters variations. The problem with those having a non-deterministic behavior is that we do not know if perturbations breaking the stationary condition, or leading the system out of their boundaries, will be presented.

## 4 EFF Estimation

From the average estimation, its low computational complexity is a remarkable advantage. In cases when a unique parameter is used in combination with an adequate FF [16] it presents a better performance compared to other hybrid versions [7,17].

Within the state of the art, FF is implemented to modify the covariance from a system state, but the descriptions are complex due to the number of operations, which increase in order of the parameter matrix. Each FF affects with different intensity the estimation results, having the exponential kind the most accepted, due to the past information tends to lose weight through the evolution of the system following the tendency of the exponential function (4) [18], whose base is the number  $e$ , and  $C$  and  $arg$  the coefficient and argument that affects its behavior.

$$\exp = Ce^{arg} \quad (4)$$

Two functions presented in different calculations, and that are not extensively used to modify the Forgetting Factor (FF), are the *sign* (5) and the *absolute* (5). Each of them gives different properties from magnitudes without increasing considerably the complexity.

$$|x| = \begin{cases} x & \text{if } x \geq 0, \\ -x & \text{if } x < 0, \end{cases} \quad (5)$$

$$\text{sgn}(x) = \begin{cases} 1 & \text{if } x > 0, \\ 0 & \text{if } x = 0, \\ -1 & \text{if } x < 0. \end{cases} \quad (6)$$

A comparison of both functions is developed to determine which is more useful for the error correction in the estimation-identification process. Fig. 3 shows the results.

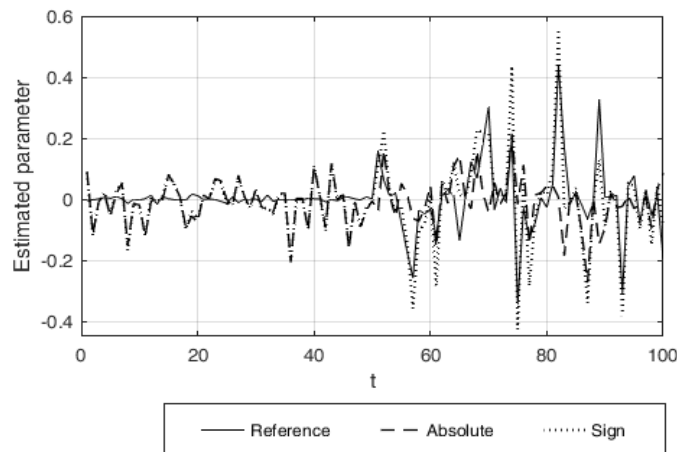


**Fig. 3.** Comparison of the sign and absolute function in the approximation of a signal.

As in shown in Fig. 3, comparing both functions to approximate a reference with different magnitudes of variations, the sign function performs better, so this is the one selected. It is also possible to see that when the reference tends to zero, both approximations are similar, obtaining a more remarkable variation when the error is different from zero.

Considering the error identification as an innovation process and the principal argument for the exponential correction factor, as well as the characteristics given by the sign function, it is proposed in [19] the use of the Exponential Forgetting Factor (EFF) (7).

$$EFF_t = \text{sgn}(\hat{A}_t)e^{\text{sgn}(\hat{A}_t)e_{rt}}. \tag{7}$$

This factor is applied to modify the first average estimation and obtaining a second estimation as indicated in (8)

$$\hat{A}_t = \hat{A}_t + EFF_t - \text{sgn}(\hat{A}_t). \tag{8}$$

To obtain the final identified output is necessary to apply (8) in (2); obtaining a corrected estimation in two complete iterations. The block diagram in Fig. 4 summarizes the procedure, where the dotted lines indicate the second estimation stage.

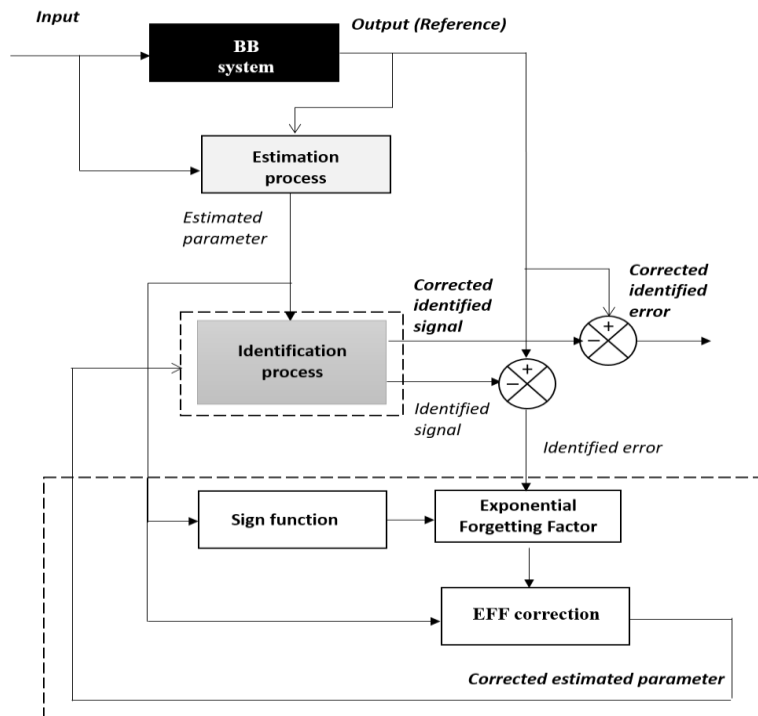


**Fig. 4.** Estimation-Identification block diagram, with two stages of correction using the sign function and the Exponential Forgetting Factor (EFF).

## 5 Application Example

The estimation-identification process analyzed in time is focused on the shape of a signal. To visualize the effectiveness of the EFF correction, the method is applied in a simple tracking trajectory problem.

According to [20], the initial trajectory assigned to a flight could be adjusted through time to optimize the path with the objective of avoid accidents and to take advantage of the wind flow [21]. Searching benefits in security, reduction of the fuel consumption and environment pollution.

Being the reference signal a trajectory from one point to another given in latitude and longitudinal coordinates, first the Recursive Least Square (RLS) and the Least Square Methods (LSM) are compared.

To implement these first two methods is necessary to determine the longitude of the filter and their initial parameter values. Longitude could be between  $l$  to  $n$ , being  $n$  the biggest value, and the initial parameters between  $0$  and  $l$ .

In Fig. 5 different filters size and their execution time are presented. This data was obtained considering the input as a random signal and output signal from the reference trajectory.

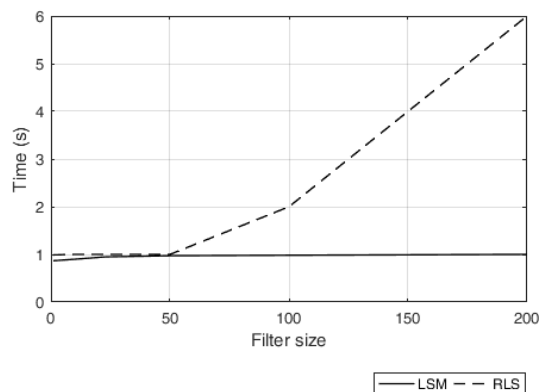


**Fig. 5.** Comparison in execution time between using the Least Square Method (LSM) and the Recursive Least Square (RLS).

From Fig. 5 is easy to appreciate that an increment in the filter size implies increasing the execution time. Thus, a second is performed to identify which filter, LSM or RLS methods, approximates better the reference and with what size. Fig. 6 shows these performances considering filters of size  $l$ ,  $23$  and  $50$ .

The  $23$  size LSM was the best adapted to the reference, while any size of the RLS method could not approximate the trajectory.

From previous results, it is decided to use the LMS ( $23$ ) as reference to compare the correction through the EFF estimation. Fig. 8 shows the approximation to the reference comparison, and Fig. 9 the error obtained with each method, where the LSM has an approximate of  $2.5\%$  error while the EFF  $6\%$ .

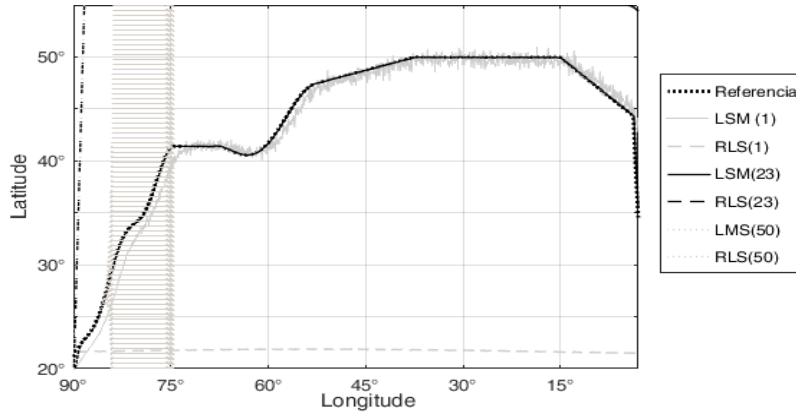


Fig. 6. Comparison of the LSM and RLS performance for different filter sizes.

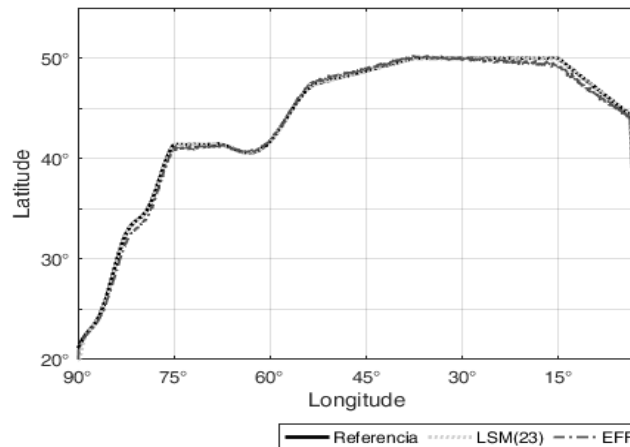


Fig. 7. Performance in the tracking trajectory problem using the LSM and the EFF methods.

In addition to this, another comparison is performed, but now using the CPU-time from the Matlab® interface to measure how much time they take to accomplish the estimation. Fig. 9 presents the results, where the EFF estimation takes less time than the LSM method.

## 6 Conclusions

With the development of the present paper, it was possible to compare a parameter estimation - system identification process by using an Exponential Forgetting Factor (EFF), reducing the influence of past data in comparison to the traditional Least Square Method (LSM) and the Recursive Last Square (RLS).

The identification obtained with the LSM and the EFF was similar and better than that one obtained with the RLS, for the considered signal reference. When using the

adequate size filter for the LSM the error tends to zero, nevertheless, when using the EFF it is not necessary to define initial parameters and its execution time is 75%, approximately, lower than the one LSM presents.

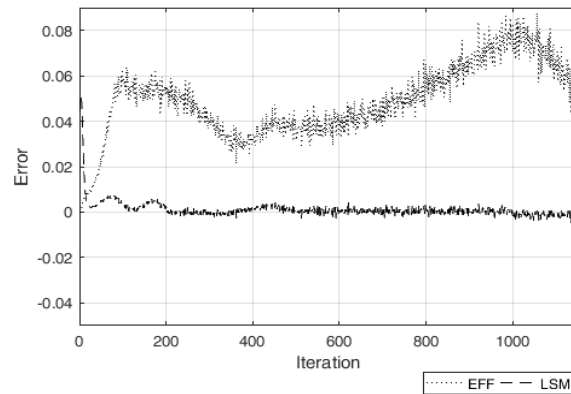


**Fig. 8.** Error obtained when LSM and EFF methods are applied to identify a reference.

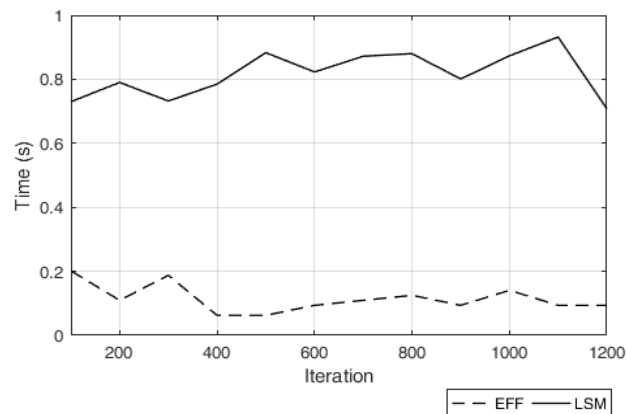


**Fig. 9.** Execution time taken from the *cputime* given by Matlab for the tracking trajectory problem, measured for different number of iterations and comparing the EFF and the LSM.

It is necessary to compare more Forgetting Factor (FF) configurations to determine which is the best, but for now the combination of the sign function of the estimated parameter, in average, and the error magnitude, as presented in this work, gives useful results when time restrictions are presented.

## References

1. Bakshi, U., Bakshi, V.: Automatic Control Systems. Technical Publications (2009)
2. García, R. P. Ñ.: Apuntes de sistemas de control. Editorial club Universitario (2003)

3. Ugalde, H., Carmina, J., Reyes, J., Mantilla, J.: Computational cost improvement of neural network models in black box nonlinear system identification. *Neurocomputing*, 166, 96–108 (2015)
4. Godjevac, J. Neuro-fuzzy controllers: design and application. In: PPUR presses polytechniques (1997)
5. Qiu, F., Jensen, J. R.: Opening the black box of neural networks for remote sensing image classification. *International Journal of Remote Sensing*, 25(9), 1749–1768 (2004)
6. Wnag, J.: Adaptive control for nonlinear systems using decomposed neural network. *Cybernetics & systems* 29 (1), 73–83 (1998)
7. Aguilar, K., Medel, J., Fernández, J., Viguera, E.: Neural net gains estimation based on an equivalent model. *Computational Intelligence and Neuroscience* 2016 (2016)
8. Aguilar, K., Zagaceta, M., Medel, J.: Adaptation of weights in a neuron using an integrated filter. *Research in Computing Science*, 100, 139–147 (2015)
9. Parkum, J. Pulsen, N., Holst, J.: Recursive forgetting algorithms. *Internacional Journal of Control* 55(1), 109–128 (1992)
10. Nishiyama, K.: A new approach to introducing a forgetting factor into the normalized least mean squares algorithm. *Signal Processing* 114, 19–23 (2015)
11. Badoni, M., Singh, A., Singh, B.: Variable forgetting factor recursive least square control algorithm for dstatcom. *IEEE Transactions on Power Delivery* 30(5), 2353–2361 (2015)
12. Yinling, J., Beiyang, J.: Multi-model neural network sliding mode control for robotic manipulators. In: *Mechatronics and Control (ICMC), International Conference on IEEE*, 2431–2435 (2015)
13. Chand, A., Kawanishi, M., Narikiyo, T.: Parameter estimation for the pitching dynamics of a flapping-wing flying robot. In: *IEEE International Conference on Advanced Intelligent Mechatronics (AIM) IEEE*, 1552–1558 (2015)
14. Aguilar, K., Urbieto, R., Medel, J.: Stochastic System Model Evaluated with First and Second Order Filters. *Research in Computing Science* 118, 127–136 (2016)
15. Juárez, M., Parrazales, R., Orozco, R.: Estimador estocástico para un sistema tipo caja negra. *Revista mexicana de física* 57(3), 204–210 (2011)
16. Albu, F.: Improved variable forgetting factor recursive least square algorithm. In: *Control Automation Robotics & Vision (ICARCV), 12th International Conference on IEEE*, pp. 1789–1793 (2012)
17. Henwood, N.: Estimation en ligne de paramètres de machines électriques pour véhicule en vue d'un suivi de la température de ses composants. PhD thesis, Ecole Nationale Supérieure des Mines de Paris (2014)
18. Antonio, N., Pedro, C., Manuel, M.: Conceptos básicos de filtrado, estimación e identificación. *IEEE Transactions on Power Delivery* 30(5), 2353–2361 (2015)
19. Aguilar, K.: Filtro digital para la estimación de parámetros variantes usando el factor de olvido exponencial. Thesis, Centro de Investigación en Computación IPN (2015)
20. Altus, S.: Effective flight plans can help Airlines economize. *Boeing Aero* (2009)
21. Cattani, L., Eagle, P.: Aircraft identification, trajectory tracking and prediction. Tech. rep. DTIC Document (1995)



# Análisis de readmisión hospitalaria de pacientes diabéticos mediante aprendizaje computacional

Germán Cuaya-Simbro<sup>1</sup>, Elias Ruiz<sup>1</sup>, Angélica Muñoz-Meléndez<sup>2</sup>,  
Eduardo F. Morales<sup>2</sup>

<sup>1</sup> Instituto Tecnológico Superior de Oriente del Estado de Hidalgo, Apan Hidalgo,  
México

<sup>2</sup> Instituto Nacional de Astrofísica, Óptica y Electrónica, Tonantzintla, Puebla,  
México

{gcuaya, eruiz}@itesa.edu.mx, {amunoz,emorales}@inaoep.mx

**Resumen.** La disminución de la tasa de readmisión hospitalaria temprana es una situación de interés debido a que esto generalmente es debido a complicaciones de alguna enfermedad en los pacientes. En México es particularmente importante la prevención de la readmisión temprana de pacientes diabéticos, puesto que esto está asociado a complicaciones derivadas de la enfermedad, como pueden ser problemas en los ojos, riñones, nervios, corazón, entre otros. Existen trabajos en donde se describen métodos computacionales para el diagnóstico de diabetes [10,4], pero en estos trabajos no se hace un análisis de los factores relacionados a las complicaciones de la enfermedad. En este artículo, se presenta un análisis basado en técnicas de aprendizaje computacional para estimar las variables más importantes asociadas a la readmisión hospitalaria en pacientes con diabetes. La metodología presentada contempla el uso de métodos de selección de atributos y selección de instancias mediante técnicas supervisadas y no supervisadas, así como la construcción de clasificadores con la información obtenida, finalmente, se presentan y se discuten los valores de precisión y recuerdo de los clasificadores para mostrar la efectividad de éstos en la predicción de readmisión temprana de pacientes diabéticos. Los resultados muestran las ventajas del uso de la metodología propuesta para la identificación de la información relevante asociada a la prevención de readmisión hospitalaria.

**Palabras clave:** selección de atributos, agrupamiento, clasificación, readmisión hospitalaria.

## Hospital Readmission Analysis of Diabetic Patients through Computational Learning

**Abstract.** The decrease in the rate of early hospital readmission is a situation of interest because this is usually due to complications of some

disease in the patients. In Mexico, the prevention of early readmission of diabetic patients is particularly important, since this is associated with complications derived from the disease, such as problems in the eyes, kidneys, nerves, heart, among others. There are works describing computational methods for the diagnosis of diabetes [10,4], but in these works an analysis of the factors related to the complications of the disease is not done. In this article, we present an analysis based on computational learning techniques to estimate the most important variables associated with hospital readmission in patients with diabetes. The presented methodology contemplates the use of methods of selection of attributes and selection of instances by means of supervised and unsupervised techniques, as well as the construction of classifiers with the obtained information, finally, the values of precision and memory of the classifiers are presented and discussed. to show the effectiveness of these in the prediction of early readmission of diabetic patients. The results show the advantages of using the proposed methodology for the identification of relevant information associated with the prevention of hospital readmission.

**Keywords:** attributes selection, grouping, classification, hospital readmission.

## 1. Introducción

Actualmente los modelos de inteligencia computacional son usados cada vez con mayor frecuencia en el ámbito médico, como herramientas para el diagnóstico de enfermedades [6]. Sin embargo, es de especial interés usar las herramientas de inteligencia computacional en aplicaciones no solamente de diagnóstico, sino de predicción, en particular, es de suma importancia prevenir la aparición o complicación de enfermedades, lo cual generalmente implica una pronta (temprana) readmisión hospitalaria de un paciente.

En los hospitales es importante tener un índice bajo de readmisión hospitalaria [1] la cual es derivada de la complicación de algún padecimiento, como pueden ser cardiovascular, respiratorio, digestivo, diabetes, por mencionar algunos. Algunos países han creado programas para reducir la readmisión hospitalaria [12], con el objetivo de reducir los costos de salud y de mejorar la calidad de vida de los pacientes. Es importante señalar que, el reducir la readmisión hospitalaria implica la prevención y/o predicción de ésta.

La diabetes es una enfermedad con una incidencia cada vez más alta en el mundo [5,11]. En particular, en México es una enfermedad de alerta en hospitales [13]. Actualmente los hospitales se encuentran realizando esfuerzos en materia de diagnóstico preventivo hacia la población en general. Diagnosticar pre-diabetes o hacer recomendaciones de mejores hábitos de alimentación y ejercicio para pacientes con predisposición a ella tiene un impacto en la reducción de costos para las instituciones de salud y en una mejoría para la calidad de vida del paciente [2].

En contraste con lo anterior, poco se ha estudiado y discutido sobre aquellos pacientes diagnosticados con diabetes y los cuales tuvieron que ser reingresados al hospital en un corto tiempo por alguna complicación de la enfermedad, lo cual tiene implicaciones graves para la salud del paciente, en ocasiones la muerte. La mayoría de estas situaciones son ocasionadas debido a que un paciente llega a medicina general o a especialidades que no corresponden al tratamiento de la diabetes (endocrinología), lo que puede derivar en una complicación de la enfermedad como pueden ser, problemas en riones, pies, ojos o piel, corazón, entre otras. Dichas complicaciones pueden ser evitadas, pero se requiere un diagnóstico acertado y preventivo. Por este motivo, resulta importante contar con estrategias que permitan ayudar a predecir posibles complicaciones asociadas a la diabetes, lo cual generalmente deriva en una readmisión hospitalaria temprana, y en específico determinar los factores que están asociados a dicha readmisión.

En este trabajo de investigación se presenta un análisis de la información de una base de datos con registros de pacientes diagnosticados con diabetes los cuales fueron readmitidos en el hospital, determinando por medio de aprendizaje computacional aquellas variables que están asociadas a una readmisión temprana (en un periodo de tiempo menor a 30 días) y mostrando como el uso de este tipo de técnicas puede apoyar en la identificación de factores asociados a la complicación de enfermedades, en específico la diabetes.

## **2. Antecedentes**

Debido a la importancia de la diabetes a nivel mundial, se han reportado diversos trabajos que utilizan técnicas de aprendizaje computacional para diagnosticar diabetes en pacientes [10,4]. La mayoría de dichos trabajos, utilizan reglas de decisión o clasificadores SVM (*Support Vector Machine*) en un enfoque supervisado. Sin embargo, su enfoque es principalmente el diagnóstico, no la predicción y/o prevención de las complicaciones de alguna enfermedad.

Por otro lado, existen trabajos que reportan el análisis de información para prevenir o predecir la readmisión de pacientes, como se presenta en [19] donde realizan un caso de estudio sobre una determinada raza para verificar la readmisión de pacientes pertenecientes a ésta en un lapso menor a 30 días, utilizando un enfoque basado en un algoritmo de redes bayesianas. En [20] hacen un análisis del impacto de la hemoglobina glicosilada con respecto de los niveles de reincidencia del paciente diabético al hospital a lo largo de varios meses, los autores concluyen que la probabilidad de readmisión está ligada al diagnóstico primario del paciente y a las acciones para mantener los niveles de hemoglobina glicosilada bajo control. Igualmente, en [14] muestran la importancia de tener un control glucémico al dar de alta al paciente para reducir el riesgo de reingreso en la población mexicana, aunque la mayor razón de reingreso fue debido a infecciones y enfermedades cardiovasculares. Los trabajos citados parten del análisis de información *a priori*, proporcionada generalmente por los expertos (en particular la consideraciones de variables a utilizar), en contraste al trabajo realizado en

esta investigación, se propone el análisis mediante aprendizaje computacional de los datos para determinar los factores o variables asociados a la complicación de una enfermedad la cual derive en la readmisión del paciente, en específico en pacientes diabéticos. La identificación correcta de los factores de riesgo asociados a complicaciones de cierta enfermedad propiciara un mejor pronóstico.

Existen diversas técnicas del aprendizaje computacional para analizar datos a fin de seleccionar atributos o variables de interés, seleccionar instancias o ejemplos, mejorar la clasificación a partir de datos entre otras, por ejemplo, [8,15]. Es por esto que en este trabajo se presentan resultados de la aplicación de diferentes algoritmos estándar de selección de variables, agrupamiento, y clasificación, para la identificación de factores de riesgo asociados a complicaciones de la diabetes, lo cual implica una readmisión temprana del paciente. Los métodos de selección de variable, de agrupamiento y de clasificación fueron aplicados a través Weka, el cual es un software para minería de datos que permite realizar clasificación y selección de atributos [7].

### 3. Metodología

En este trabajo se utilizó la base de datos descrita en [20]. Esta base de datos cuenta con 101,766 visitas de pacientes (registros) los cuales fueron hospitalizados y a quienes se les asignó un número de identificación. Cada paciente tiene registrado un número determinado de visitas, esto es, un paciente en esta base de datos puede tener registradas 4 visitas, y otro paciente puede tener asociado solo 1 visita. En una visita se toman la información de la Tabla 1 la cual cuenta con 55 atributos.

**Tabla 1.** Nombre y tipo de dato de los atributos de la base de datos. Información detallada de la tabla puede ser consultada en [20].

| Atr. | Nombre del atributo      | Tipo     | Atr. | Nombre del atributo         | Tipo     |
|------|--------------------------|----------|------|-----------------------------|----------|
| 1    | Encounter ID             | Numérico | 15   | Num. of medications         | Numérico |
| 2    | Patient number           | Numérico | 16   | Num. of outpatient visits   | Numérico |
| 3    | Race                     | Nominal  | 17   | Num. of emergency visits    | Numérico |
| 4    | Gender                   | Nominal  | 18   | Num. of inpatient visits    | Numérico |
| 5    | Age                      | Nominal  | 19   | Diagnosis 1                 | Nominal  |
| 6    | Weight                   | Numérico | 20   | Diagnosis 2                 | Nominal  |
| 7    | Admission type           | Nominal  | 21   | Diagnosis 3                 | Nominal  |
| 8    | Discharge disposition    | Nominal  | 22   | Number of diagnoses         | Numérico |
| 9    | Admission source         | Nominal  | 23   | Glucose serum test result   | Nominal  |
| 10   | Time in hospital         | Numérico | 24   | A1c test result             | Nominal  |
| 11   | Payer code               | Nominal  | 25   | Change of medications       | Nominal  |
| 12   | Medical specialty        | Nominal  | 26   | Diabetes medications        | Nominal  |
| 13   | Number of lab procedures | Numérico | 27   | 24 features for medications | Nominal  |
| 14   | Number of procedures     | Numérico | 28   | Readmitted                  | Nominal  |

Cada visita registrada indica si el paciente fue readmitido antes de 30 días (clase 1), después de 30 días o ya no fueron readmitidos (clase 0), atributo *readmitted*. El análisis desarrollado identifica información relevante asociada a la readmisión temprana del paciente, y la relevancia de la información evaluada

mediante la construcción y evaluación de clasificadores, posteriormente se utilizan técnicas de agrupamiento para complementar o enriquecer la información relevante. Este proceso es descrito con detalle a continuación:

1. Se redujo el número de instancias mediante un enfoque supervisado de eliminación de registros incompletos.
2. Se realizó una conversión supervisada a datos numéricos de todos los atributos nominales.
3. Se ordenó la base de datos de acuerdo al atributo “Identificador de visita” (*Encounter ID*).
4. Se separó la base de datos de acuerdo al número de visitas de cada paciente, esto es, se creó una base de datos con la información de aquellos pacientes con únicamente 1 visita,  $M_1$ , posteriormente se construye una nueva base de datos con la información de los pacientes que tuvieron al menos 2 visitas,  $M_2$ , cabe señalar que la información contenida en esta nueva base de datos sólo está la información de la segunda visita de los pacientes dado que la información correspondiente a la primera visita ya se tiene almacenada en  $M_1$ . Se continúa con este proceso hasta tener por separada la información de cada una de las visitas de los pacientes. Una vez acabado este proceso se obtuvo un total de 26 bases de datos, esto es,  $M_1, M_2, \dots, M_{26}$ , donde  $|M_1| = 34321$ ,  $|M_2| = 6484$ ,  $|M_3| = 2259$ ,  $\dots$ ,  $|M_{26}| = 1$ .
5. Se determinó trabajar solamente con la información de los pacientes que tienen al menos 3 visitas registradas, esto es, se usó sólo la información de  $M_1$ ,  $M_2$ , y  $M_3$ , debido a que el objetivo de este trabajo es prevenir las complicaciones de la diabetes, es decir, prevenir las readmisiones tempranas asociadas a esta enfermedad.
6. Se realizó un proceso de uniformidad de las bases de datos anteriores, buscando tener la misma información en cada una de ellas, tomando como referencias los elementos contenidos en  $M_3$ , 2259, y eliminando los elementos diferentes en  $M_1$  y  $M_2$ . Así,  $|M_1| = |M_2| = |M_3| = 2259$ .
7. Se filtró la información de las bases de datos conservando únicamente aquellos pacientes (instancias) que fueron diagnosticados con algún tipo de diabetes, atributos *Diagnosis 1*, *2* o *3*. Así,  $|M_1| = |M_2| = |M_3| = 485$ .
8. Se unió la información de las 3 bases de datos anteriores en una sola de tal modo que se obtuvo la base de datos con la que se trabajó,  $BD_{all}$ , donde  $DB_{all} = M_1 \cup M_2 \cup M_3$ ,  $|DB_{all}| = 1455$ .
9. Se realizó selección de atributos [8] mediante la regla  $V_{sel} = \bigcup_{j=1}^n S_j$ , donde  $S_j$  es el conjunto de variables obtenidas por un método de selección de atributos. En los experimentos  $n = 5$  y el umbral de cada  $S_j$  fue fijado a los seis primeros resultados. Los métodos de selección de atributos utilizados fueron: método basado en correlación [9], método basado en correlación de *Pearson*, método basado en ganancia de información, y método basado en selección de atributos mediante el uso de reglas. Así el conjunto de variables  $V_{sel}$  obtenido tiene 13 elementos los cuales son mostrados en la Tabla 2. De acuerdo a las variables seleccionadas se creó una base de datos conservando únicamente dichas variables  $DB_{sv}$ .

**Tabla 2.** Variables escogidas por los métodos de selección de variables. Las variables con el número 27\* corresponden a nombres de medicamentos consumidos por el paciente.

| No. Atributo | Nombre del atributo        | No. Atributo | Nombre del atributo        |
|--------------|----------------------------|--------------|----------------------------|
| 18           | Number of inpatient visits | 27*          | glimepiride                |
| 22           | Number of diagnoses        | 8            | Discharge disposition      |
| 27*          | Insulin                    | 26           | Diabetes medications       |
| 27*          | glipizide-metformin        | 17           | Number of emergency visits |
| 27*          | metformin-rosiglitazone    | 19           | Diagnosis 1                |
| 10           | Time in hospital           | 20           | Diagnosis 2                |
| 27*          | repaglinide                |              |                            |

10. Se procesó la información de  $DB_{all}$  con una técnica de aprendizaje no supervisado (k-medias de 2 grupos) para pesar de manera simple los ejemplos más fáciles de aprender y con ellos entrenar el modelo supervisado. Este procedimiento es una técnica simplificada de *boosting*. De lo anterior se obtienen 2 bases de datos, instancias correctamente aprendidas  $DB_{corr}$  y las incorrectamente aprendidas  $DB_{incorr}$ .
11. Finalmente se realizó clasificación de los datos utilizando técnicas de aprendizaje supervisado para cada conjunto de datos, tales como Redes Bayesianas [16], *bagging* [3], árboles [18] y vectores de soporte [17].

Un diagrama que ilustra el proceso de análisis de la información para determinar los factores relevantes asociados readmisión temprana de pacientes diabéticos a causa de complicaciones es presentado en las Figuras 1 y 2.

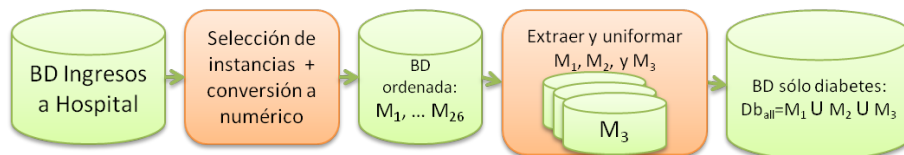


**Fig. 1.** Diagrama del pre-procesamiento de la información. Al final se consideran solamente pacientes con diagnóstico de diabetes.

#### 4. Resultados y discusión

Para mostrar la efectividad del uso de la metodología propuesta en este trabajo se construyeron 4 clasificadores, utilizando las diferentes bases de datos generadas durante el proceso de análisis de la información,  $DB_{all}$  base de datos con todos los atributos,  $DB_{sv}$  base de datos con las variables de la Tabla 2,  $DB_{corr}$  base de datos con las instancias correctamente aprendidas en el proceso de agrupamiento.

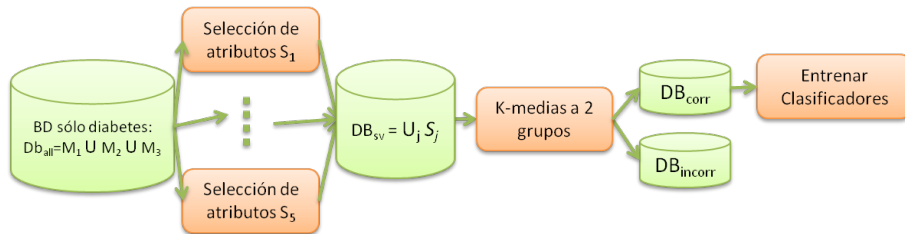


**Fig. 2.** Diagrama del proceso de análisis de la información el cual consiste en hacer selección de atributos, agrupamiento y clasificación.

Las métricas que se usaron para evaluar cada uno de los clasificadores fueron precisión, recuerdo y medida F.

La precisión se define como  $\frac{VP}{VP+FP}$ , donde VP son los verdaderos positivos (casos correctamente estimados) y FP son los falsos positivos (casos erróneamente clasificados como positivos). Esto es, es la proporción de instancias relevantes obtenidas respecto a las instancias recuperadas.

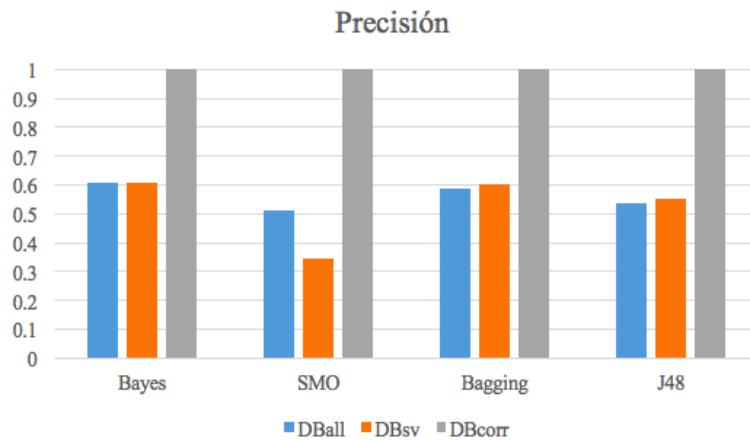


**Fig. 3.** Valor de precisión de los clasificadores con las diferentes bases de datos.

El recuerdo se define como  $\frac{VP}{VP+FN}$ , donde FN son los falsos negativos (casos erróneamente clasificados como negativos). Es decir, indica la proporción de instancias relevantes que se han recuperado sobre la cantidad total de instancias relevantes.

La medida F trata de establecer un compromiso entre la precisión y el recuerdo, evitando caer en una sobre representación de alguno de los dos. Se

define como se muestra en la Ecuación 1:

$$Medida F = \frac{2(precisión)(recuerdo)}{precisión + recuerdo} \quad (1)$$

Las Figuras 3, 4, 5 muestran los valores de las medidas de evaluación de los diferentes clasificadores construidos con las diferentes bases de datos.

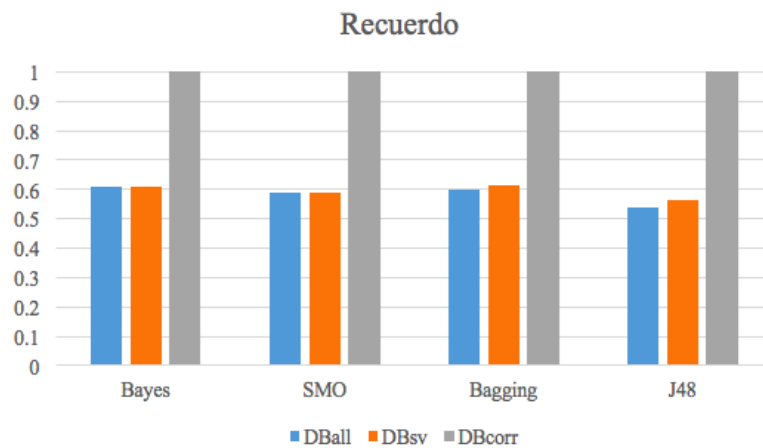


Fig. 4. Valor de recuerdo de los clasificadores con las diferentes bases de datos.

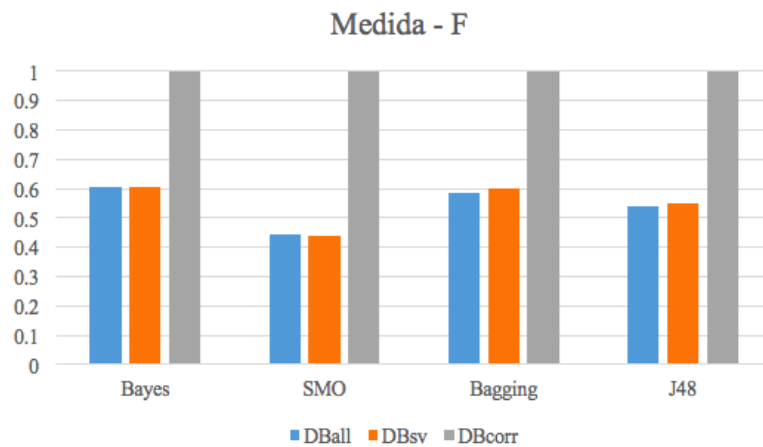


Fig. 5. Valor de la medida-F de los clasificadores con las diferentes bases de datos.

Como se puede observar los clasificadores construidos con las variables relevantes de la Tabla 2, tienen un desempeño similar a los clasificadores que fueron construidos utilizando todas las variables, esto es, se han determinado variables relevantes asociadas a la readmisión temprana debido a complicaciones de la diabetes.

Es de interés y de discusión los resultados obtenidos con la base de datos  $DB_{corr}$ , en principio esta base de datos es más pequeña que las bases  $DB_{all}$  y  $DB_{sv}$ ,  $|DB_{corr}| = 723$ , el uso de agrupamiento permitió reducir el problema y analizar la información más relevante, debido a que las instancias consideradas en dicho conjunto de datos son muy similares y al momento de construir clasificadores con dicha información podemos determinar las relaciones y la relevancia de dichas variables, dado que obtenemos modelo más efectivos en términos de precisión, recuerdo y medida-F.

Con un análisis más detallado de los modelos creados con  $DB_{corr}$  permitió observar variables tales como la insulina la cual está estrechamente asociada a la detección de un riesgo de readmisión hospitalaria temprana, lo cual a partir de la simple selección de atributos no era posible determinar, así debe tenerse en cuenta que determinar subconjunto de forma supervisada ayuda en la explicación de las relaciones de las variables respecto a la clase de interés, readmisión.

Este análisis es complementario a la información mostrada en la Tabla 2 y debe de ser considerada por los expertos en el dominio para diseñar y conducir estudios más especializados en donde sólo se incorpore la información relevante y se descarte información que de acuerdo a los resultados no aporta información para la determinación de readmisión en un periodo menor a 30 días.

## 5. Conclusiones y trabajo futuro

Se presenta una metodología la cual permite la identificación de los factores relacionados a la readmisión hospitalaria temprana debido a complicaciones en pacientes diabéticos.

La selección de atributos en conjunto con el agrupamiento de instancias similares permite determinar las principales relaciones entre las variables y mejorar los modelos de prevención de readmisión hospitalaria temprana.

Se discuten las posibles ventajas del uso de la metodología propuesta desde el punto de vista computacional y además de las ventajas del uso de las variables relevantes desde el punto de vista clínico. Dando con ello un panorama de como técnicas de aprendizaje automático pueden apoyar en procesos de prevención médica, en este caso la prevención de readmisión temprana de pacientes diabéticos.

Como trabajo futuro, se extenderán el conjunto de pruebas para validar la efectividad de la metodología propuesta. Estas pruebas pueden involucrar el uso de todo el conjunto de datos, uso de datos filtrados por edad, entre otras. De la misma forma y con el objetivo de evaluar la efectividad de la metodología se probará ésta con diferentes bases de datos, tal como bases de datos médicas, climáticas o financieras, por mencionar algunas. Finalmente, con el objetivo de

medir la relevancia de la información se propone la validación de los resultados obtenidos, específicamente la selección de variables, con expertos en el dominio, para verificar si los resultados encontrados tienen validez desde el punto de vista clínico.

## Referencias

1. Alonso Martínez, J.L., Llorente Diez, B., Echegaray Agara, M., Urbietta Echezarreta, M.A., Gonzalez Arencibia, C.: Reingreso hospitalario en Medicina Interna. *Anales de Medicina Interna* 18, 28 – 34 (05 2001)
2. Barquera, S., Campos-Nonato, I., Aguilar-Salinas, C., Lopez-Ridaura, R., Arredondo, A., Rivera-Dommarco, J.a.: Diabetes in Mexico: cost and management of diabetes and its complications and challenges for health policy. *Global Health* 9, 9 (2013), <http://www.ncbi.nlm.nih.gov/pmc/articles/PMC3599194/>
3. Breiman, L.: Bagging predictors. *Machine Learning* 24(2), 123–140 (1996), <https://doi.org/10.1007/BF00058655>
4. Fatima, M., Pasha, M.: Survey of machine learning algorithms for disease diagnostic. *Journal of Intelligent Learning Systems and Applications* 9, 1–16 (2017), [www.scirp.org/journal/PaperInformation.aspx?PaperID=73781](http://www.scirp.org/journal/PaperInformation.aspx?PaperID=73781)
5. Forouhi, N.G., Wareham, N.J.: Epidemiology of diabetes. *Medicine (Abingdon)* 42(12), 698–702 (Dec 2014), <http://www.ncbi.nlm.nih.gov/pmc/articles/PMC4282306/>, s1357-3039(14)00271-0[PII]
6. Foster, K.R., Koprowski, R., Skufca, J.D.: Machine learning, medical diagnosis, and biomedical engineering research - commentary. *Biomed Eng Online* 13, 94–94 (Jul 2014), <http://www.ncbi.nlm.nih.gov/pmc/articles/PMC4105825/>, 1475-925X-13-94[PII]
7. Frank, E., Hall, M.A., Holmes, G., Kirkby, R., Pfahringer, B., Witten, I.H., Trigg, L.: Weka-a machine learning workbench for data mining. In: Maimon, O., Rokach, L. (eds.) *Data Mining and Knowledge Discovery Handbook*, 2nd ed., pp. 1269–1277. Springer (2010), [https://doi.org/10.1007/978-0-387-09823-4\\_66](https://doi.org/10.1007/978-0-387-09823-4_66)
8. Guyon, I., Elisseeff, A.: An introduction to variable and feature selection. *Journal of Machine Learning Research* 3, 1157–1182 (2003), <http://www.jmlr.org/papers/v3/guyon03a.html>
9. Hall, M.A.: Correlation-based feature selection for discrete and numeric class machine learning. In: Langley, P. (ed.) *Proceedings of the Seventeenth International Conference on Machine Learning (ICML 2000)*, Stanford University, Stanford, CA, USA, June 29 - July 2, 2000. pp. 359–366. Morgan Kaufmann (2000)
10. Kavakiotis, I., Tsave, O., Salifoglou, A., Maglaveras, N., Vlahavas, I., Chouvarda, I.: Machine learning and data mining methods in diabetes research. *Computational and Structural Biotechnology Journal* 15, 104 – 116 (2017), <http://www.sciencedirect.com/science/article/pii/S2001037016300733>
11. Mayer-Davis, E.J., Lawrence, J.M., Dabelea, D., Divers, J., Isom, S., Dolan, L., Imperatore, G., Linder, B., Marcovina, S., Pettitt, D.J., Pihoker, C., Saydah, S., Wagenknecht, L.: Incidence trends of type 1 and type 2 diabetes among youths, 2002-2012. *New England Journal of Medicine* 376(15), 1419–1429 (2017), <http://dx.doi.org/10.1056/NEJMoa1610187>, PMID: 28402773
12. McIlvennan, C.K., Eapen, Z.J., Allen, L.A.: Hospital readmissions reduction program. *Circulation* 131, 1796–1803 (May 2015), <http://www.ncbi.nlm.nih.gov/pmc/articles/PMC4439931/>

13. Meza, R., Barrientos-Gutierrez, T., Rojas-Martinez, R., Reynoso-Noveron, N., Palacio-Mejia, L.S., Lazcano-Ponce, E., Hernandez-Avila, M.: Burden of type 2 diabetes in Mexico: Past, current and future prevalence and incidence rates. *Preventive medicine* 81, 445–450 (2015), <http://www.ncbi.nlm.nih.gov/pmc/articles/PMC4679631/>
14. Molina-Corona, A., Zonana-Nacach, A.: Readmisin hospitalaria de pacientes diabeticos: seguimiento de 12 meses. *Revista Mdica del Instituto Mexicano del Seguro Social* 5, 469–474 (2010)
15. Olvera-López, J.A., Carrasco-Ochoa, J.A., Martínez Trinidad, J.F., Kittler, J.: A review of instance selection methods. *Artif. Intell. Rev.* 34(2), 133–143 (2010), <https://doi.org/10.1007/s10462-010-9165-y>
16. Pearl, J.: Probabilistic reasoning in intelligent systems - networks of plausible inference. Morgan Kaufmann series in representation and reasoning, Morgan Kaufmann (1989)
17. Platt, J.C.: Sequential minimal optimization: A fast algorithm for training support vector machines. Tech. rep., *Advances in Kernel Methods - support Vector Learning* (1998)
18. Quinlan, J.R.: C4.5: Programs for Machine Learning. Morgan Kaufmann (1993)
19. Shameer, K., Johnson, K.W., Yahi, A., Miotto, R., Li, L., Ricks, D., Jebakaran, J., Kovatch, P., Sengupta, P.P., Gelijns, A., Moskovitz, A., Darrow, B., Reich, D.L., Kasarskis, A., Tatonetti, N.P., Pinney, S., Dudley, J.t.: Predictive modeling of hospital readmission rates using electronic medical record-wide machine learning: A case-study using Mount Sinai heart failure cohort. In: *Pacific Symposium on Biocomputing*. Pacific Symposium on Biocomputing. vol. 22, pp. 276–287 (2016), <http://www.ncbi.nlm.nih.gov/pmc/articles/PMC5362124/>
20. Strack, B., DeShazo, J.P., Gennings, C., Olmo, J.L., Ventura, S., Cios, K.J., Clore, J.N.: Impact of HbA1c measurement on hospital readmission rates: Analysis of 70,000 clinical database patient records. *BioMed Research International* 2014, 11 (2014), <http://dx.doi.org/10.1155/2014/781670>



# The Mexican *Magical Towns* Traveling Salesman Problem: Preliminary Results

Sandra J. Gutiérrez, Nareli Cruz-Cortés, Hiram Calvo,  
Marco A. Moreno-Armendáriz

Instituto Politécnico Nacional, Centro de Investigación en Computación,  
CDMX, Mexico

B160499@sagitario.cic.ipn.mx, nareli@cic.ipn.mx, hcalvo@cic.ipn.mx,  
mam.armendariz@cic.ipn.mx

**Abstract.** The Traveling Salesman Problem (TSP) is a classical NP-hard combinatorial problem that has been intensively studied through several decades. A large amount of literature is dedicated to this problem. TSP can be directly applied to some real life problems, and to be generalized to some other set of important combinatorial problems. Nowadays, a large collection of TSP instances can be found such as TSPLIB and National TSP webpage, among others. In this paper we experiment with a different TSP instance, that is, a set of 111 Mexican towns (called *Magical Towns*), by applying five different algorithms: (1) Ant Colony Optimization, (2) Particle Swarm Optimization, (3) Greedy Metaheuristic (4) Lin-Kernighan and (5) Hybrid Metaheuristic. The best results were obtained by the hybrid metaheuristic, with a final cost function of 120.65.

**Keywords:** ant colony optimization, Lin-Kernighan, *MAX-MIN* ant system, traveling salesman problem, *magical towns*.

## 1 Introduction

The Traveling Salesmen Problem (TSP) is one of the problems in mathematics and computer science which is easy to understand and needs much effort to solve. The idea of the problem is to find the shortest path for a salesman starting from a given city, visiting  $n$  cities only once and finally arriving at the city of origin.

Much of the work on the TSP is motivated by its use as a platform for analyzing the performance of general methods that can be applied to a wide range of discrete optimization problems. This is not to say, however, that the TSP does not find applications in many fields. Indeed, the numerous direct applications of the TSP bring life to the research area and help to direct future work.

A large collection of TSP instances can be found along the specialized literature, for instance TSPLIB<sup>1</sup>, National TSP webpage<sup>2</sup>, art constructed by solving instances of the TSP<sup>3</sup>, among many others. However, there is almost no published work related to Mexican instances.

On the other hand, a Mexican Magical Town certificate is awarded to places that preserve and display tradition, beauty and culture through symbolic attributes, legends and history. The *Magical Towns Program* is a proposal made by Mexico's Ministry of Tourism launched in 2001 and, by 2017, a total of 111 towns and villages in all 31 states have been awarded the title *Magical Town*. The main objective of this program is to invite to visit this kind of towns that provide a magical experience with a typical illustration of an authentic Mexican village, natural beauty landscapes, folklore and historical sites, in order to increase profits from travel and tourism.

In this paper we apply some heuristic algorithms in a specific TSP problem, in this case Mexican *Magical Towns*. Specifically, a comparison among the following algorithms is presented: two bio-inspired algorithms: Particle Swarm Optimization [1], *Max-Min* Ant System [2], besides the best-known algorithm for TSP proposed by Lin & Kerningham [3], a simple greedy strategy and an hybrid algorithm. Our comparative study shows that the algorithm with the best results is the hybrid algorithm.

The rest of the paper will proceed as follows: the following section establishes the TSP solved with different artificial intelligence (AI) techniques and describes some routing planning problems in Mexico. Some optimization metaheuristics used in this paper are described in Section 3. The methodology for this investigation is presented in Section 4. Computational results and discussion are presented in Section 5. Finally, future work and conclusions are presented in Section 6.

## 2 Traveling Salesman Problem

The most used representation of TSP is an edge-weighted graph  $G = (V, E)$  with  $V$  being set of  $n = |V|$  nodes or vertices representing cities and  $E \subseteq V \times V$  being set of directed edges or arcs. Each arc  $(i, j) \in E$  is assigned with a value of length  $d_{ij}$  which is distance between cities  $i$  and  $j$  with  $i, j \in V$ . TSP can be either asymmetric or symmetric in nature. In case of asymmetric TSP, distance between pair of nodes  $i, j$  is dependent on direction of traversing edge or arc i.e. there is at least one arc  $(i, j)$  for which  $d_{ij} \neq d_{ji}$ . In contrast, in symmetric TSP the relation  $d_{ij} = d_{ji}$  holds for all arcs in  $E$ . The goal in TSP is thus to find minimum length Hamiltonian Circuit of graph, where Hamiltonian Circuit is a closed path visiting each of  $n$  nodes of  $G$  exactly once. Thus, an optimal solution to TSP is permutation  $\pi$  of node index  $1, \dots, n$  such that length  $f(\pi)$

<sup>1</sup> <https://www.iwr.uni-heidelberg.de/groups/comopt/software/TSPLIB95/>

<sup>2</sup> <http://www.math.uwaterloo.ca/tsp/world/countries.html>

<sup>3</sup> <http://www2.oberlin.edu/math/faculty/bosch/tspart-page.html>

is minimal, where  $f(\pi)$  is the objective or cost function, given by equation 1 [4]:

$$f(\pi) = \sum_{i=1}^{n-1} d_{\pi(i)\pi(i+1)} + d_{\pi(n)\pi(1)}. \quad (1)$$

Besides the minimization of the total travel distance, other objectives could be considered too, for instance, minimization of travel time, minimization of money (using free ways), etc.

TSP is a classical NP-hard combinatorial problem that has been intensively studied among several decades using heuristics like iterated-local search, branch and bound and graph coloring. Even evolutionary algorithms, ant colony optimization (ACO) algorithms and hybridization of techniques have been used [5].

## 2.1 Mexican TSP

To our knowledge, there have been only few studies about routing optimization in Mexico. In [6] and [7] authors presents a novel method using ant colonies for optimizing patrolling routes for personnel working in public security and the case study is municipality of Cuautitlán Izcalli in Mexico. Also in [8] authors design a routing planning software with the aim of distance minimization and travel cost for State of Puebla using dynamic programming and Floyd algorithm. Finally, in [9] authors use minimum spanning tree to collect trash across Atizapán de Zaragoza, México, while in [10], they use nearest neighborhoods to optimize the collect of platforms across the country. These works are related to our paper, but there are not about Mexican TSP instances.

## 3 Optimization Heuristics and Metaheuristics

### 3.1 MAX - MIN Ant System (MMAS)

A main ant colony optimization algorithm (ACO) is Ant System (AS), a bio-inspired metaheuristic proposed by M. Dorigo [2]. In AS the real ant behavior is used as methaphor to get the best suitable path by artificial agents, its working is based on a chemical substance called *pheromone* which is released by the ants on their path, it helps ants to locate each other in order to get location of the nearest source of food. The higher the pheromone level, the greater the number of ants following that path [11].

Each  $k$  ant generates a complete tour by choosing the cities according to a probabilistic state transition rule given by equation 2, if  $c_{ij} \in \mathbf{N}(s^P)$ , otherwise  $p_{ij}^k = 0$  [2]:

$$p_{ij}^k = \frac{\tau_{ij}^\alpha \cdot \eta_{ij}^\beta}{\sum_{c_{il} \in \mathbf{N}(s^P)} \tau_{il}^\alpha \cdot \eta_{il}^\beta}, \quad (2)$$

where  $\tau_{ij}$  is the pheromone associated with cities  $i$  and  $j$ ,  $\eta_{ij} = 1/d_{ij}$ ,  $d_{ij}$  is the distance between cities  $i$  and  $j$ ,  $\mathbf{N}(s^P)$  is the set of cities that remain to be

visited, edges  $(i, l)$  where  $l$  is a city not yet visited. The parameters  $\alpha$  and  $\beta$  control the influence between pheromone and heuristic information  $\eta_{ij}$ .

Ants prefer to move to cities which are connected by short edges with a high amount of pheromone. Once all ants have completed their tours the following updating rule is applied: a fraction of the pheromone evaporates on all edges (edges that are not refreshed become less desirable), and then each ant deposits an amount of pheromone on edges which belong to its tour in proportion to how short its tour was.

In [12] authors include *MAX - MIN AS*, it is an improved version in which only the best ant updates the pheromone trails and the value of the pheromone is bound. The pheromone update rule is shown in equation 3:

$$\tau_{ij} \leftarrow [(1 - \rho) \cdot \tau_{ij} + \Delta\tau_{ij}^{best}]_{\tau_{min}}^{\tau_{max}}, \quad (3)$$

where  $\rho$  is the evaporation rate,  $\Delta\tau_{ij}^{best}$  is the quantity of pheromone laid on edge  $(i, j)$  by the best ant,  $\tau_{min}$  and  $\tau_{max}$  are the upper and lower bounds, respectively, which are typically obtained empirically and tuned on the specific problem considered. If  $(i, j)$  belongs to the best tour  $\Delta\tau_{ij}^{best}$  is equal to  $1/L_{best}$ , otherwise it is equal to zero, and  $L_{best}$  is the length of the tour of the best ant. There have been many works related to solving TSP using *MM AS* presented in [13] and [14].

### 3.2 Particle Swarm Optimization for TSP

The particle swarm optimization (PSO) is a popular metaheuristic based on social behaviour of flock of birds and school of fish; it was originally presented by Kennedy and Eberhart [15]. In PSO, each particle represents a potential solution with an initial velocity and moves to a new position. At each iteration, every particle calculates its velocity and updates its position according to equations 4 and 5, respectively [1]:

$$V_i^{(t)} = wV_i^{(t-1)} \otimes c_1r_1(P_i - X_i^{(t-1)}) \otimes c_2r_2(G - X_i^{(t-1)}), \quad (4)$$

$$X_i^{(t)} = X_i^{(t-1)} + V_i^{(t)}. \quad (5)$$

It is very important to mention that original PSO was only for continuous search spaces and because TSP is discrete, combinatorial problem, some modifications must be made. To solve TSP with PSO, each particle represents a complete tour as a feasible solution and velocity is a measure to update the tour for better solution. Many prominent PSO based methods use Swap Sequence (SS) for velocity. A SS is a collection of several Swap Operators (SOs) and each one indicates two positions in a tour, those might be swapped. All SOs of a SS are applied on a particle's tour maintaining order and hence implications of the SS transforms the TSP tour into a new one.

In equation 4,  $c_1$  and  $c_2$  are learning factors,  $r_1$  and  $r_2$  are random values between 0 and 1,  $P_i$  is the previous best tour,  $G$  is the best tour particles ever

encountered,  $P_i - X_i^{(t-1)}$  means to obtain SOs needed to make  $X_i^{(t-1)}$  sequence equal to  $P_i$  sequence, which is the same for  $G - X_i^{(t-1)}$ ,  $c_1 r_1 (P_i - X_i^{(t-1)})$  means all SOs for  $(P_i - X_i^{(t-1)})$  should be maintained with the probability of  $c_1 r_1$ , which is the same for  $c_2 r_2 (G - X_i^{(t-1)})$ , and  $w$  is the scaling factor of influence of the previous velocity in present velocity. Each particle moves to a new tour solution  $X_i^{(t)}$  applying all SS on its previous solution  $X_i^{(t-1)}$  using equation 5. A SS is the union of SOs,  $SS = (SO_1, SO_2, \dots, SO_n)$ .

The operator  $\otimes$  defines the merging operation. If  $SS_1 = SO(1, 2), SO(5, 2)$  and  $SS_2 = SO(5, 3), SO(4, 1)$ , the new swap sequence is:

$$SS(new) = SS_1 \otimes SS_2 = SO(1, 2), SO(5, 2), SO(5, 3), SO(4, 1).$$

Finally if the new solution  $X_i^{(t)}$  is superior to  $P_i$ , update  $P_i$ , and do the same for  $G$ . Some relevant works that used this metaheuristic were presented in [16] and [17].

### 3.3 Greedy Algorithms

A greedy algorithm is a mathematical process that follows the problem solving heuristic of making the locally optimal choice at each stage, deciding which next step will provide the most obvious benefit with the aim of finding a global optimum, in this case chooses the nearest city no matter where it starts, but availability of nearest cities it is important [18]. The advantage of using a greedy algorithm is that solutions to smaller instances of the problem can be straightforward and easy to understand. The disadvantage is that it is entirely possible that the most optimal short-term solutions may lead to the worst possible long-term outcome [19].

### 3.4 Lin-Kernighan

The Lin-Kernighan (LK) algorithm belongs to the class called *local search algorithms*. It was first presented by Lin and Kernighan in [20]. This algorithm is highly effective for generating optimal solutions for the symmetric TSP [21,22,23]. However, the design and implementation of an algorithm based on this heuristic is not trivial. Basically, it is a generalization of the  $k$ -opt local search. The  $k$ -opt neighborhood includes all the TSP tours that can be obtained by removing  $k$  edges from the original tour  $T$  and adding  $k$  edges such that the resulting tour is feasible. Lin-Kernighan explores only parts of the  $k$ -opt neighborhood that seem to be most promising: it removes a edge from a given tour, then the resulting path is rearranged looking for a minimization of its cost. To make the tour feasible again, only one edge must be added to close up the tour. Then, it is possible that the final aggregated edge does not minimize the total cost because this was not considered during the minimization process.

### 3.5 Hybrid Metaheuristics

Research in metaheuristics for combinatorial optimization problems has lately experienced a remarkable shift towards the hybridization of metaheuristics with other techniques for optimization. Simultaneously, the focus of research has changed from being rather algorithm-oriented to being more problem-oriented. Nowadays the focus is on solving the problem at hand in the best way possible, rather than promoting a certain metaheuristic. This new approach is full of a multitude of powerful hybrid algorithms that were obtained by combining components from several different optimization techniques [24].

## 4 Methodology

The algorithms to solve Mexican *Magical Towns* TSP were *MMAS*, *PSO*, *LK*, greedy and hybrid algorithms. All algorithms were implemented in Matlab<sup>®</sup>.

The database of *magical towns* coordinates<sup>4</sup> was incomplete, there were missing towns<sup>5</sup>, so we manually completed it by searching in Google Maps the coordinates of the missing towns<sup>6</sup>. At the end, the list contains 111 coordinates (latitude and longitude) of *magical towns*.

### 4.1 Experimental Setup

Experiments were run in a Personal Computer with Windows 10 Pro 64-bits, with processor i7-4790@3.6 GHz and 8 GB RAM. The number of experiments for all algorithms was 30. Parameters for the AS and PSO algorithms are shown in Table 1 and Table 2, respectively, according to the most used parameters in the state of the art.

**Table 1.** Algorithm parameters for AS.

| Parameter | $m$ | $\rho$ | $\alpha$ | $\beta$ | Iterations |
|-----------|-----|--------|----------|---------|------------|
| Value     | 111 | 0.1    | 1        | 2       | 100000     |

<sup>4</sup> <http://www.gpstec.mx/coordenadas-gps-de-los-pueblos-magicos-de-mexico-2014/>

<sup>5</sup> <http://hellodf.com/la-lista-definitiva-de-todos-los-pueblos-magicos-que-hay-que-conocer-en-mexico/>

<sup>6</sup> Available at (1)<http://iarp.cic.ipn.mx/~magicaltowns> and (2)<https://www.dropbox.com/sh/dtqodj41x29tmxz/AABQPfo3xHD8M4n19wKkF-ha?dl=0>

**Table 2.** Algorithm parameters for PSO.

| Parameter | Particles | Neighborhoods | Velocity | Iterations | $c_1$ | $c_2$ | $w$ |
|-----------|-----------|---------------|----------|------------|-------|-------|-----|
| Value     | 333       | 5             | 56       | 500        | 2     | 2     | 1   |

In Table 2, the velocity is the number of swap operators (SOs), i.e. the length of swap sequence (SS), in this case 56 random values between 1 and 111, which represent the indexes to change in the corresponding tour.

## 5 Results and Discussion

In this section we present our results of applying five techniques to solve TSPs using optimization metaheuristics. Table 3 shows the average performance of 30 experiments of *MAX-MIN* AS, PSO, Greedy, LK and an hybrid (PSO and LK) algorithms.

**Table 3.** Cost function values of algorithms.

| Algorithm         | Best          | Worst         | Average       | Time [s] |
|-------------------|---------------|---------------|---------------|----------|
| <i>MMAS</i>       | 134.14        | 228.68        | 136.81        | 37.27    |
| PSO               | 129.53        | 138.70        | 134.87        | 28.04    |
| Greedy            | 140.83        | 168.06        | 154.39        | 0.32     |
| LK                | 121.81        | 693.22        | 138.67        | 0.31     |
| <b>PSO and LK</b> | <b>120.65</b> | <b>129.53</b> | <b>124.21</b> | 0.28     |

It is interesting to note that distance between best and worst tour in AS is more significant than PSO, it shows that PSO has a faster convergence behavior than AS, maybe because ant system has an explorative tendency with the parameters selected and in PSO particles for a swarm in which, at the end, all have similar solutions. In Figure 1(a) the obtained tour using *MMAS* algorithm is shown.

Moreover, in PSO the initial velocity, i.e. the length of SS, influences the population diversity, values between 10 and 111 were tested along the experiments, the higher the value of population diversity, the more influence has the particle velocity. In Figure 1(b) the obtained tour using PSO algorithm is shown.

Furthermore in Figure 1(c) and 1(d) we shown the obtained tour using the greedy and LK ( $k = 2$ ) algorithms, respectively.

The optimal tour was found by applying an hybrid heuristic with PSO and LK algorithms, with a final cost function of 120.65<sup>7</sup>. In Figure 2 the obtained tour using hybrid heuristic is shown.

<sup>7</sup> Available at (1) <http://iarp.cic.ipn.mx/~magicaltowns>, and (2) <https://www.dropbox.com/sh/dtqodj41x29tmxz/AABQPfo3xHD8M4n19wKkF-ha?dl=0>

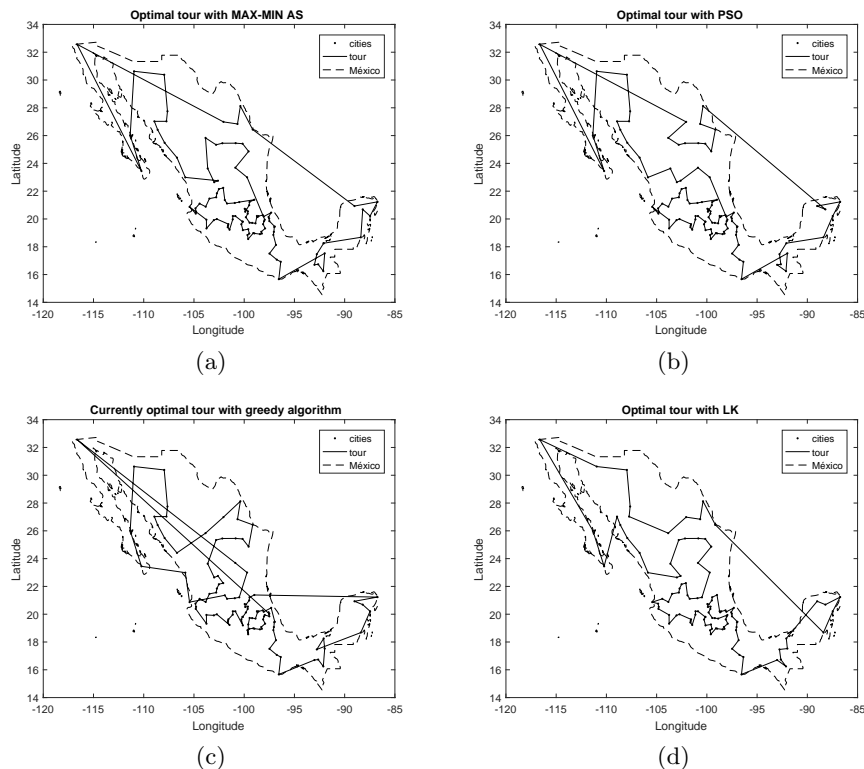


Fig. 1. Best tours using metaheuristics: (a) *MMAS*, (b) *PSO*, (c) Greedy, (d) *LK*.

## 6 Future Work and Conclusions

The experimental results show that the Mexican *Magical Towns* Traveling Salesman Problem could be solved applying different optimization metaheuristics like *MMAS*, *PSO*, greedy, *LK* and an hybrid technique.

However, using two metaheuristic results in a powerful combinations that finds the optimal tour for the 111 Mexican *Magical Towns*, with a final cost function value of 120.65. We think this results came from combining explorations and exploitation from *PSO* algorithm and then add *LK* algorithm which performs locally search and tries to improve the best solution from *PSO* algorithm.

As future work, the *MMAS*, *PSO*, *LK* and greedy algorithms can be analyzed for future enhancement such that new research could be focused to investigate which parameters are the best according to the Mexican *Magical Towns* TSP. A series of hybrid AI algorithms still needs to be applied to the dataset, like genetic algorithm, artificial bee colony, simulated annealing, etc.

On the other hand, the dataset only includes the euclidean distance between cities and it is important to take into consideration the real distance according

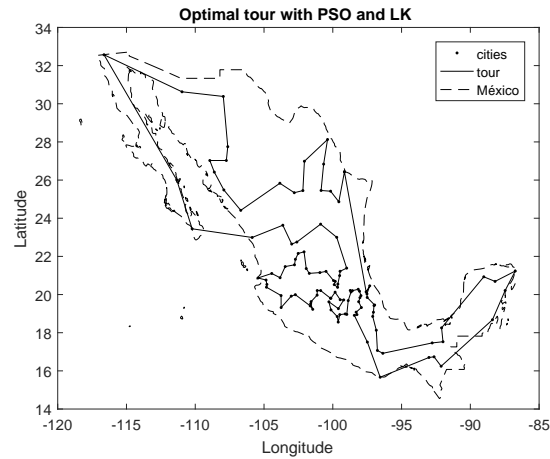


Fig. 2. Best tour using an hybrid metaheuristic.

to routes marked in a map. Nowadays, it is even possible to know the different routes, the traffic and estimated time through the different apps that use a GPS.

**Acknowledgments.** Work done under support Government of Mexico (Instituto Politécnico Nacional, SNI, SIP-IPN, COFAA-IPN, BEIFI-IPN and CONACyT) for providing necessary support. The authors would like to thank the reviewers for the useful comments, their time, effort, and engagement to making this manuscript better.

## References

1. Akhand, M. A. H., Akter, S., Rashid, M. A. and Yaakob, S. B.: Velocity Tentative PSO: An Optimal Velocity Implementation based Particle Swarm Optimization to Solve Traveling Salesman Problem. *International Journal of Computer Science* 42(3):221–232 (2015)
2. Dorigo M., Gambardella L.C.: Ant Colony System: A Cooperative Learning Approach to the Traveling Salesman Problem. *IEEE Transactions on Evolutionary Computation*, 1:1–24 (1997)
3. Karapetyana, D., Gutina, G.: Lin-Kernighan Heuristic Adaptations for the Generalized Traveling Salesman Problem. *European Journal of Operational Research* 208(3), 221–232 (2011)
4. Chahuan, C., Gupta, R., Pathak, K.: Survey of Methods of Solving TSP along with its Implementation using Dynamic Programming Approach. *International Journal of Computer Applications*, 52(4):12–19 (2012)
5. Blum, C., Puchinger J., Raidl, G.R., Roli A.: Hybrid metaheuristics in combinatorial optimization: A survey. *Applied Soft Computing* 11:4135–4151 (2011)
6. Calvo, H., Godoy-Calderon S., Moreno-Armendáriz, M.A., Martínez-Hernández V.M.: Patrolling Routes Optimization Using Ant Colonies. In: 7th Mexican Conference on Pattern Recognition, pp.302–312, Mexico (2015)

7. Calvo, H., Godoy-Calderon S., Moreno-Armendáriz, M.A., Martínez-Hernández V.M.: Forecasting, clustering and patrolling criminal activities, *J. Intelligent Data Analysis*, 21(3):697–720 (2017)
8. Montiel R.: Un Planificador de Rutas Turísticas para el Estado de Puebla. In: 7th Congreso Internacional de Cómputo en Optimización y Software, pp.221–232, M.A. Cruz-Chávez Press, Estado de México (2011)
9. Reyes, R.: Diseño del programa de recolección de desechos sólidos domiciliarios para el municipio de Atizapán de Zaragoza como aplicación del problema del agente viajero. Undergraduate dissertation, Instituto Politécnico Nacional (2005)
10. Soto, C.: Modelo para optimizar la recolección de tarimas en una empresa arrendadora: Caso de estudio. Masters thesis, Instituto Politécnico Nacional (2008)
11. Raman, V., Singh, N.: Review of different heuristic algorithms for solving Traveling Salesman Problem. *International Journal of Advanced Research in Computer Science*, 8(5):423–425 (2017)
12. Stutzle, T., Hoos, H.H.: MAXMIN Ant System. *Future Generation Computer Systems*, 16(8):889–914 (2000)
13. Stutzle, T., Hoos, H.: MAX-MIN Ant System and Local Search for the Traveling Salesman Problem. In: *IEEE International Conference on Evolutionary Computation*, pp. 309–314, Indianapolis (1997)
14. Dorigo, M., Maniezzo, V., Colorni, A.: Ant System: Optimization by a Colony of Cooperating Agent. In: *IEEE Transactions on Systems, Man and Cybernetics-Part B: Cynernetics*, 26(1):29–41 (1996)
15. Eberhart, R. C., Kennedy, J.: A new optimizer using particle swarm theory. In: 6th International Symposium on Micromachine and Human Science, pp. 39–43, Nagoya, Japan (1995)
16. Yan, X., Zhang, C., Luo, W., Li, W., Chen, W., Liu, H.: Solve Traveling Salesman Problem Using Particle Swarm Optimization Algorithm. *International Journal of Computer Science*, 9(6):264–271 (2012)
17. Zhang, J., Si, W.: Improved Enhanced Self-Tentative PSO Algorithm for TSP. In: 6th IEEE International Conference on Natural Computing, pp.2638–2641, Yantai, Shandong (2010)
18. Gutin, G., Yeo, A., Zverovich, A.: Traveling salesman should not be greedy: domination analysis of greedy-type heuristics for the TSP. *Discrete Applied Mathematics*, 117(1):81–86 (2002)
19. Bang-Jensen, J., Gutin, G., Yeo, A.: When the greedy algorithm fails. *Discrete Optimization*, 1(2):121–127 (2004)
20. Lin, S., Kernighan, B.W.: An effective Heuristic Algorithm for the Traveling-Salesman Problem. *Operations Research*, 21(2):498–516 (1973)
21. Helsgaun, K.: An effective implementation of K-opt moves for the Lin-Kernighan TSP heuristic. Doctoral dissertation, Roskilde University (2006)
22. Applegate, D., Cook, W., Rohe, A.: Chained Lin-Kernighan for large traveling salesman problems. *INFORMS Journal on Computing*, 15(1):82–92 (2003)
23. Helsgaun, K.: Solving the equality generalized traveling salesman problem using the LinKernighanHelsgaun Algorithm. *Mathematical Programming Computation*, 7(3):269–287 (2015)
24. Blum, C., Puchinger, J., Raidl, G. R., Roli, A.: Hybrid metaheuristics in combinatorial optimization: A survey. *Applied Soft Computing*, 11(6):4135–4151 (2011)

Impreso en los Talleres Gráficos  
de la Dirección de Publicaciones  
del Instituto Politécnico Nacional  
Tresguerras 27, Centro Histórico, México, D.F.  
noviembre de 2017  
Printing 500 / Edición 500 ejemplares

